Mathematical Modelling of Drug Delivery to Solid Tumour

by

Wenbo ZHAN

A Thesis submitted in fulfilment of the requirements for the degree of

Doctor of Philosophy and Diploma of Imperial College London

Department of Chemical Engineering

Imperial College London

September 2014

觀

Abstract

Effective delivery of therapeutic agents to tumour cells is essential to the success of most cancer treatment therapies except for surgery. The transport of drug in solid tumour involves multiple biophysical and biochemical processes which are strongly dependent on the physicochemical properties of the drug and biological properties of the tumour. Owing to the complexities involved, mathematical models are playing an increasingly important role in identifying the factors leading to inadequate drug delivery to tumours. In this study, a computational model is developed which incorporates real tumour geometry reconstructed from magnetic resonance images, drug transport through the tumour vasculature and interstitial space, as well as drug uptake by tumour cells. The effectiveness of anticancer therapy is evaluated based on the percentage of survival tumour cells by directly solving the corresponding pharmacodynamics equation using predicted intracellular drug concentration.

Computational simulations have been performed for the delivery of doxorubicin through various delivery modes, including bolus injection and continuous infusion of doxorubicin in free form, and thermo-sensitive liposome mediated doxorubicin delivery activated by high intensity focused ultrasound. Predicted results show that continuous infusion is far more effective than bolus injection in maintaining high levels of intracellular drug concentration, thereby increasing drug uptake by tumour cells. Moreover, multiple-administration is found to be more effective in improving the cytotoxic effect of drug compared to a single administration.

The effect of heterogeneous distribution of microvasculature on drug transport in a realistic model of liver tumour is investigated, and the results indicate that although tumour interstitial fluid pressure is almost uniform, drug concentration is sensitive to the heterogeneous distribution of microvasculature within a tumour. Results from three prostate tumours of different sizes suggest a nonlinear relationship between transvascular transport of anticancer drugs and tumour size.

Numerical simulations of thermo-sensitive liposome-mediated drug delivery coupled with high intensity focused ultrasound heating demonstrate the potential advantage of this novel drug delivery system for localised treatment while minimising drug concentration in normal tissue.

Acknowledgement

This thesis represents not only the result of my hard work over the last four years, but also invaluable supports from sincere and kind people in my life.

First and foremost, I am grateful to my supervisor Professor Xiao Yun Xu. She has been professionally and personally supportive since the day I applied for a Ph.D. position at Imperial College. My Ph.D. experience would not have been as stimulating and productive without her contributions of ideas and time. I appreciate her motivational enthusiasm and great patience to guide me through the tough time in the Ph.D. pursuit.

Many people have helped and taught me immensely during this project. Thank you to Professor Wladyslaw Gedroyc for kindly providing MR images and answering all my questions. I would like to acknowledge Professor Simon Thom who gave me many suggestions from clinical aspects to help improve my work. The time of working with Professor Nigel Wood is unforgettable because of his great enthusiasm and appreciable willingness. I also want to express my special thanks to Dr. Xin Zhang for sharing knowledge of thermo-sensitive liposome and providing useful suggestions based on his experiments. Generous help was also given by Dr. Cong Liu, who helped me a lot in deepening understanding of drug transport processes.

Our group has become a source of friendship, kind help and collaboration. My time at the college could not have been as colourful or joyful without any of these. Thanks to Drs. Ryo Torii, Zhou Cheng and Chrysa Anna Kousera, my fellow colleagues Afet Mehmet, Zhongjie Wang, Harkamaljot Kandail, Shelly Singh, Oluwatoyin Fatona, Ana Crispin Corzo, Boram Gu, Claudia Menichini and Andris Piebalgs. I wish you all the best.

My time in the U.K. was made enjoyable and cheerful because of many friends. I cherish the time spent with friends in London, trips to other UK cities and abroad. Many thanks to my friends for their long-lasting friendship over years. Da Gao and Wenbo Dong's visits were surprising gifts to me. Heartfelt thanks to Yijiu Jiang for his fraternal supports in the past years.

Last but not the least, I am deeply indebted to my parents for their love and encouragement under any circumstances. They raised me with a love of science and supported me in all reasonable pursuits. It is my great honour and happiness to be a member of the family. Thank you.

Declaration

I hereby declare that the work represented in this thesis was originated entirely from me. Information derived from the published and unpublished work of others has been acknowledged in the text and references are given in the bibliography.

Wenbo ZHAN

Imperial College London, September 2014

Contents

List of Figures

12

13

15

List of Tables

1. Introduction

Cancer is a major cause of mortality and morbidity in the developed and developing countries. Currently, cancer is treated primarily by surgery, radiation therapy and chemotherapy. Novel approaches, such as gene therapy, immunotherapy and antiangiogenesis therapy, have been developed extensively and are likely to become clinically available in the next few decades. Except for surgery, effective delivery of therapeutic agents to tumour cells is the key to success for these therapies. Therefore, in this thesis, the essential physical and biochemical processes involved in drug delivery to solid tumours are studied. This chapter presents the relevant background and preliminaries of the project. The objectives and strategies of the research are then defined, which is followed by an outline of the thesis.

1.1. Background

1.1.1. Cancer

Cancer is a set of diseases characterized by unregulated cell growth leading to invasion of surrounding tissues and spread to other parts of the body [1]. Cancer cells can divide and grow uncontrollably, forming malignant tumours and finally invading nearby normal tissues. Up to now, over 200 types of cancer have been discovered. As shown in Figure 1-1, the high mortality rate associated with cancer makes it one of the most serious life-threatening diseases in the world. Around 159,000 people died from cancer in the UK in 2011, indicating 252 deaths for every 100,000 people.

Death per 100,000 Population*

- 116.0+
- 99.6 – 116.0
- 89.7 – 99.6
- 73.3 – 89.7
- <73.3
- No Data

*All cancers except non-melanoma skin cancer
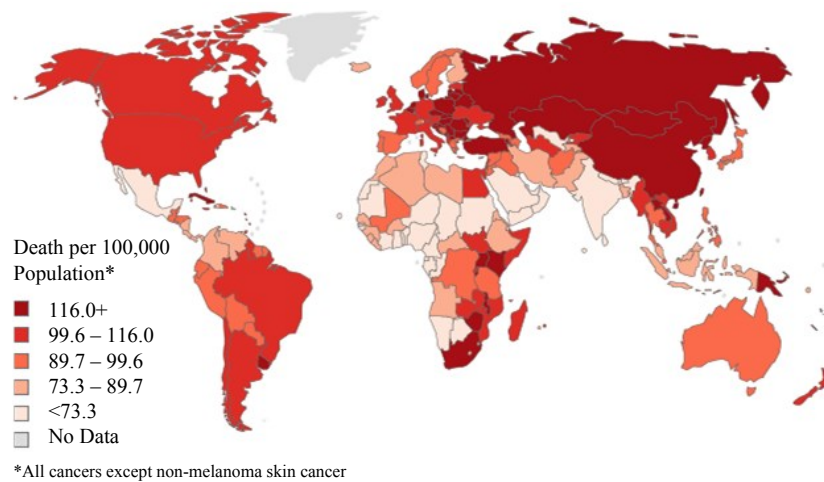
Figure 1-1. World cancer death 2012

The causes of cancer are diverse, complex and not totally understood [2]. Various factors have been suggested to increase the risk of cancer, including pollution, radiation, industrial products and certain types of infections caused by damaged genes or combined with existing genetic faults within cells. Cancerous mutations of proliferation related genes, proto-oncogenes and/or tumour suppressor genes, drive cancer cells to go on duplicating themselves.

Cancer seems to develop progressively [2]. As cancer cells expand, the original space becomes insufficient for their uncontrolled growth, resulting in invasion of increasing number of cells to the adjacent normal tissues. In order to acquire oxygen and nutrition to support cancer growth, normal cells are signalled to help develop new blood vessels. These vessels tend to be leaky and with abnormal geometric properties, which are different from blood vessels in normal tissues. In

addition, cancer cells can migrate from the primary cancer and spread to more distant parts of the body through the blood stream or lymphatic system to establish new colonies of cancer cells. These new settlements, termed metastases, are the major cause of death since vital organs can be damaged by cancer cells [1]. Ideally, treatments should start before cancer cells invade into other organs.

1.1.2. Anticancer Therapy

Various anticancer treatments are available in clinics, and the choice of these treatments is strongly dependent on the location, growth stage of cancer as well as the health condition of patients, *etc*. The main anticancer therapies are outlined below.

(1) Surgery

Surgery is cutting away tissue from patient's body. Given that it is a local treatment, surgery may cure a localised cancer that is totally contained in one area before metastases taking place. In surgery, tumour and some of its surrounding normal tissues are removed to make the margin clear. Considering that cancer may invade the lymphatic system, the nearest lymph nodes are also removed. This is a preferred treatment for cancer, and can offer a complete cure in some cases [1].

After spreading of cancer cells, surgery usually cannot cure the cancer, but may also help patients live longer and reduce/control pain. Another application of surgery is to prevent or reduce the risk of cancer. People at a high risk of a particular type of cancer (*e.g.* bowel or breast cancer) may choose surgery to remove the relevant tissue.

Surgery is limited by the type of cancer. Certain types of cancer are difficult to be removed due to their location, and insufficient removal may result in regrowth of cancer. On the other hand, spalling of cancer cells during surgery may cause the spread of cancer cells.

(2) Chemotherapy

Chemotherapy is the use of cytotoxic or cytostatic drugs that respectively kill malignant cells or prevent them from proliferating. The effectiveness of chemotherapy strongly depends on the

amount of drugs accumulated in the tumour, exposure duration to drugs and the proportion of cell population that is proliferating.

There are more than 100 different anticancer drugs currently available and new drugs are being developed all the time. The choice of drugs is highly related to the type and stage of tumour. Chemotherapy kills tumour cells by damaging the genes that make cells divide, or it may interrupt the chemical process involved in cell division. The process affected by normal chemotherapy drugs are summarized in Table 1-1.

Table 1-1. Processes affected by chemotherapeutic drugs [1]

Drug	Process Affected	Cancer Treated
Cisplatin	DNA synthesis	Ovary, Testis
Methotrexate	Dihydrofolate reductase	Breast, Placenta
5-Fluorouracil	Thymidylate synthase, RNA synthesis	Stomach, Breast, Colorectal
Doxorubicin	DNA & RNA synthesis	Lung, Breast, Leukaemia
Vincristine	Tubulin polymerisation	Lymphoma, Testis

Chemotherapy is a systemic treatment. Drugs are circulated around the body in the bloodstream and can reach cells almost anywhere. Without specifying the target, normal cells can also be killed and hence the normal function of tissue can be compromised. This is known as side effects, which can seriously offset the treatment outcome. Side effects vary according to the drug, but there are some most common side effects, as shown in Table 1-2.

Table 1-2. Common side effects caused by chemotherapeutic drugs [1]

Drug	Side Effects
Cisplatin	Nephrotoxicity, Ototoxicity, *etc*
Methotrexate	Myelosuppression, Alopecia, Dermatitis, *etc*
5-Fluorouracil	Myelosuppression, Cardiac toxicity, *etc*
Doxorubicin	Cardiomyopathy, Myelosuppression, Leukopenia, *etc*
Vincristine	Chemotherapy-induced peripheral neuropathy, Hyponatremia, *etc*

During chemotherapy, drugs often stop the bone marrow from generating enough blood cells. Without adequate white blood cells, risks of developing infections will increase, which low levels of red blood cells result in the shortage of nutrition and oxygen supply, causing

breathlessness and tiredness. Most drugs cause hair loss, but this effect is temporary and hair starts to grow back a few weeks after chemotherapy ends.

Changes in the way that liver, kidney, lung and heart work can also be caused by chemotherapy drugs. These changes are usually temporary, but can be permanent for some patients. Doxorubicin is a typical anticancer drug, and its most serious side effect is cardiomyopathy, which can lead to heart failure. In order to minimise the risk for this, the total dose of doxorubicin in a life cycle is limited to 550 mg per unit body surface area [3].

(3) Radiotherapy

Radiation is applied to kill malignant tumour cells by causing irreversible damages to DNA within cancer cells. Since tumour stem cells are not as sensitive as cycling cells to radiation, the entire treatment process may last longer than other types of treatment. According to the way radiation is used, basically there are two types of radiotherapy: external radiotherapy and internal radiotherapy.

In external radiotherapy, a narrow radiation beam with high intensity is generated to a well identified area of the patient's body. X-ray and gamma ray are the most common radiation used clinically. Since radiation can pass through the body, superficial and deep-seated tumours can be treated without surgical trauma. Given that the treated area is well identified before radiotherapy, damage to adjacent and overlying normal cells can be minimized by re-directing the radiation beam to restrict the radiation dose only being focused in tumour.

In internal radiotherapy, radioactive implants are inserted within or close to the target tumour, and a radioactive liquid is administrated orally or injected first, which is then transported by the circulation system. The radioactive component of the liquid is called isotope, which is designed to attach to a 'bioconjugate' molecule, such as an antibody, to cause the liquid to be taken up by tumour cells.

Although radiotherapy is a local treatment, some normal cells are inevitably killed, resulting in undesirable side effects. During the treatment, tiredness is a common side effect since healthy cells need to be repaired or the level of blood cells drops. In addition, radiotherapy can also cause side effects in particular organs, such as in the head, neck or chest.

(4) Novel and Emerging Therapies

High intensity focused ultrasound (HIFU) is a novel and fast developing therapy [4]. High frequency ultrasound waves are emitted from an ultrasound transducer, and the waves deliver a strong beam to the targeted region in order to elevate the temperature to kill tumour cells. It is a highly targeted and localised treatment. Because of the non-invasive nature of the sound wave used, the associated side effect is less than the other treatment methods. Patients may feel localised pain in the first 3~4 days.

Photodynamic therapy (PDT) is usually used to treat non-melanoma skin cancer [5]. Drugs (known as photosensitiser) are firstly administrated to add a specific type of light sensitivity to tumour cells, which are then killed by exposure to this light. However, PDT can make skin and eyes sensitive to light, and may cause death of nearby normal cells.

Gene therapy involves inserting specific genes into malignant or normal cells in order to modify their gene expressions. Either viral or non-viral agents can be used to deliver the specific genes, and viral must be attenuated before used. This therapy is with high specificity, but is still in development stage. A number of early stage clinical trials have been carried out [6-8].

Clinically, the treatment methods are strongly dependent on the type, location and growth stage of tumour as well as the health condition of patient. Usually, various treatments are combined in order to improve the overall treatment outcome. Most of these therapies depend on effective delivery of therapeutic agents to the targeted tumour.

1.1.3. Thermo-Sensitive Liposome-Mediated Drug Delivery

For an effective delivery, adequate therapeutic agents should reach the tumour while drug accumulation in normal tissues needs to be prevented or reduced in order to minimize side effects. Since most therapeutic agents are carried by systemic bloodstream to the entire body, their usages are hence limited. As an improvement, thermo-sensitive liposome-mediated drug delivery has been developed to overcome this shortcoming.

Anticancer drugs are encapsulated by thermo-sensitive liposomal particles which are administrated into the blood stream as usual [9]. Ideally, these particles should retain their load at body temperature, and rapidly release the encapsulated drugs within a locally heated tumour

region. The fast release is due to liposome thermo-responsiveness, which arises from a phase transition of the constituent lipids and the associated conformational variations in the lipid bilayers [10-12].

Localised heating can be achieved by various means, including: microwave, radiofrequency electric current, laser, and HIFU transducer [13]. The sound wave generated by HIFU transducer is a mature technology which has been adopted in HIFU treatment alone without the use of drugs, and is found to have very few side effects.

1.2. Objectives of the Study

The delivery of anticancer drugs consists of multiple processes, as the drugs must make their way into the blood vessels of the tumour, pass through the vessel wall to enter the interstitial space and be taken up by tumour cells. On the one hand, these processes are dependent on the physicochemical properties of the drugs, such as diffusivity and drug binding to cellular macromolecules. On the other hand, the biological properties of a tumour, including tumour vasculature, extracellular matrix components, interstitial fluid pressure, tumour cell density and tissue structure and composition, also serve as determinants in these processes. Unfortunately, the structure and morphology of microvessels in malignant tumours is highly abnormal and heterogeneous, which create a great barrier for effective delivery of drugs to cancer cells.

The overall aim of this project is to develop a multi-physics model for the simulation of transport processes of therapeutic agents in solid tumours. The main focus of this project is on the development of transport models for free drug and drug loaded thermal-sensitive liposomes, with the following specific objectives:

(1) To develop a mathematical model for the transport of anticancer drugs in their free form;
(2) To determine the optimal administration mode and schedule for maximum accumulation of drugs in tumour cells;
(3) To develop a mathematical model for the transport of drug-loaded thermosensitive liposomes;
(4) To fulfil objective (3), a bioheat transfer model with HIFU heating needs to be developed;
(5) To examine the effect of different drug delivery modes on drug distribution in solid tumours.

A research strategy has been developed in order to accomplish these objectives. The mathematical models are applied to realistic tumour models reconstructed from magnetic resonance images (MRI). In the basic tumour models, a uniform microvasculature is assumed. This assumption is subsequently relaxed by incorporating microvasculature heterogeneity derived from *in vivo* MRI data, and the effect of microvasculature distribution on drug concentration in tumour is investigated. Finally, the drug delivery model is coupled with the bioheat transfer model under HIFU heating in order to study thermal-sensitive liposome-mediated drug delivery.

1.3. Structure of This Thesis

This thesis includes seven chapters, which are organized in a logical sequence. In Chapter 2, a comprehensive survey of literature is given for the research to cover tumour properties, drug delivery modes and drug transport processes. In Chapter 3, mathematical models utilized to achieve the objectives and their implementations are described. Chapters 4, 5 and 6 present the findings and analysis of results of drug transport process and treatment efficacy with various administration modes and biological properties. Chapter 4 compares the bolus injection and continuous infusion, and Chapter 5 investigates the influence of heterogeneous vasculature and the size of tumour. Chapter 6 focuses on drug transport under thermal-sensitive liposome-mediated drug delivery. Finally, conclusions and suggestions for future work are outlined in Chapter 7.

2. Literature Review

In this chapter, a comprehensive review of the literature on topics related to drug transport in solid tumour is given. Firstly, the unique characteristics of solid tumour are described, which serves as an introduction to the microenvironment in tumour. This is followed by a review of previous studies of drug delivery modes, covering both medical and mathematical modelling aspects. Finally, the key processes involved in drug delivery to solid tumour are summarized.

2.1. Characteristics of Solid Tumour

Different from normal tissues, solid tumours have abnormal characteristics that may strongly influence the transport of anticancer drugs to and within tumours.

2.1.1. Tumour Vasculature

Microcirculation plays an important role in the delivery of anticancer agents to solid tumours [14-16]. Small tumours with a diameter less than 2 mm are perfused by blood from their host normal tissues [17]. With the growth of a tumour, new blood vessels are formed either through recruitment from pre-existing network of the host tissue or resulting from the angiogenic response of tumours [18, 19]. Both morphological features and functions of tumour vasculature differ from those in normal tissues.
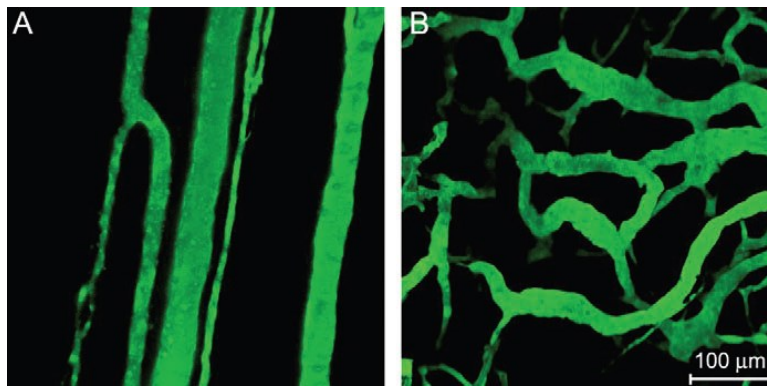
Figure 2-1. Normal and tumor vasculature.

A) Normal vasculature: vessels are aligned in a well-organized manner; B) Tumor vasculature: vessels are dilated with non-uniform diameters and random branching patterns (extracted from [20])

Tumour vasculature becomes tortuous, elongated, and often dilated as a result of tumour growth (Figure 2-1). The morphological structure of vessels can also change in the growing process of a tumour, with some features that are rarely present in normal tissues. As shown in Figure 2-2, trifurcation is a typical pattern which is frequently seen in tumour vasculature. Loops can be found in both arterial and venous trees in tumours, and there are two types: self-loop and true loop [21]. Self-loops are planar loops consisting of only two vessels without any other side branches, whereas true loops are non-planar composed of several vessel segments with many branches. Polygonal structure exists in the tumour capillary meshwork. Venous convolution is

often observed in close proximity to the feeding/draining vessels. The result of this kind of vascular architecture may lead to plasma skimming and heterogeneous vessel haematocrit levels.
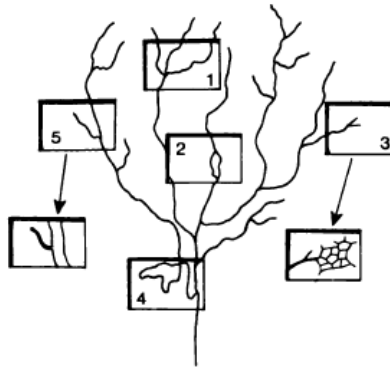
Figure 2-2. Typical architecture of blood vessels in solid tumour (extracted from [21])

Including (1) trifurcations, (2) self-loop, (3) characteristic polygonal structure of the capillary meshwork, (4) venous convolutions, and (5) small (20~40 μm) vessels branching off of large (200 μm) vessels

The diameters of arterioles and venules decrease monotonically as branching order increases. Comparisons presented in Table 2-1 [21-24] show that blood vessels in tumour have a large diameter, which may exceed the size of anticancer agents (<1~2 μm for free drugs and 100 nm for liposome particles [25, 26]). Comparisons between unit volume of tumour and normal tissue show that the length, surface area and fraction of vasculature volume are significantly larger in tumours.

Table 2-1. Morphological features of tumour microvasculature

| | Diameter (μm) | | Length | Surface Area | Vascular Volume |
	Capillary	Venules	(cm/mm^3)	(mm^2/mm^3)	Fraction (%)
In Tumour	5~20	15~70	36	70	50
In Normal Tissue	5~8	12~50	160	20	20

One of the unique characteristics of tumour vasculature is its high leakiness. The abnormal structure of vessel wall in tumours [27-29] may be one of the reasons. Large inter-endothelial junctions, increased numbers of fenestrations, vesicles and vesico-vacuolar channels, and a lack of normal basement membrane are often found in tumour vessels [30, 31]. Perivascular cells have abnormal morphology and heterogeneous association with tumour vessels. In correspondence to these structural alterations in the tumour vessel wall, the cut-off size of pores on tumour microvasculature is in the range of 100~780 nm, varying according to the location and growth stage of the tumour [26, 32, 33]. Compared to the pore size of 2~6 nm in most normal

tissues [34-36] and 40~150 nm in kidney, liver and spleen [37, 38], tumour vasculature with large pores is favourable for anticancer drugs to pass through, and thereby easing the drug delivery process.

The distribution of tumour vasculature depends strongly on the location and growth stage of the tumour. In theory, four regions can be categorized based on the type and function of tumour vasculature [39]: (1) necrotic region with no functional vasculature; (2) semi-necrotic regions with capillary, pre- and post-capillary extended; (3) stabilized microcirculation region characterised mainly by venules, veins and a few arterioles; and (4) tumour advance front with arterioles, capillaries and venules. Jain simplified this region-categorization as necrotic region, semi-necrotic region and well-vascularised region along the radial distance [40], as shown in Figure 2-3.
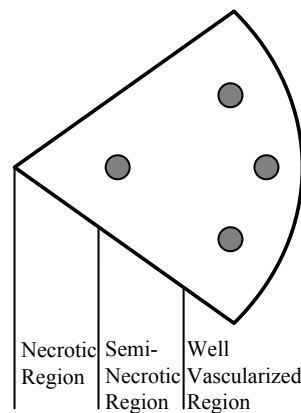
Figure 2-3. Regions in Solid Tumour (extracted from [40])

In reality, two types of vascular structure can be observed from *in vivo* images [41]. In tumours with peripheral vascularisation, the centre is poorly perfused and vessels are located mainly in the periphery. These may also occur in fully grown tumours that have already invaded into normal tissues. In tumours with central vascularisation, vessels proliferate from the centre and form a tree-like structure. In this case, vessel volume in the centre is higher than that in the periphery of the tumour.

2.1.2. Blood Flow Rate

Given that anticancer agents are carried by the blood stream to the target solid tumour, tumour blood flow rate may greatly influence the transport of drugs. Under the assumption of steady and

fully developed flow and ignoring geometric complexities, the volumetric flow rate in a tumour vascular network is proportional to the pressure difference between its arterial and venous ends, and inversely proportional to blood viscosity and geometric resistance [42].

Microvasculature pressure at the arterial ends is found to be similar in both tumour and normal tissue [43], but pressure in the venular side is significantly lower in a tumour when compared to normal tissue [17]. Because most blood vessels in tumours are veins whilst arteries mainly exist in tumour advance front region [41], the driving force for blood flow is greater at the periphery. This is one possible reason for the heterogeneous distribution of blood flow in tumour [39, 44].

Viscous resistance depends on plasma viscosity and parameters describing the number, size and rigidity of red blood cells, while geometric resistance is directly associated with the morphological features of microvessels, such as the number of vessels, branching patterns, diameter and length [42]. Both of these resistances may be altered by changes in environmental or internal conditions. Compared to normal tissue, greater resistance is found in tumours owing to the drainage force from the tumour cells and proteins existing in the extracellular space, as well as the large vessel diameter and long vessel length.

Table 2-2. Mean blood flow rate in human tumour and normal tissue (ml/g/min) [45].

	Brain	Lymphatic	Breast	Uterus	Liver
Tumour	0.50	0.45	0.23	0.33	0.12
Normal Tissue	0.57	0.40	0.83	0.13	1.05

A number of studies of blood flow in human tumours and their holding tissues have concluded that there is a wide range of variations in blood flow rate even for the same type of tumour [45]. Comparisons summarized in Table 2-2 show that the difference in mean blood flow rate between tumours and normal tissues depend strongly on their location.

2.1.3. Lymphatic Drainage

The lymphatic system is a part of the circulatory system spreading into many organs. Lymphatic vessels are structurally similar to capillaries, with a wall formed by a single layer of endothelial cells [46]. However, the lymphatic wall is more permeable than the capillary wall and is not size-selective [17]. Its main function is to return interstitial fluid back to the blood stream partly due

to the low pressure in lymphatics, and to clear extracellular matrix deposits, such as proteins, from the interstitial space in most normal tissues [47]. The diameter of lymphatic vessels in tissue is around 40 μm, and the velocity is in the range of 1.4~20 μm/s, with an average value of 8 μm/s [46]. Hence, drugs can be constantly cleared in regions with a high density of functional lymphatic vessels.

2.1.4. Interstitial Fluid Pressure

The interstitial space of a tumour is complex partly due to the extracellular matrix and non-uniform vasculature distribution [46]. The pressure in a tumour can exceed atmospheric by greater than 4200 Pa [46, 48]. This high pressure can be attributed to: (1) insufficient normal removal of interstitial fluid due to lack of lymphatics; (2) high permeability of tumour vasculature, and (3) vascular collapse caused by cell proliferation in a confined volume [15].

Models of microenvironment as complex as interstitial space of a tissue require a proper description of its microstructure. The organization of capillaries in tumours is random owing to the abnormal morphological features, and the inter-capillary distance is usually 2~3 orders of magnitude smaller than the length scale for drug transport [49], hence a useful model can be based on percolation description of porous media governed by Darcy's law [46].

A theoretical platform has been set by Baxter and Jain [49] for transvascular exchange and extravascular transport of fluid and macromolecules in tumour based on Darcy's law describing the interstitial space as a porous media. Validated by experimental data, their simulations of tumour microenvironments in both tissue-isolated and subcutaneous tumours indicate that interstitial fluid pressure in a tumour is higher than in normal tissue with a uniform distribution in the centre even if in the presence of a necrotic core, and there is a sharp drop of interstitial pressure at the periphery of the tumour [49-51].

2.2. Modes of Drug Delivery to Solid Tumour

The route and method of drug administrated affect the kinetics of bio-distribution and elimination, therefore, the effectiveness of chemotherapy [46]. Modern pharmaceutical science provides many options for drug administration to meet specific requirements in clinical anticancer treatments.

2.2.1. Traditional Administration

Anticancer drug administration traditionally includes oral delivery and intravenous injection. Because eating is one of the most common acts in daily life, oral intake is always preferred. It is painless, uncomplicated and self-administrated [46]. However, due to the fact that many drugs are degraded within the gastrointestinal tract, or cannot be sufficiently absorbed, the treatment efficacy is seriously compromised.

Drug delivered by intravenous infusion is therefore adopted to offer a more rapid and efficient therapeutic outcome. With this administration method, nearly 100% of the drug is bioavailable and the plasma concentration level can also be controlled continuously [46]. The disadvantages, such as risk of overdose and infection, can also be avoided. Nowadays, intravenous injection is the most common administration mode in anticancer treatment.

Studies on infusion duration were attempted with an aim to maximise intracellular drug concentration and reduce side effects. Noticing that high plasma concentration of doxorubicin may cause serious cardiotoxicity [3, 52], Legha [53] prolonged the infusion duration to 48 hours or 96 hours in treatments for 21 patients, while the other 30 control patients received standard intravenous injection with the same clinical dose. It was found that plasma levels of doxorubicin were reduced by continuous infusion, thereby reducing the risk of cardiotoxicity. Comparison also showed that the anticancer efficacy was not compromised.

Similar clinical studies were carried out by Hortobagyi [54]. The initial group of breast cancer patients were treated by doxorubicin with bolus injection while in the other group doxorubicin was administrated via a central venous catheter over a 48-hour or 96-hour continuous infusion schedule. Anticancer treatment outcomes revealed that there were no differences between these two groups, but continuous infusion was less cardiotoxic than bolus injection.

El-Kareh and Secomb [55] suggested that shorter infusion duration might improve treatment efficacy, and explored it by numerical studies. The anticancer efficacy is reflected by survival cell fraction based on the predicted peak intracellular concentration over the entire treatment period. Comparison between bolus injection and continuous infusion of 50, 100, 150 and 200 minutes indicated that infusion duration had a strong influence on the predicted outcome. An optimal duration for continuous infusion was found to be within 1 to 3 hours.

2.2.2. Nanoparticle-Mediated Delivery

In order to reduce the risk of side effects caused by high drug concentration in normal tissues, cytotoxic drugs are encapsulated in nanoparticles, typically liposomes, before being intravenously administrated into blood stream [56, 57]. The term "liposome" was firstly introduced to describe one or more concentric lipid bilayers enclosing an equal number of aqueous media which can be entrapped in the core during formation [46, 58]. Usually, liposomes are designed to be in the range of 70 to 200 nm in diameter in order to increase its circulation time in the blood stream [59]. Decreasing the diameter of liposome to less than 70 nm would result in 70% of the injected dose being accumulated in liver, while larger liposomal particles with a diameter greater than 200 nm are more likely to be taken up by the spleen, resulting in a reduced level in blood [60].

Because of phagocytosis by cells of the reticuloendothelial system, liposomes disappear rapidly in the blood stream [46]. Hence, modifications on the liposome structure are required. Polyethylene Glycol (PEG) is now widely adopted as an important component in liposomal layer in order to prolong the circulation of liposomal nanoparticles in the blood stream. The drug concentration, therefore, can be maintained at a sufficient high level for effective cell killing [56, 61]. The pharmacokinetics of liposome-mediated doxorubicin in cancer patients was qualitatively analysed by comparing with the same dose of doxorubicin delivered in free form [62]. Results have shown clearly that liposome-mediated delivery can reduce plasma clearance and increase doxorubicin concentration within tumours. Plasma elimination of doxorubicin-loaded liposomes follows a bi-exponential decay function with half-lives of 2 and 45 hours [62].

In vivo experiments on human prostate carcinoma, which is implanted subcutaneously into nude Swiss mice, demonstrated that liposome-encapsulated doxorubicin could enhance the therapeutic efficacy owing to reduced systemic elimination, increase penetration in tumour and prolong liposome presence with slow drug release [63]. To assess the clinical benefit of liposome-encapsulated doxorubicin, 297 patients with metastatic breast cancer with no prior chemotherapy were randomized to receive 60 mg/m^2 liposome-encapsulated doxorubicin or conventional doxorubicin in combination with 600 mg/m^2 of cyclophosphamide until disease progression or unacceptable toxicity was reached [64]. Results showed that liposome-encapsulated doxorubicin could significantly reduce cardiotoxicity and improve the therapeutic effectiveness.

Controlled release is important in making chemotherapy a localised treatment. With a thermo-sensitive liposomal membrane, in theory, no drug can be released until it is heated beyond its phase transition temperature [65]. A large number of experimental studies have been carried out to meet this goal. Thermo-sensitive liposomes sterically stabilized in human plasma have been developed by Gaber [66], while Unezkazi [67] and Lindner [68] developed improved formulations to offer both prolonged circulation and thermo-sensitivity. Optimization study on liposome particle was carried out by Tagami [69] to reduce the release rate at body temperature while maximising the release rate at mild hyperthermia.

Fast temperature elevation can be obtained by laser, microwaves, radiofrequency electric current [13] and high intensity focus ultrasound (HIFU) [70]. Ultrasound has been used clinically to apply thermal therapy non-invasively at targets that are unavailable to other heating methods [71]. Staruch tested localised drug release with HIFU heating by *in vivo* experiments on rabbits [72, 73]. In their experiments, a HIFU beam was scanned in a circular trajectory to heat a given region in normal thigh [72] and tumour [73] to $43^{\circ}C$ lasting for 20~30 minutes. Localised heating is controlled by MRI thermometry. Encapsulated doxorubicin with thermo-sensitive liposome was intravenously administrated during hyperthermia. Comparison between heated and unheated regions indicated that MRI-controlled HIFU hyperthermia could enhance local drug delivery.

Temperature elevation in a liver tumour was predicated by numerical studies in Sheu's work [74]. Based on a patient-specific liver model, the large hepatic artery was modelled explicitly to investigate the impact of blood flow on temperature elevation. However, neither the real geometry of hepatic tumour nor drug release was included in this study.

Researchers also investigated HIFU heating modes in order to achieve a homogeneous temperature profile in tumour. Based on a 2-D idealized circular model, variables in fast scanning method with a short sonication duration for HIFU treatment were examined [75]. Results showed that fast scanning method could produce a planned lesion regardless of its scanning path. The final temperature profiles were highly dependent on the applied power and tissue perfusion. Theoretical and experimental studies [76, 77] suggested that signal point fixed-gain proportional-integral control coupled with multiple heating points along a rapid scanned trajectory could result in a homogeneous temperature profile in a given region.

2.2.3. Polymer Implant

Apart from nanoparticle-mediated delivery, a polymer implant is another delivery method developed to overcome the lack of targeting in common methods. The anticancer drug is firstly dissolved in polymers, and then the drug needs to diffuse through the polymer after being implanted and finally dissolve into the extracellular space of tumour. A number of polymeric materials have now been approved for clinical use. The most extensive type is non-degradable hydrophobic polymers. The development of biodegradable polymers with the advantage that no residual material remains in the tissue has enabled more anticancer agents with low diffusivity to be delivered to solid tumours [46]. However the design of these polymers is complex since large quantities of potentially harmful products may be released in the body.

Wang [78] showed that implanting IgG-loaded polymer in the cavity left after surgical removal of a tumour may improve the anticancer efficacy. However, Teo [79] found that surgical removal of the tumour alone could only enhance drug delivery in bis-chloroethylnitrosourea (BCNU) treatment in limited time. Intratumoural administration with optimization is capable to improve treatment efficacy and reduce drug concentration in normal tissue [80, 81].

2.3. Drug Transport in Solid Tumour

Systemic administration is the main delivery method for chemotherapeutic agents. Following its administration into the blood stream, anticancer drug experiences sequential processes before reaching the targeted tumour cells. These processes (shown in Figure 2-4) are described in detail below.
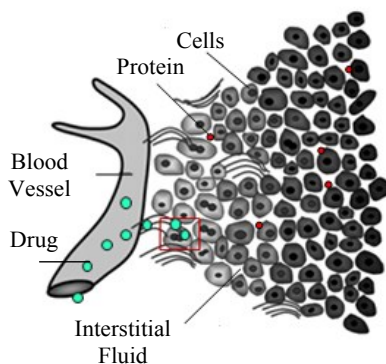
Figure 2-4. Schematic diagram of drug transport

2.3.1. Transport within Blood Vessel

After administration, therapeutic agents begin to circulate in the systemic circulation to all over the body. Drug transport within blood stream is determined by drug properties and the *in vivo* environment. Drugs that are transported via the blood may disperse into tissue when passing by. In addition, kidney and other organs can eliminate drugs from the circulation system by filtering plasma continuously, and thereby compromising the treatment effect. This function of renal excretion is known as plasma clearance, which may vary according to the drug type [82-84].
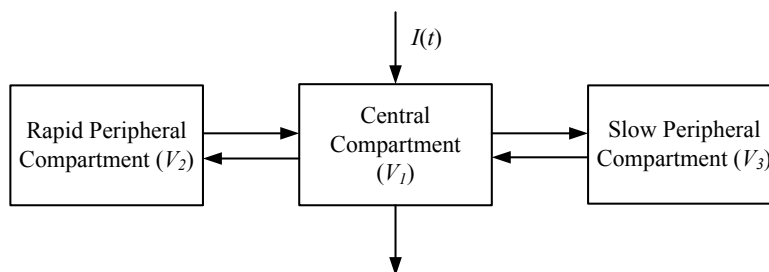
Figure 2-5. Schematic diagram of three-compartment model

Pharmacokinetics is classically represented by compartment models describing drug plasma concentration as a function of time, $I(t)$. A human body can be represented as three compartments with the volume distribution at steady state shown in Figure 2-5: the central compartment (V_1) for blood plasma, rapid (V_2) and slow (V_3) peripheral compartments corresponding to dense and sparse vessel volumes, respectively. Drugs in the central compartment can be cleared out, and there are two-way exchanges between the central and peripheral compartments, as shown in Figure 2-5. A two-compartment model has also been adopted in mathematical modelling of the delivery of anticancer agents, which consists of a central compartment and periphery compartment, with inter-compartmental exchange taking place in both directions.

Plasma concentration is associated with plasma clearance, dosage and administration mode. The pharmacokinetics of doxorubicin has been evaluated in the plasma of 12 breast cancer patients receiving no prior treatment [85]. Drug concentration was obtained by testing plasma samples collected at various times after administration. The successive half-lives were 0.08 hour, 0.822 hour and 18.9 hour, indicating that a three-component exponential function would be better suited for doxorubicin concentration in blood plasma.

In addition to red blood cells, white blood cells and platelets, blood also contains a range of proteins. Extensive bindings between these proteins and drugs have been observed in clinical and experimental conditions. Plasma pharmacokinetics of doxorubicin with a 15 minutes continuous infusion were studied in 10 breast cancer patients [86]. By applying high performance liquid chromatography, Green found that 75±2.7% of the total plasma concentration of doxorubicin was bound with protein over the whole range of observed concentrations. This high rate of binding can effectively reduce the plasma concentration of free doxorubicin and affect the amount of drug reaching tumour cells. On the other hand, the retention of drug in blood can be extended because of the low plasma clearance rate of protein [17].

2.3.2.   Transport through Blood Vessels

Being transported within the circulatory system, some drugs can be extravasated to the interstitial space owing to the high permeability of tumour vasculature. Drug transport through the vasculature wall depends on convection and diffusion.

Drug transport by convection is associated with fluid flux across the vessel wall. This fluid movement is determined by hydrostatic and osmotic pressure difference between the lumen and interstitium. Drug transport by diffusion is driven by the concentration gradient between blood and interstitial fluid, and is also related to the permeability and area of blood vessels for drug exchange. This implies that drug can also be transported back to blood when the gradient reverses. Although drugs can be carried by endothelial cells, transcytosis has been found to play a minor role when compared with convection and diffusion [17].

The pore model is widely adopted in numerical study of drug transport through blood vessels. Deen [87] reviewed studies of the hindered transport through pores on membrane that were aimed at predicting applicable transport coefficients from fundamental information, such as the size, shape and electrical charge of the solutes and pores in liquid-filled pores. The pioneering work on drug transport in solid tumour was conducted by Baxter and Jain. Employing the pore model described in Deen's work [87], they developed a general mathematical platform for trans-vascular and interstitial transport of fluid and macromolecules [49, 50, 88, 89].

Through application to an idealized tumour core model, Eikenberry [90] investigated the delivery of soluble doxorubicin from a capillary to its surrounding tumour mass to examine the

penetration of doxorubicin under different dosage regimens and microenvironment in solid tumour. Drug infusion duration was found to be an important factor in determining the spatial profile of tumour cell killing, and extending the infusion duration or fractionating the dose would help improve the treatment effect. Numerical results showed that only a limited amount of doxorubicin could be delivered into solid tumours.

The application of a pore model was extended by El-Kareh and Secomb [55] to study liposome-mediated delivery of doxorubicin to solid tumours. A mathematical model was developed and applied to compare the performance of various administration modes of both free form and liposomal encapsulated doxorubicin. The treatment outcome was predicated based on peak intracellular concentration without considering the dynamics of tumour cell density. Their simulation results indicated that continuous infusion with an optimal infusion duration yielded the best treatment efficacy, and there was a clear advantage of thermo-sensitive liposomal delivery at some doses but only if the blood was not significantly heated.

2.3.3. Transport in Interstitial Space

Following extravasation, drugs move in the interstitial space to reach tumour cells. The main pathways for drug movements are also attributed to convection and diffusion, which are highly dependent on interstitial fluid pressure and interstitial fluid velocity within tumour. Drug convection in interstitium is determined by hydraulic conductivity and pressure gradient, and diffusion depends on the concentration gradient and diffusion coefficient. Diffusion within a tissue is slower than diffusion through a medium filled with interstitial fluid, due to the presence of cells [46]. The composition of the extracellular space also affects the diffusivity of compounds through tissue, especially for macromolecules which are mostly influenced by the presence of proteins in interstitial fluid. The fact that diffusivity also depends on the architecture of tissue [46] means that the diffusion coefficient for the same drug can be different in tumour and normal tissue.

In the work of Netti [91], the tumour was modelled as a poroelastic material. The aim was to determine the mechanisms regulating interstitial fluid pressure and develop methods to overcome the interstitial fluid pressure barrier in drug delivery. Experimental and numerical results demonstrated that higher uptake of macromolecular would result from periodic modulation of

blood pressure rather than acute or chronic increase of intravascular pressure. Hence pressure elevation caused by drug administration would have a limited effect on drug delivery.

Goh [51] develop a 2-D simulation platform to investigate the spatial and temporal variation of doxorubicin concentration in hepatoma. The model geometry was reconstructed from patient-specific CT images, including the necrotic core, viable tumour and its surrounding normal tissue. Increase in vascular pressure caused by intravenous bolus injection was considered, and the predicated results showed that interstitial fluid pressure stabilized fairly quickly. The results also indicated that diffusion was the dominant transport mechanism. It was concluded that doxorubicin transport to solid tumour was strongly dependent on the vascular exchange area, doxorubicin cellular metabolism and DNA binding kinetics.

The effect of transient interstitial fluid flow on drug delivery in brain tumour was addressed by Teo [79]. After surgical removal of the necrotic core, polymer wafers that contained bis-chloroethylnitrosourea (BCNU) were implanted in the cavity. The mathematical platform established by Goh [51] was applied to simulate the intra-tumoural release of BCNU and its penetration through resection cavity to the tumour. The interstitial fluid flow was found to reach equilibrium in less than 3 hours, and surgery could only enhance drug delivery temporally.

Owing to the presence of a variety of proteins and nucleic acids in the interstitial space, extensive binding may take place. Experimental studies have shown that binding can delay drug transport [92-94]. In an experiment on thyroid cancer cells, 5-fluorouracil, cisplatin and inulin were found to be evenly distributed in cell spheroids within 15 minutes [17, 93, 94], while doxorubicin, methotrexate and paclitaxel, which bind to macromolecules, remained in the periphery of spheroids [95-97]. Since a tumour is always surrounded by normal tissues and interstitial fluid velocity is higher at the periphery of tumour than in the centre, drug exchange can also take place between tumour and normal tissues.

Based on a computational reaction-diffusion model, Tzafriri [80] examined drug release from intra-tumourally injected microspheres and drug transport in an idealized tumour model accounting for binding in tumour interstitial fluid. Their simulation results suggested that extracellular drug concentration was spatially heterogeneous in the initial period following drug administration. It was concluded that increasing the duration of drug release might prolong the

exposure duration of anticancer drug but lower the plateau drug concentration. This implied that intratumoural drug release could be optimized to improve treatment efficacy.

Baxter and Jain [88] developed a general theoretical framework to examine the effect of binding on concentration profiles of macromolecules. A high binding affinity was predicted to be most efficacious except for certain conditions of necrotic cores and low vascular permeability. Doxorubicin was also found to bind extensively with proteins, mainly albumin, in both plasma and interstitial fluid [55]. Due to the lack of *in vivo* experimental data, Eikenberry [90] assumed that doxorubicin binding and unbinding in both plasma and interstitial fluid shared the same rates, which were obtained based on experimental data [86]. Coupled with other drug transport processes including transvascular and interstitial movement, drug binding was investigated in a tumour core model. Their simulation results showed that most of the doxorubicin in extracellular space existed in bound form.

2.3.4. Transport to Lymphatic System

The lack of a functional lymphatic system has been observed in solid tumours [49, 50]. The limited existence of the lymphatic system can significantly reduce the clearance of large molecular weight drugs and hence increase their retention in interstitial fluid. These are typically liposome, nanoparticles and macromolecular drugs. On the other hand, without effective drainage of interstitial fluid from the extracellular space, interstitial fluid pressure will increase, which will in turn affect the drug exchange between blood and interstitial space.

Based on previous work on interstitial fluid pressure and drug convection, Baxter and Jain [50] used a similar model to examine the effect of lymphatics on interstitial fluid pressure distribution and concentration distribution of macromolecules (*e.g.* antibody). Their results suggested that substances could be rapidly removed by lymphatics, if present in tumour, which would result in much lower concentration levels.

2.3.5. Transport through Cell Membrane

After migrating in the interstitial space, drug can pass through cell membrane to enter tumour cells. The main mechanisms for molecular transit across membranes are passive diffusion, diffusion through channels, facilitated and active transport which involves the participation of

transmembrane proteins that bind a specific solute [46]. Drug transport through cell membrane is a dynamics process, with influx and efflux occurring simultaneously [46, 90]. Dordal [98] monitored cellular uptake of fluorescence-labelled doxorubicin in human lymphoma cells by a flow cytometry assay with a rapid-injection system. The experimental data was then analysed by a pharmacokinetic model to find the relation between drug concentration and cellular uptake.

Tumour cells can become resistant to anticancer drugs. One of the complex resistance mechanisms is related to a 1.7×10^5 Da membrane protein named P-glycoprotein (P-gp). Being insensitive to a wide variety of chemicals, P-gp is capable of actively transporting certain types of anticancer drugs, including doxorubicin and vincristine. Luu [99] developed a mathematical model to capture the efflux of doxorubicin resulting from drug mediated P-gp induction, and they concluded that their mathematical model could be utilized to optimize dosing strategies in order to minimize P-gp induction and thereby improving treatment efficacy.

El-Kareh and Secomb [55] included the dynamic process of cellular uptake and efflux in a symmetric tumour model to investigate the influence of administration modes. Friedmen [100] adopted a simplified model to fit cellular uptake rate data that showed saturation in both intra- and extra-cellular concentrations. Kerr's [101] experiments provided the experimental support to this mathematical model. Cell uptake and efflux were analysed by human non-small cell lung tumour cells in monolayer culture, and the relation between intracellular drug concentration and cytotoxicity was obtained. A similar model was improved by Eikenberry [90] and then adopted by Liu [102] to investigate the effects of ATP-binding cassette transporter-based acquired drug resistance mechanisms at the cellular and tissue scale.

2.3.6.   Cell Killing

After phagocytosis by tumour cells, drugs may destroy the genes that cause cells to divide or interrupt the chemical process involved in cell division, and thereby killing cells. The rate of cell killing has been found to be strongly dependent on extracellular and intracellular drug concentrations, and several models have been proposed to describe this relationship.

The cytotoxicity of drug was firstly assumed to be a function of area under the extracellular concentration-time curve (AUC_e) [103]. Ozawa [104] derived a cell kill kinetics equation for cell cycle phase-non-specific agents, and tested the equation by fitting to experimental results based

on Chinese hamster V79 cells. It was concluded that the cell killing action of cell cycle phase-non-specific drugs could be described by a pharmacodynamics model with the concentration-time product. Eichholtz-Wirth [105] treated Chinese hamster cells and Hela cells with doxorubicin, and found the surviving cell fraction was proportional to the product of extracellular drug concentration and exposure time. The experimental data also showed a non-linear relation between extra- and intra-cellular concentrations.

Although there is evidence that drug can kill cells without entering them, cell death is believed to be mainly dependent on intracellular concentration [1, 106]. Alternative models including intracellular drug concentration and cellular pharmacodynamics have been proposed. A cellular pharmacodynamics model for cisplatin was proposed by El-Kareh and Secomb [107] to relate cell killing to the peak value of intracellular concentration over the entire treatment period. The kinetics equations were modified for doxorubicin to reflect survival cell fraction [55, 90]. However, this model is incapable to tracking the dynamic variation of tumour cell density.

Given that chemotherapy is a dynamic process including cell proliferation, physical degradation and cell killing caused by drugs, a dynamic model was suggested to evaluate the temporal variation of cytotoxic effect of anticancer drugs [102]. Lankelma [108] proposed a pharmacodynamics model for doxorubicin, where cell killing was described as a function of intracellular concentration history. Drug accumulation history in cells was calculated using cellular drug transport parameters derived from doxorubicin uptake and efflux measurements on MCF-7 cells attached to culture dishes. Eliaz [109] developed a model taking into account the cell proliferation rate, the cell killing rate, the average intracellular concentration and a lag time for cell killing. The model was applied to free doxorubicin and doxorubicin encapsulated in liposome targeted to melanoma cells in culture.

2.4. Summary

A detailed review of tumour characteristics, drug delivery methods and transport processes indicates that all these three aspects depend on and interact with each other during anti-tumour treatment. Although previous studies summarized in this chapter have addressed the complex interplays among these factors to a certain extent, a systematic study that accounts for all these physical and biological aspects is lacking. This is what the current project aims to achieve, and

the integrated mathematical model developed in this project will serve as a platform to compare and optimise different strategies in chemotherapy.

3. Mathematical Models and Numerical Procedures

In this chapter, a detailed description of mathematical models and their implementations are given. The mathematical equations are described first; these include equations governing the interstitial fluid flow in tumour and normal tissues, mass transport and cellular uptake of anticancer agents, and heat transfer in response to the application of HIFU for activation of drug release from thermo-sensitive liposomes. Model parameters as well as relevant physical and transport properties are then discussed. Finally, numerical methods to implement the mathematical models are presented.

3.1. Mathematical Models

Drug properties are the key factors in anticancer treatments. In addition, drug transport also depends on the interstitial fluid flow in tumour and its holding tissue, and the properties of tumour cells have impacts on the cell killing as well. To include these relationships, the current modelling platform consist of descriptions of interstitial fluid flow, transport for none-encapsulated and thermo-sensitive liposome-mediated drugs, pharmacodynamics of tumour cells and bioheat transfer model introduced by high intensity focus ultrasound heating for thermo-sensitive liposome-mediated drugs only. Given the mentioned fact that the large size difference exist between a tumour and its vasculature, a commonly adopted approach for study on drug transport is treating the vasculature as a source term in the governing equations, without considering its morphological features. The main assumptions are as follows: (1) the interstitial fluid is incompressible, Newtonian fluid with homogeneous properties in tumour and surrounding normal tissue, respectively; (2) all tumour cells are stationary, identical and alive initially; (3) the simulation duration is significantly shorter than the timescale for tumour growth, and thereby the physiological parameters and geometry are independent of time.

The mathematical models consist of the mass and momentum conservation equations for interstitial fluid flow, mass transfer equations for the free and bound drug, transport equations for liposome encapsulated drug, as well as equations describing the intracellular drug concentration and pharmacodynamics. First, the interstitial fluid flow equations are solved to provide the basic biomechanical environment for drug transport. This is followed by solution of the mass transfer equations for drug transport, which is described schematically in Figure 3-1 (a) and (b) for direct infusion, and thermo-sensitive liposome-mediated delivery of doxorubicin, respectively. Briefly, the tumour region consists of three compartments: blood, extracellular space and tumour cells. Within each compartment, letters F, B and L represent free, bound and liposome encapsulated doxorubicin, respectively.

The dynamics process in drug delivery includes association/disassociation with protein at the rate k_{as} and k_{ds} respectively, drug exchange between blood and extracellular space, and influx/efflux of drugs from extracellular space to tumour cells. The rate of cell killing is governed by a pharmacodynamics model based on the predicted intracellular concentration of anticancer drugs. In the case of thermo-sensitive liposome-mediated drug delivery, an additional equation

describing the transport of liposomes is needed. The detailed descriptions of each section of mathematical models are listed below.

(a)

(b)
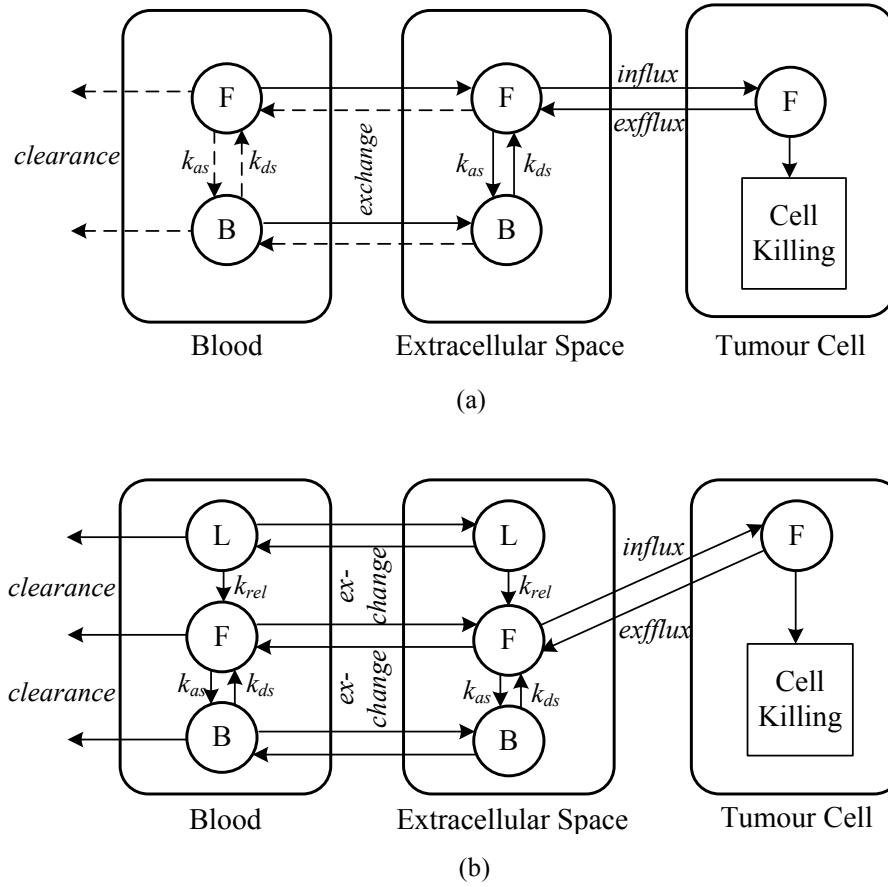
Figure 3-1. Drug transport with (a) continuous infusion of drug in its free form, and (b) thermo-sensitive liposome-mediated drug delivery

3.1.1. Interstitial Fluid Flow

The mass conservation equation for interstitial fluid is given by

$$\nabla \cdot \boldsymbol{v} = F_v - F_{ly} \tag{3-1}$$

where $\boldsymbol{v}$ is the velocity of the interstitial fluid, F_v and F_{ly} are the source and sink terms, accounting for the gain of interstitial fluid from blood vessels, and fluid absorption rate by the lymphatics, respectively. F_v and F_{ly} can be determined by Starling's law

$$F_v = K_v \frac{S}{V}\left[p_v - p_i - \sigma_T\left(\pi_v - \pi_i\right)\right] \tag{3-2}$$

where K_v is the hydraulic conductivity of the microvascular wall, S/V is the surface area of blood vessels per unit volume of tumour tissue, p_v and p_i are the vascular and interstitial fluid pressures, respectively, σ_T represents the average osmotic reflection coefficient for plasma protein, π_v is the osmotic pressure of the plasma, and π_i is that of interstitial fluid.

The lymphatic drainage, F_{ly}, is related to the pressure difference between the interstitial fluid and lymphatics.

$$F_{ly} = K_{ly} \frac{S_{ly}}{V}\left(p_i - p_{ly}\right) \tag{3-3}$$

where K_{ly} is the hydraulic conductivity of the lymphatic wall, S_{ly}/V is the surface area of lymphatic vessels per unit volume of tumour tissue, and p_{ly} is the intra-lymphatic pressure.

The tumour and its surrounding tissues are treated as porous media, which can be justified as the inter-capillary distance (33-98 μm [21, 110]) is typically 2-3 orders of magnitude smaller than the length scale for drug transport. The corresponding momentum equation is given by

$$\frac{\partial(\rho v)}{\partial t} + \nabla \cdot \left(\rho v v\right) = -\nabla p_i + \nabla \cdot \tau + F \tag{3-4}$$

where the stress tensor τ is expressed as

$$\tau = \mu[\nabla v + (\nabla v)^T] - \frac{2}{3}\mu(\nabla \cdot v)I \tag{3-5}$$

where ρ and μ is the density and dynamic viscosity of interstitial fluid, respectively. I is the unit tensor. The last term in equation (3-4), F, represents the Darcian resistance to fluid flow through porous media and is given by

$$F = W\mu v + \frac{1}{2}C\rho|v|v \tag{3-6}$$

and W is a diagonal matrix with all diagonal elements calculated as

$$W = \kappa^{-1} \tag{3-7}$$

where C is the prescribed matrix of the inertial loss term, and κ is the permeability of the interstitial space. Since the interstitial fluid velocity is very slow ($|v| \ll 1$) [49], the inertial loss term can be neglected when compared to the Darcian resistance. In addition, the interstitial fluid is treated as incompressible with a constant viscosity. Hence, equation (3-6) can be reduced to

$$F = W \mu v \tag{3-8}$$

3.1.2. Drug Transport

Drug transport is governed by the convection-diffusion equations for the free and bound drug in the interstitial fluid. Free doxorubicin concentration in the interstitial fluid (C_{fe}) is described by

$$\frac{\partial C_{fe}}{\partial t} + \nabla \cdot \left(C_{fe} v \right) = D_{fe} \nabla^2 C_{fe} + S_i \tag{3-9}$$

where D_{fe} is the diffusion coefficient of free doxorubicin. The source term, S_i, is the net rate of doxorubicin gained from the surrounding environment, which is given by

$$S_i = S_v + S_b + S_u \tag{3-10}$$

here S_v, S_b and S_u represent the net rate of doxorubicin gained from the blood/lymphatic vessels, association/dissociation with bound doxorubicin-protein and influx/efflux from tumour cells, respectively.

$$S_v = F_{fp} - F_{fl} \tag{3-11}$$

where F_{fp} is the doxorubicin gained from the blood capillaries in tumour and normal tissues, and F_{fl} is the loss of doxorubicin to the lymphatic vessels per unit volume of tissue. Using the pore model [49, 50, 87, 89] for trans-capillary exchange, F_{fp} and F_{fl} can be expressed as

$$F_{fp} = F_v \left(1 - \sigma_d \right) C_{fp} + P_{fe} \frac{S}{V} \left(C_{fp} - C_{fe} \right) \frac{\mathrm{Pe}_f}{e^{\mathrm{Pe}_f} - 1} \tag{3-12}$$

$$F_{fl} = F_{ly} C_{fe} \tag{3-13}$$

where C_{fp} is the concentration of doxorubicin in blood plasma, σ_d is the osmotic reflection coefficient for the drug molecules, and P_{fe} is the permeability of vasculature wall to free doxorubicin. Pe_f is the trans-capillary Peclet number defined as

$$Pe_f = \frac{F_v(1-\sigma_d)}{P_{fe}\dfrac{S}{V}}$$

(3-14)

The net doxorubicin gained due to protein binding and cellular uptake is governed by

$$S_b = k_d C_{be} - k_a C_{fe}$$

(3-15)

$$S_u = D_c \varepsilon - D_c \zeta$$

(3-16)

where D_c is the tumour cell density, k_a and k_d are the doxorubicin-protein binding and dissociation rates, respectively.

The convection-diffusion equation for bound doxorubicin (C_{be}) is similar to equation (3-9) except for the source terms.

$$\frac{\partial C_{be}}{\partial t} + \nabla \cdot (C_{be}v) = D_{be}\nabla^2 C_{be} + F_{be} - S_b$$

(3-17)

where D_{be} is the diffusion coefficient of the bound doxorubicin-protein, and F_{be} accounts for the gain of bound doxorubicin from blood vessels, which is given by

$$F_{be} = F_v(1-\sigma_d)C_{bp} + P_{be}\frac{S}{V}(C_{bp} - C_{be})\frac{Pe_b}{e^{Pe_b}-1}$$

(3-18)

where P_{be} is the permeability of the vessel wall to bound doxorubicin, and C_{bp} is the bound doxorubicin concentration in the plasma. The trans-capillary Peclet number is

$$Pe_b = \frac{F_v(1-\sigma_d)}{P_{be}\dfrac{S}{V}}$$

(3-19)

Since only unbound doxorubicin can pass through the cell membrane [55, 90], the rate of cellular uptake is a function of free doxorubicin concentration in the interstitial fluid.

$$\frac{\partial C_i}{\partial t} = \zeta - \varepsilon \tag{3-20}$$

$$\zeta = V_{max} \frac{C_{fe}}{C_{fe} + k_e \varphi} \tag{3-21}$$

$$\varepsilon = V_{max} \frac{C_i}{C_i + k_i} \tag{3-22}$$

where C_i is the intracellular doxorubicin concentration, and V_{max} is the rate of trans-membrane transport, ζ and ε are cellular uptake and efflux functions, k_e and k_i are constants obtained from experimental data, and φ is the volume fraction of extracellular space.

3.1.3. Thermo-Sensitive Liposome-Mediated Drug Transport

Additional equations are required to describe the transport of liposome encapsulated doxorubicin, in order to solve separately the encapsulated drug concentration and released drug concentration. Equations for the transport of released drug, including those for free drug concentration in plasma and interstitial fluid, bound drug concentration in plasma and interstitial fluid as well as intracellular concentration, are described using the same equations given in the preceding section.

Similar to equation (3-9), the liposome encapsulated drug concentration in the interstitial fluid (C_{le}) is governed by

$$\frac{\partial C_{le}}{\partial t} + \nabla \cdot (C_{le} \mathbf{v}) = D_l \nabla^2 C_{le} + S_l \tag{3-23}$$

where D_l is the diffusion coefficient of liposomes. The source term, S_l is the net rate of liposomes gained from the surrounding environment, which is given by

$$S_l = S_{lp} - S_r \tag{3-24}$$

Here, S_{lp} represents the liposomes gained from plasma, and S_r represents released drug in the interstitial fluid. S_{lp} can be calculated by

$$S_{lp} = F_{lp} - F_{ll} \tag{3-25}$$

where F_{lp} is the liposomes gained from the capillaries in tumour and normal tissues, and F_{ll} is the loss of liposomes through the lymphatic vessels per unit volume of tissue. Values for F_{lp} and F_{ll} can be obtained using the pore model described by Equations (3-12) to (3-14) but with transport properties corresponding to the thermo-sensitive liposome.

The amount of released doxorubicin in the interstitial fluid, S_r, is given by

$$S_r = k_{rel} C_{le} \tag{3-26}$$

where k_{rel} is the release rate of doxorubicin from liposome.

The free doxorubicin concentration in blood plasma (C_{fp}) is governed by

$$\frac{\partial C_{fp}}{\partial t} = S_r - \frac{V_T}{V_B} F_{fp} - CL_{fp} C_{fp} - \left(k_a C_{fp} - k_d C_{bp} \right) \tag{3-27}$$

where F_{fp} represents the free doxorubicin crossing the capillary wall into the interstitial fluid. V_T and V_B are tumour volume and blood plasma volume, respectively. CL_{fp} is the plasma clearance of drug. k_a and k_d are the association and disassociation rates with proteins.

The bound doxorubicin concentration in blood plasma (C_{bp}) is given by

$$\frac{\partial C_{bp}}{\partial t} = \left(k_a C_{fp} - k_d C_{bp} \right) - \frac{V_T}{V_B} F_{be} - CL_{bp} C_{bp} \tag{3-28}$$

where CL_{bp} is the plasma clearance of bound doxorubicin.

The free doxorubicin concentration in interstitial fluid (C_{fe}) is described by Equation (3-9), except that the source term contains an additional contribution from S_r, as described below.

$$S_i = S_v + S_b + S_u + S_r \tag{3-29}$$

Expressions for the terms on the right hand side have been given previously (see equations (3-11) to (3-16) and (3-26)).

3.1.4. Pharmacodynamics Model

The change of tumour cell density with time is described by a pharmacodynamics model as given below [109].

$$\frac{dD_c}{dt} = -\frac{f_{max}C_i}{EC_{50}+C_i}D_c + k_p D_c - k_g D_c^2 \tag{3-30}$$

The first term on the right hand side represents the anticancer effect, where f_{max} is the cell-kill rate constant and EC_{50} is the drug concentration producing 50% of f_{max}. k_p and k_g are cell proliferation rate constant and physiological degradation rate, respectively. In this study, cell proliferation and physiologic degradation are assumed to have reached equilibrium at the start of each treatment.

3.1.5. Heat Transfer under High Intensity Focused Ultrasound (HIFU) Heating

In localized heating in anti-tumour therapy, both blood and tissue including the tumour and its holding tissue are heated. Energy balances for tissue and blood are illustrated in Figure 3-2 (a) and (b), respectively.
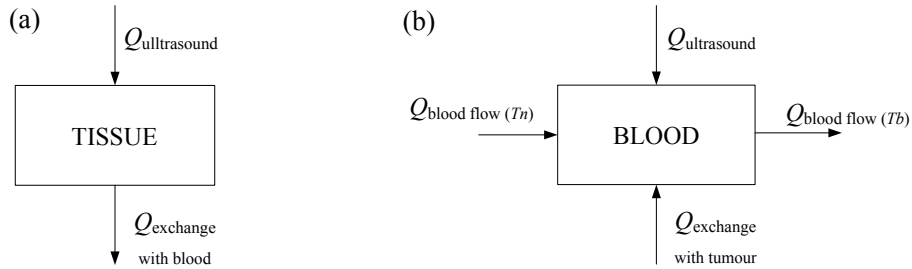
Figure 3-2. Schematic representation of heat transfer under HIFU heating in (a) tumour and (b) blood

The temperature (T) of tissue and blood can be calculated by solving the following energy balance equations [74, 111]:

$$\rho_t c_t \frac{\partial T_t}{\partial t} = k_t \nabla^2 T_t - \rho_b c_b w_b (T_t - T_b) + q_t \tag{3-31}$$

$$\rho_b c_b \frac{\partial T_b}{\partial t} = k_b \nabla^2 T_b + \rho_b c_b w_b (T_t - T_b) - \rho_b c_b w_b (T_b - T_n) + q_b \tag{3-32}$$

where ρ is the density, c is the specific heat, k is the thermal conductivity, and w is the perfusion rate of blood flow. q represents the ultrasound power deposition, and subscripts b and t represent blood and tissue, respectively. T_n is the normal body temperature, which is assumed to be 37 °C.

In reality, heating of biological tissue by HIFU also contains the effect of acoustic non-linearity [112, 113]. However, studies show that the non-linear wave propagation can be ignored if a focal intensity is within the range of 100~1000 W/cm^2 and the peak negative pressure in the range of 1~4 MPa [74, 114]. The ultrasound power deposition per unit volume is assumed to be proportional to the local acoustic intensity I_a as follows

$$q = 2\alpha I_a \tag{3-33}$$

where α is the absorption coefficient, and the intensity I_a is defined as:

$$I_a = {p_a^2} \big/ {2\rho v_a} \tag{3-34}$$

v_a is the speed of ultrasound, and p_a is the acoustic pressure which is represented by the real parts of the following equation

$$p_a = i k_{ac} \rho v_a \psi \tag{3-35}$$

here k_{ac} represents the acoustic velocity potential, and is given by

$$k_{ac} = {\omega} \big/ {v_a} = {2\pi} \big/ {\lambda} \tag{3-36}$$

ω is the angular frequency, and λ is the wave length of ultrasound.

For a spherical concave radiator S (Figure 3-3) with a uniform normal velocity, if the diameter or width of a slightly curved radiator is large compared to the wave-length, the resulting acoustic velocity potential, Ψ, in a restricted region can be written as [115]

$$\psi(R,\theta) = \frac{\boldsymbol{u}}{2\pi} \int_0^{2\pi} \int_0^b s^{-1} e^{-ik_{ac}d} R_1 dR_1 d\beta \tag{3-37}$$

where $\boldsymbol{u}$ is the normal velocity of a slightly curved radiating surface, which is represented by

$$\boldsymbol{u} = u_0 e^{i\omega t} \tag{3-38}$$

here u_0 is a constant and t is time. In Equation (3-37), d is the distance from a point on the radiator to a field point, which is given by

$$d = \sqrt{R^2 - 2Rr_1 \sin\theta \cos\beta + zR_1^2} \tag{3-39}$$

$$z = 1 - 2hR\cos\theta / b^2 \tag{3-40}$$

$$r_1 = R_1 \sqrt{1 - \left(R_1^2 / 4A^2\right)} \tag{3-41}$$

Referring to Figure 3-3, the ultrasound radiator is represented by the thick lines and the heated point is Q. A and a are the radius of curvature and radius of the circular boundary, respectively, h is the depth of the concave surface and b is the chord from the transducer centre O to the radiator boundary.
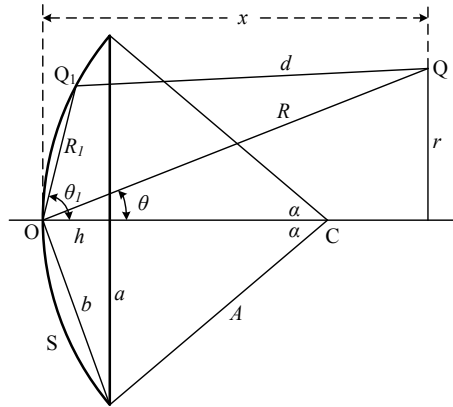
Figure 3-3. Dimensions and coordinates of a spherical radiator [115].

3.2. Model Parameters

Since the growth of tumour and normal tissues is ignored, all the geometric and transport parameters used in this study are assumed to be independent of time. Values adopted for these are summarized in Tables 3-1, 3-2 and 3-3 at the end of this Chapter for parameters related to the tissue, liposome and doxorubicin, respectively. Justifications for the choices of some of the parameters are given below.

3.2.1. Tissue Related Transport Parameters

Blood vessel surface area to tissue volume ratio (*S/V*)

The ratio of surface area of blood vessel to tissue volume has a direct influence on the amount of anticancer drug in the interstitial fluid. Its value depends strongly on the type of tissue and stage of tumour growth [116]. Pappenheimer *et al.* measured this in normal tissues [117], while Baxter and Jain [49] recommended using 70 cm^{-1} and 200 cm^{-1} for normal and tumour tissues, respectively. The effect of this parameter on anticancer efficacy and its derivation from *in vivo* MR images will be discussed in Chapter 5.

Tumour cell density (*Dc*)

The volume fraction of extracellular space in a tumour tissue ranges from 0.2 to 0.6 [118]. Assuming an average tumour cell diameter, Eikenberry [90] estimated that tumour cell density ranged from 9.55×10^{15} to 1.53×10^{16} cells/m^3. During chemotherapy treatment, tumour cell density may change as a result of drug uptake, cell proliferation and physiological degradation.

3.2.2. Drug Related Transport Parameters

Vascular Permeability (*P*)

Vascular permeability coefficient measures the capacity of a blood vessel (often capillary in tumour) wall to allow for the flow of substances in and out of the vasculature. The structure of vessel wall and the molecular size of the transported substance are key determinants of permeability [110].

(1) Free & bound doxorubicin

Estimates of this parameter reported in the literature usually correspond to 'effective permeability', which is on the order of 10^{-7} m/s for albumin in both tumour and normal tissues. For Sulforhodamine B (*MW*=559 Da), its permeability in normal tissue is 3.4×10^{-7} m/s [119]. Patent is another agent with a similar molecular weight (566 Da) to that of doxorubicin, and its permeability is 3.95×10^{-7} m/s in normal tissue of male frog [120]. Eikenberry [90] assumed the effective permeability of free doxorubicin in tumour to be in the range of 8.1×10^{-7} and 3.7×10^{-6} m/s, whereas Ribba *et al*. [121] used 3.0×10^{-6} m/s in their simulation work. Compared with

normal tissues, Gerlowski and Jain [122] found the vessel wall permeability to be 8 times higher in tumour tissues. Using *MW* for interpolation, Goh [51] assumed the permeability of doxorubicin in tumour tissue to be nearly 8 times higher than in normal tissue. In the present study, values of permeability in tumour and normal tissues are assumed to be 3.0×10^{-6} m/s and 3.75×10^{-7} m/s, respectively. Wu *et al.* [119] measured the permeability of albumin (corresponding to albumin-bound doxorubicin) in both tumour and granulating tissues, and found the corresponding vasculature permeability to be $7.8 \pm 1.2 \times 10^{-9}$ m/s and $2.5 \pm 0.8 \times 10^{-9}$ m/s, respectively. In this thesis, their average value is adopted as the permeability of albumin-bound doxorubicin.

(2) Liposome encapsulated doxorubicin

The permeability of polyethylene glycol coated liposomes of 100 nm through tumour capillaries was measured at 37 $^{\circ}$C by Yuan *et al.* [26] and Wu *et al.* [25] as 2.0×10^{-10} and $3.42 \pm 0.78 \times 10^{-9}$ m/s, respectively. In normal granulation tissues permeability of the same liposomes was $8.0 \sim 9.0 \times 10^{-10}$ m/s at the same temperature [25, 26].

Diffusion Coefficient (*D*)

Diffusion coefficient is the constant of proportionality between the molar flux owing to molecular diffusion and the gradient in the concentration of the species, which is also known as the driving force for diffusion.

(1) Free and bound doxorubicin

Diffusion coefficient is related to the molecular weight (*MW*) of the substance [15]. The relationship between diffusion coefficient in water and molecular weight can be represented by [15, 123]

$$D_w = a_{d1}(MW)^{-a_{d2}} \tag{3-45}$$

This equation is used to fit the diffusion coefficients of common anticancer agents in water [124] (Figure 3-4). Since doxorubicin has a *MW* of 544 Da, its diffusion coefficient in water at 37 $^{\circ}$C could be estimated as 3.83×10^{-10} m^2/s. It has also been found that diffusion coefficient in neoplastic tissue deviates from free diffusion in water [118]. For *MW*s in the range of 376 Da and

66,900 Da, the ratio of diffusion coefficient in tumour (D) to that in water (D_W) was found to be linearly related to MW

$$\frac{D}{D_w} = a_{d3}\, MW + a_{d4} \tag{3-46}$$

Using equation (3-46), the ratio for doxorubicin is 0.8885 and the diffusion coefficient of doxorubicin in tumour is 3.40×10^{-10} m^2/s (Figure 3-4 (b)).

At 37 ^{o}C, the relationship between diffusion coefficient (D) and MW in normal tissues may be obtained from *in vitro* experimental data [125].

$$D = 1.778\times10^{-8}\left(MW\right)^{-0.75} \;\; \left(32 < MW < 69000\right) \tag{3-47}$$

Based on equation (3-47), the diffusion coefficient of doxorubicin in normal tissues is calculated as 1.58×10^{-10} m^2/s.
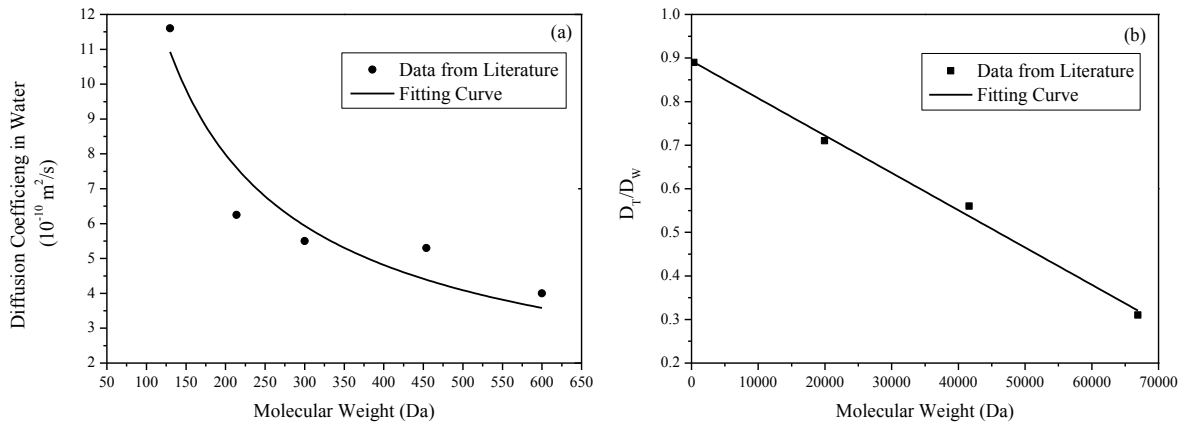
Figure 3-4. Estimation of doxorubicin diffusion coefficient in tumour tissue. (a) The diffusion coefficient of anticancer drugs in water as a function of molecular weight, using equation (3-45) [15, 123]. For the best fitted curve for experimental data in reference [124], a_{d1} = 380.44, a_{d2} = 0.73. (b) The relation between diffusion coefficient ratio (tumour to water) and molecular weight. For the best fitted line using equation (3-46) to fit experimental data from reference [118], a_{d3} = -8.55948 $\times10^{-6}$, a_{d4} = 0.89317.

Doxorubicin can bind with high molecular weight proteins (*e.g.* albumin [90]) in the interstitial fluid. In such a case, the diffusion coefficient of the bound component depends mainly on the protein (*e.g.* albumin). The effective diffusion coefficient for albumin in VX2 carcinoma was measured as 8.89×10^{-12} m^2/s [90]. Since the bound component has a MW of approximately 69

kDa [51], its diffusion coefficient in normal tissue estimated by Equation (3-47) is 4.17×10^{-12} m^2/s.

(2) Liposome encapsulated doxorubicin

For diffusion of spherical particles through liquid at low Reynolds number, the diffusion coefficient in water can be calculated by solving the Einstein-Stokes equation [15].

$$D_w = k_B T^* \Big/ 6\pi\mu r \tag{3-48}$$

where k_B is Boltzmann's constant, T^* is the absolute temperature, μ is viscosity and r is the radius of spherical particle. Assuming the liposomes are spherical with a uniform diameter of 100 nm, their diffusion coefficient at 37°C is $5.82 \times 10^{-12}\,m^2/s$.

Yuan found that for liposome particles of 90 nm in diameter, the ratio of permeability in tumour and diffusion coefficient in water was around 20 m^{-1} [110], and the permeability was $2.0 \pm 1.6 \times 10^{-10}$ m/s [26]. Based on these results, the diffusion coefficient is $1.0 \pm 0.8 \times 10^{-11}$ m^2/s. Based on the Einstein-Stokes equation, the diffusion coefficient is inversely related to the particle radius. Hence, the diffusion coefficient of liposomes with 100 nm diameter is estimated to be $9.0 \pm 7.2 \times 10^{-12}$ m^2/s. The diffusion coefficients in tumour and normal tissues adopted in this thesis are $9.0 \times 10^{-12}\,m^2/s$ and $5.8 \times 10^{-12}\,m^2/s$, respectively.

Reflection Coefficient (σ)

The reflection coefficient determines the efficiency of the oncotic pressure gradient in driving transport across the vascular wall. It is related to the sizes of drug and pores on the vasculature wall [126]. For the same drug, this parameter may vary in different types of tissues [127]. Wolf *et al*. [128] measured the reflection coefficient for albumin and found this to be 0.82 ± 0.08. The sizes of albumin and liposome are 3.5 nm and 100 nm, respectively. The reflection coefficient for liposome is estimated to be greater than 0.90, hence it is assumed to be 0.95 in this study.

Drug Dose (D_d)

As a common anticancer drug, doxorubicin is widely used in chemotherapy to treat various types of cancer, such as lymphoma, genitourinary, thyroid, and stomach cancer [3]. By interacting with

DNA in cells, doxorubicin can inhibit the process of DNA replication. Because of this mechanism of action, high concentration of doxorubicin in normal tissues can cause serious damage to healthy cells, known as side effects. In clinical therapy, the most serious toxicity is life-threatening cardiomyopathy [129, 130], leading to heart failure. Side effects set a limit to the lifetime dose a patient can receive, which is approximately 550 mg per unit body surface area [3]. The dose of doxorubicin in clinical use is related to the patient's body surface area. In each treatment cycle, the dose is between 50 to 75 mg/m^2 [3].

Plasma Pharmacokinetics (C_v)

Doxorubicin concentration in blood plasma is modelled as an exponential decaying function of time. The form of equations depends on the infusion mode.

For continuous infusion, a tri-exponential decay is assumed based on the plasma pharmacokinetics of doxorubicin [55, 90].

$$\begin{cases} C_v = \dfrac{D_d}{T_d}\left[\left(\dfrac{A_1}{\alpha_1}\left(1-e^{-\alpha_1 t}\right)+\dfrac{A_2}{\alpha_2}\left(1-e^{-\alpha_2 t}\right)+\dfrac{A_3}{\alpha_3}\left(1-e^{-\alpha_3 t}\right)\right)\right] & (t < T) \\ C_v = \dfrac{D_d}{T_d}\left[\dfrac{A_1}{\alpha_1}\left(e^{\alpha_1 T}-1\right)e^{-\alpha_1 t}+\dfrac{A_2}{\alpha_2}\left(e^{\alpha_2 T}-1\right)e^{-\alpha_2 t}+\dfrac{A_3}{\alpha_3}\left(e^{\alpha_2 t}-1\right)e^{-\alpha_2 t}\right] & (t \geq T) \end{cases}$$

(3-49)

where t refers to time, D_d is the dose of doxorubicin and T_d is the infusion duration. A_1, A_2 and A_3 are compartment parameters and α_1, α_2, α_3 are compartment clearance rate.

For bolus injection, the terms involving α_2, α_3, A_2 and A_3 represent the compartments with much slower elimination. The drug concentration is assumed to follow an exponential decay based on the plasma pharmacokinetics of doxorubicin [55, 90].

$$C_v = D_d A_1 e^{-\alpha_1 t}$$

(3-50)

Free doxorubicin in plasma can easily bind with proteins, such as albumin. Greene *et al.* [86] found that approximately 75±2.7 % doxorubicin is present in the bound form, and the percentage binding is independent of doxorubicin and albumin concentrations. Hence for direct infusion, the free (C_{fp}) and bound (C_{bp}) doxorubicin concentrations in plasma are given by:

$$C_{fp} = sC_v$$
$$C_{bp} = (1-s)C_v$$

(3-51)

where s is the percentage of bound doxorubicin, which is 25% in this study.

3.3. Implementations of Mathematical Models

Usually the location where anticancer agents are administrated into a patient's body is remote from the tumour, hence the influence of drug infusion on blood pressure in the tumour is ignored. In addition, drug transport processes are assumed to have no influence on the interstitial fluid pressure because of the small size of anticancer agents. In order to generate initial conditions for the time-dependent numerical simulation, the interstitial fluid flow equations are firstly solved to obtain a steady-state solution in the entire computational domain. Following this, the obtained pressure and velocity values are applied at time zero for the simulation of drug transport and cellular uptake in order to predict the treatment efficacy. The mathematical equations described above are implemented into ANSYS Fluent, which is described in the following section.

3.3.1. ANSYS Fluent

ANSYS FLUENT is a widely used CFD code based on the finite volume method (FVM). The physical domain is firstly divided into a large number of computational cells forming a computational grid on which control volumes are defined where the variable of interest is located in the centroid. Governing equations in the differential forms are then integrated over each of the control volumes until the residual between two adjunct iterations is less than a given tolerance. The conservation principle for the variables in each control volume is expressed by the resulting discretised equation.

The employed solution algorithm is the SIMPLEC which uses a relationship between velocity and pressure corrections to enforce mass conservation and to obtain the pressure field. The momentum, mass and heat transfer equations are discretised using the second order UPWIND scheme, in which quantities at cell faces are computed using a multi-dimensional linear reconstruction approach [131]. In this approach, higher-order accuracy is achieved at cell faces through a Taylor series expansion of the cell-centred solution about the cell centroid. For

transient problems, a fully implicit second order backward Euler scheme is adopted, which is unconditionally stable with respect to time step size. The Gauss-Seidel method is adopted to update values at nodal points by using the previously computed results as soon as they become available.

3.3.2. User Defined Routines for Drug Transport

Mass transfer equations describing the transport of drugs are coded in C programming language by using the User Defined Scalar (known as UDS), which is a function for user defined programme be dynamically loaded with FLUENT.

These equations are solved based on the interstitial fluid field resolved by solving the continuity and momentum equations. Drug transport equations are also discretised using the second order UPWIND scheme, and the tolerance controlling the convergence is set to be 1×10^{-8}.

3.3.3. User Defined Routines for Heat Transfer

Heat transfer under HIFU heating in blood and tissue is also incorporated via UDS. These equations are solved with the drug transport equations when simulating thermo-sensitive liposome-mediated drug delivery. The second order UPWIND scheme is adopted for spatial discretisation and the convergence tolerance is set as 1×10^{-10}.

3.3.4. Boundary Conditions

In order to solve the above equations numerically and to ensure physiological relevance of the solutions, each of the dependent variable equations requires meaningful values at the boundary of the computational domain. These values are known as boundary conditions. Typical boundaries involved in the problems dealt with in this thesis include: interface between tumour regions, tumour-normal tissue interface and external surface of normal tissue. The specification of boundary conditions is problem-dependent, hence details will be given for each problem described in individual chapters.

3.4. Summary

The numerical methods and tools described above were applied to a realistic prostate tumour with a focus on understanding the transport steps of non-encapsulated drugs (Chapter 4), a liver

tumour with a focus on elucidating the effect of heterogeneous distribution of blood vessels and 3 prostate tumours with a focus on examining the effect of tumour size and microvascular density (Chapter 5), and a realistic prostate tumour with a focus on investigating the thermo-sensitive liposome-mediated drug delivery with hyperthermia induced by high intensity focused ultrasound (Chapter 6). All computations were carried out on an HP Compaq 8100 Elite CMT PC.

Table 3-1. Parameters for tumour and normal tissues.

Parameter	Definition	Unit	Tumour Tissue	Normal Tissue	Reference
S/V	Surface area of blood vessels per unit tissue volume	m^{-1}	20000	7000	[49-51, 88]
K_v	Hydraulic conductivity of the micro-vascular wall	m/Pa·s	2.10×10^{-11}	2.70×10^{-12}	[49-51, 88]
ρ	Density of interstitial fluid	kg/m^3	1000	1000	[51]
μ	Dynamic viscosity of interstitial fluid	kg/m·s	0.00078	0.00078	[51]
$1/\kappa$	Permeability of the interstitial space	m^{-2}	4.56×10^{16}	2.21×10^{17}	[49-51, 88]
p_v	Vascular fluid pressure	Pa	2080	2080	[49-51, 88]
π_v	Osmotic pressure of the plasma	Pa	2666	2666	[49-51, 88]
π_i	Osmotic pressure of interstitial fluid	Pa	2000	1333	[49-51, 88]
σ_T	Average osmotic reflection coefficient for plasma proteins		0.82	0.91	[49-51, 88]
$K_{ly}S_{ly}/V$	Hydraulic conductivity of the lymphatic wall times surface area of lymphatic vessels per unit volume of tumour tissue	$(Pa \cdot s)^{-1}$	0	4.17×10^{-7}	[51]
p_{ly}	Intra-lymphatic pressure	Pa	0	0	[51]
D_c	Cell density	$10^5 cell/m^3$	1×10^{10}	-	[90]
V_T	Total tumour volume	m^3	5×10^{-5}	3×10^{-4}	[55]
V_B	Total blood volume in body	m^3	5×10^{-2}	5×10^{-2}	[55]

Table 3-2. Parameters for liposome

Parameter	Definition	Unit	in Tumour	in Normal Tissue	Reference
P_l	Liposome permeability of vasculature wall	m/s	3.42×10^{-9}	8.50×10^{-10}	[25, 26]
D	Liposome diffusion coefficient	m^2/s	9.0×10^{-12}	5.8×10^{-12}	[25, 110]
σ_l	Reflection coefficient for liposome		0.95	1.0	-
CL_{lp}	Plasma clearance in tumour	s^{-1}	2.228×10^{-4}	2.228×10^{-4}	[62]

Table 3-3. Parameters for doxorubicin.

Parameter	Definition	Unit	Free Doxorubicin	Bound Doxorubicin	Reference
P_{tumour}	Permeability of vasculature wall in tumour	m/s	3.00×10^{-6}	7.80×10^{-9}	[51, 119]
P_{normal}	Permeability of vasculature wall in normal tissue	m/s	3.75×10^{-7}	2.50×10^{-9}	[51, 119]
D_{tumour}	Diffusion coefficient in interstitial fluid of tumour	m²/s	3.40×10^{-10}	8.89×10^{-12}	[15, 51, 118, 123-125]
D_{normal}	Diffusion coefficient in interstitial fluid of normal tissue	m²/s	1.58×10^{-10}	4.17×10^{-12}	[15, 51, 118, 123-125]
σ_d	Osmotic reflection coefficient		0.15	0.82	[51, 128]
k_a	Doxorubicin-protein binding rate	s⁻¹	0.833	-	[90]
k_d	Doxorubicin-protein dissociation rate	s⁻¹	-	0.278	[90]
φ	Tumour fraction extracellular space		0.4		[90]
V_{max}	Rate of trans-membrane transport	kg/10⁵cells s	4.67×10^{-15}	-	[90, 101]
k_e	Michaelis constant for transmembrane transport	kg/m³	2.19×10^{-4}	-	[90, 101]
k_i	Michaelis constant for transmembrane transport	kg/10⁵cells	1.37×10^{-12}	-	[90, 101]
f_{max}	Cell-kill rate constant	s⁻¹	1.67×10^{-5}	-	[109]
EC_{50}	Drug concentration producing 50% of f_{max}	kg/10⁵cells	5×10^{-13}	-	[109]
A_1	parameter for pharmacokinetic model	m⁻³	74.6	74.6	[85, 90]
A_2	parameter for pharmacokinetic model	m⁻³	2.49	2.49	[85, 90]
A_3	parameter for pharmacokinetic model	m⁻³	0.552	0.552	[85, 90]
α_1	compartment clearance rate	s⁻¹	2.43×10^{-3}	2.43×10^{-3}	[85, 90]
α_2	compartment clearance rate	s⁻¹	2.83×10^{-4}	2.83×10^{-4}	[85, 90]
α_3	compartment clearance rate model	s⁻¹	1.18×10^{-5}	1.18×10^{-5}	[85, 90]
k_p	Cell proliferation rate	s⁻¹	3.0×10^{-6}	-	[102]
k_g	Cell physiologic degradation rate	s⁻¹	3.0×10^{-16}	-	[102]
CL_{tumour}	Plasma clearance in tumour	s⁻¹	2.43×10^{-3}	0	[85, 114, 132, 133]
CL_{normal}	Plasma clearance in normal tissue	s⁻¹	2.43×10^{-3}	0	[85, 114, 132, 133]

4. Non-Encapsulated Drug Delivery to Solid Tumour

Intravenous administration of drugs in their free form is a traditional drug delivery method adopted in clinical treatments without specific targeting. Injected drugs undergo multiple transport processes in systemic blood stream, interstitial space and tumour cells. The role of drug transport in treatment efficacy is complicated because of nonlinear interactions between the drug and the microenvironment of tumour and surrounding normal tissues. An appropriate mathematical model is therefore needed to gain detailed understanding of the drug transport processes involved and how drug concentrations and its therapeutic effect may be influenced by infusion modes.

In this chapter, a coupled pharmacokinetics and drug transport model is applied to a real tumour geometry reconstructed from magnetic resonance image (MRI) to examine the effects of various administration modes and clinic dose levels. This is followed by comparisons of drug concentrations and survival fraction of tumour cells between 2-D and 3-D geometry models.

4.1. Model Description

The mathematic model described in Chapter 3 for free form drug administration is adopted, which incorporates the key physical and biochemical processes, including time-dependent plasma clearance, drug transport through the blood and lymphatic vessels, extracellular drug transport (convection and diffusion), drug binding with proteins, lymphatic drainage, interactions with the surrounding normal tissue and drug uptake by tumour cells. Anticancer efficacy is evaluated based on the percentage of survival tumour cells by directly solving the pharmacodynamics equation using the predicted intracellular drug concentration.

4.1.1. Model Geometry

The geometry of a prostate tumour is reconstructed from images acquired from a patient using a 3.0-Tesla MR scanner (DISCOVERY MR750, GE, Schenectady, New York, USA). Multislice anatomical images of the prostate were acquired in three orthogonal planes with echo-planer (EP) sequence, with each image comprising 256 by 256 pixels. Other imaging parameters are given in Table 4-1.

Table 4-1. MR imaging parameters

Parameter (unit)	Pixel Size (mm)	Field of View (cm)	Slice Thickness (mm)	Repetition Time (ms)	Echo Time (ms)
	1.250	32.0	7.000	4000	84.4

An example of the MR images is shown in Figure 4-1 (a) with the tumour region and its surrounding normal prostatic tissues. Transverse images are processed using image analysis software Mimics (Materialise HQ, Leuven, Belgium), and the tumour is segmented from its surrounding normal tissue based on signal intensity values. The resulting smoothed surfaces of the tumour and normal tissues are imported into ANSYS ICEM CFD to generate computational mesh for the entire volume.

The tumour shown in Figure 4-1 (b) is located at the corner of normal tissue with a dimension of 47 mm (maximum width) by 38 mm (maximum depth) in 2-D model. The final mesh consists of 64,966 triangular elements which have been tested to produce grid independent solutions.
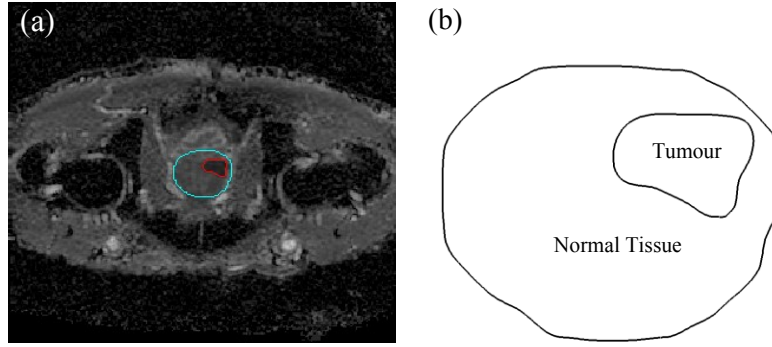
Figure 4-1. Model geometry: (a) MR image of the prostate tumour (in red) and its surrounding tissue (in pule blue); (b) the reconstructed 2-D geometry.

4.1.2. Model Parameters

The parameters describing general properties of doxorubicin, tumour and normal tissue have been given in Tables 3-1 and 3-3 in the preceding chapter. Infusion durations and doses simulated in this study are described below.

(1) Infusion Duration

Infusion duration is a key parameter in determining the pharmacokinetics of drug in blood. Previous experiments found that prolonged infusion, such as over 48 hours or 96 hours, did not contribution to better treatment efficacy [53, 54]. In a numerical study by [55], a 2-hour infusion was adopted without the consideration of cell proliferation and death as a dynamic process. Therefore, bolus injection and continuous infusion with infusion duration of 1-hour, 2-hour and 3-hour respectively, are studied.

(2) Infusion Dose

Limited by the serious side effect caused by doxorubicin, the lifetime dose a patient can receive is approximately 550 mg per unit body surface area. For each treatment cycle, the dose is between 50 to 75 mg/m^2 [3], depending on the body surface area of a patient.

Body surface area (BSA) is determined from the following formula [51]

$$BSA = \left(\frac{\text{Weight in kg}}{70 \text{ kg}} \right)^{0.73} \left(1.73 \text{ m}^2 \right) \qquad (4\text{-}1)$$

For a 70 kg patient, dosage of doxorubicin is in the range of 86.5~129.75 mg. Three dose levels, 50, 60 and 75 mg/m^2 are examined in this study.

(3) Pharmacokinetics

Doxorubicin concentration in blood plasma is usually described by an exponential function over time. Better fit to the experimental data was found by using a 3-compartment model.

For bolus injection and continuous infusion in a single administration, the plasma concentration of doxorubicin can be described by Equation (3-49) and (3-50), respectively. The plasma concentration in multiple administrations under bolus injection and continuous infusion are given below by Equation (4-2) and (4-3), respectively [134].

$$C_v = \sum_{i=1}^{n} D_d A_1 e^{-\alpha_1 \left(t^* - t_{D_i}\right)} \qquad (4\text{-}2)$$

$$C_v = \begin{cases} \sum_{i=1}^{n-1} \dfrac{D_{di}}{T_{di}} \begin{bmatrix} \dfrac{A_1}{\alpha_1}\left(1-e^{-\alpha_1 T_{di}}\right)e^{-\alpha_1\left(t^*-t_{D_i}-T_{di}\right)} \\[6pt] +\dfrac{A_2}{\alpha_2}\left(1-e^{-\alpha_2 T_{di}}\right)e^{-\alpha_2\left(t^*-t_{D_i}-T_{di}\right)} \\[6pt] +\dfrac{A_3}{\alpha_3}\left(1-e^{-\alpha_3 T_{di}}\right)e^{-\alpha_3\left(t^*-t_{D_i}-T_{di}\right)} \end{bmatrix} + \dfrac{D_{dn}}{T_{dn}}\begin{bmatrix} \dfrac{A_1}{\alpha_1}\left(1-e^{-\alpha_1\left(t^*-t_{D_n}\right)}\right) \\[6pt] +\dfrac{A_2}{\alpha_2}\left(1-e^{-\alpha_2\left(t^*-t_{D_n}\right)}\right) \\[6pt] +\dfrac{A_3}{\alpha_3}\left(1-e^{-\alpha_3\left(t^*-t_{D_n}\right)}\right) \end{bmatrix} & \left(t^*-t_{D_n} \le T_d\right) \\[30pt] \sum_{i=1}^{n} \dfrac{D_{di}}{T_{di}}\begin{bmatrix} \dfrac{A_1}{\alpha_1}\left(1-e^{-\alpha_1 T_i}\right)e^{-\alpha_1\left(t^*-t_{D_i}-T_{di}\right)} +\dfrac{A_2}{\alpha_2}\left(1-e^{-\alpha_2 T_{di}}\right)e^{-\alpha_2\left(t^*-t_{D_i}-T_{di}\right)} \\[6pt] +\dfrac{A_3}{\alpha_3}\left(1-e^{-\alpha_3 T_{di}}\right)e^{-\alpha_3\left(t^*-t_{D_i}-T_{di}\right)} \end{bmatrix} & \left(t^*-t_{D_n} > T_d\right) \end{cases} \qquad (4\text{-}3)$$

where D_d is the dose of doxorubicin and T_d is the infusion duration. A_1, A_2 and A_3 are compartment parameters and α_1, α_2, α_3 are compartment clearance rate. t^* is the time after n doses ($i = 1,2,\ldots,n$) given at time t_{Di}.

To account for the high binding rate for doxorubicin with proteins, such as albumin in blood plasma, and for the fact that the percentage of bound doxorubicin is independent of plasma concentration of doxorubicin and albumin, the free (C_{fp}) and bound (C_{bp}) doxorubicin in blood are governed by Equation (3-51), where s is the percentage of bound doxorubicin, which is 0.25 in this study [86].

4.1.3. Numerical Methods

The mathematical models described above are implemented in ANSYS-Fluent, which is a finite volume based computational fluid dynamics (CFD) code (ANSYS Inc., Canonsburg, USA). The momentum and drug transport equations are discretised using the second order UPWIND scheme, and the SIMPLEC algorithm is employed for pressure-velocity coupling. The Gauss-Seidel smoothing method is used to update values at nodal points after each iteration step. Convergence is controlled by setting residual tolerances of the momentum equation and the drug transport equations to be 1×10^{-5} and 1×10^{-8}, respectively.

In order to generate initial conditions for the transient simulation, the interstitial fluid flow equations are firstly solved to obtain a steady-state solution in the entire computational domain. Following this, the obtained pressure and velocity values are applied at time zero for the simulation of drug transport and cellular uptake (shown in Figure 4-2). The second order implicit backward Euler scheme is used for temporal discretisation, and a fixed time step size of 10 seconds is chosen. This time step is deemed sufficiently fine based on a time step sensitivity test. The initial doxorubicin concentrations are assumed to be zero in both tumour and the surrounding normal tissue.
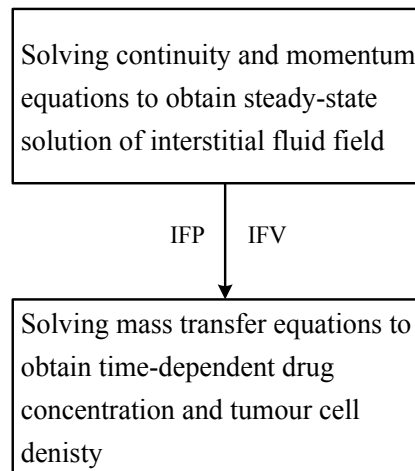
Figure 4-2. Numerical Procedures.

There are two boundary surfaces in this model: an internal boundary between the tumour tissue and normal tissue, and the outer surface of the normal tissue. At the internal boundary,

conditions of continuity of the interstitial pressure and fluid flux are applied. At the outer surface, a constant relative pressure of 0 Pa and zero flux of drug are assumed.

4.2. Results

The analysis of results obtained from the mathematical model is carried out. The interstitial fluid field is firstly examined to provide the microenvironment for drug transport and cell killing. This is followed by comparisons of administration modes and doses under single and multiple administration treatments in a clinical range. Finally, computational results obtained from the 2-D and 3-D models are compared.

4.2.1. Interstitial Fluid Field

The interstitial fluid field in tumour and normal tissues plays an important role in drug delivery. This is because on the one hand, the interstitial fluid velocity and pressure determines the drug migration in extracellular space by convention; on the other hand, transvascular pressure gradient influences the drug exchange between microvessels and the interstitial space of tumour. By solving Equations (3-1)~(3-8) described in Chapter 3 for a vascular pressure of 2080 Pa [49-51, 89], the spatial distribution of interstitial fluid pressure (IFP) is presented in Figure 4-3. There is a uniform IFP in the tumour and normal tissue. Higher IFP is found in the tumour compared with its surrounding normal tissue, and there is a large gradient in a thin layer at the interface between the two regions.
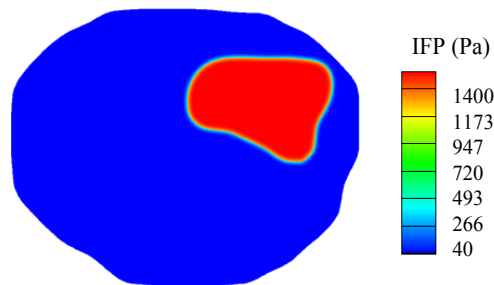
Figure 4- 3. Interstitial fluid pressure in tumour and surrounding normal tissue.

The spatial mean IFP is 1533.88 Pa in the tumour region and 40 Pa in normal tissue. These results agree with experimental studies which suggested that IFP in tumour was in the range of 586.67 Pa to 4200 Pa [48], and in normal tissue -400 Pa to 800 Pa [135]. This difference in IFP between tumour and normal tissue can be partially attributed to the special characteristics of

tumour vasculature. On the one hand, vasculature surface is enlarged because blood vessels are tortuous, elongated, and often dilated in tumour growth. The hydraulic conductivity is increased by 10-fold as a result of large pores on tumour vasculature wall [49]. This leads to a much easier fluid exchange across the blood vessel wall. On the other hand, the lack of lymphatic vessels results in less fluid being drained out of the interstitial space, causing build-up of pressure in tumour interstitial space. The IFP distribution shown in Figure 4-3 suggests that pressure-induced convection of interstitial fluid mainly occurs within a thin layer at the interface between tumour and its surrounding normal tissue.

In theory, high pressure in tumour poses a barrier for drug transport from blood to interstitial space. However, diffusion driven by concentration gradient and vasculature surface area also contributes to drug exchange between blood and interstitial space. Previous studies demonstrated that diffusion was a more important mechanism in determining drug transport across the vasculature wall because of the ineffective convection owing to the high IFP [51].

4.2.2. Single Administration Mode

In this series of simulations, the full dose of doxorubicin is administrated at the beginning of each treatment. The influences of two controllable factors, infusion duration and dose level, are examined over a period of 9 hours following drug administration.

4.2.2.1. Infusion Duration

The cytotoxic effect of doxorubicin on tumour cells is evaluated for bolus injection and continuous infusions with different infusion durations. Given that doxorubicin is carried by the blood stream into the tumour and normal tissue, its concentration in blood should be examined when evaluating its anticancer effectiveness. The time course of doxorubicin blood concentration, for a total dose of 50 mg/m^2 administered by different administration modes, is compared in Figure 4-4. Because all the drugs are administrated into blood stream in a very short period, which can be ignored in comparison with the treatment time window, drug concentration in blood under bolus injection reaches its peak at the very beginning of treatment. Without continuous supply, the concentration falls rapidly to a low level. Continuous infusion leads to different results. Since the total dose of drugs are administrated continuously in the infusion duration, drug concentration in blood increases gradually in this period. At the end of the

infusion duration, drug concentration begins to decrease. Therefore, the timing of peak drug concentration varies according to the infusion duration.
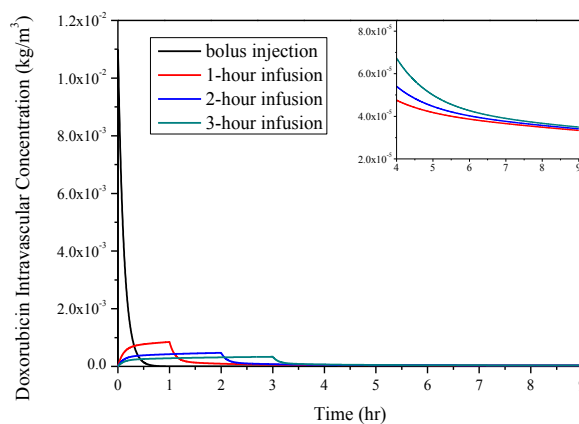
Figure 4-4. Doxorubicin concentration in plasma as a function of time after start of treatment, for bolus injection and continuous infusion of various indicated durations (dose = 50 mg/m^2).

Comparison of peak values in Figure 4-4 indicates that prolonging the infusion duration results in low peak doxorubicin blood concentration. This is because doxorubicin is being continuously cleared up after administration. Since high doxorubicin concentration in blood is associated with increased risk of cardiotoxicity, bolus injection may not be a preferred option while continuous infusion with longer duration may help reduce this risk. Comparison also shows that although fast infusion leads to higher concentrations at the beginning of the treatment, doxorubicin concentration in blood falls much faster after the infusion ends.

Free and bound doxorubicin extracellular concentrations in tumour and its surrounding normal tissue are shown in Figure 4-5 and 4-6, respectively. Regardless of the injection mode, both free and bound doxorubicin concentrations increase rapidly during the initial period following drug administration. Doxorubicin concentrations in tumour interstitial space increase faster and reach a much higher peak with bolus injection. The peak value for continuous infusion decreases with the increase in infusion duration. Although doxorubicin concentration drops to a low level after infusions end for all modes of administration, continuous infusions are able to maintain a slightly higher concentration than bolus injection. Comparing doxorubicin extracellular concentrations in Figures 4-5 and 4-6 with the concentration in blood in Figure 4-4, the concentration curves have identical shapes for a given administration mode. This means that drug concentration in blood has a direct influence on the extracellular concentration for both free and bound doxorubicin.

72
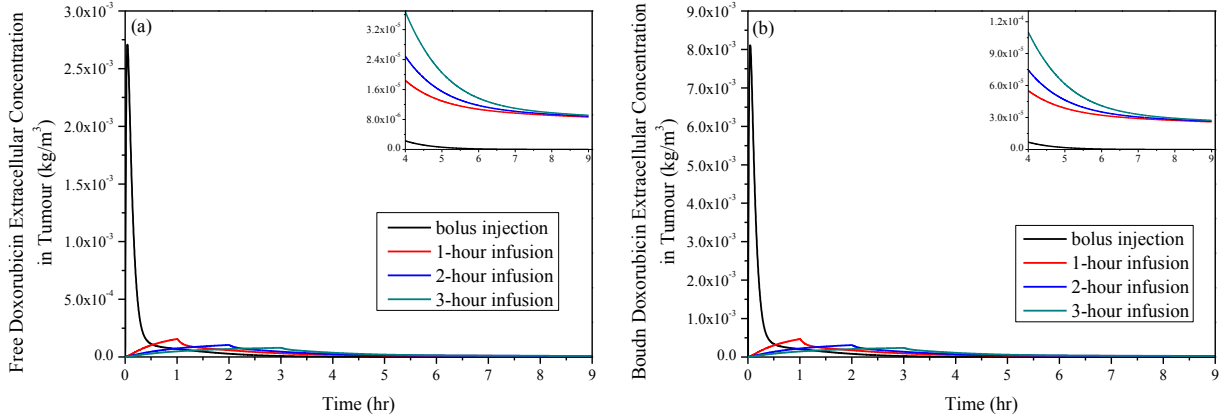
Figure 4-5. Spatial mean (a) free and (b) bound doxorubicin extracellular concentration in tumour as a function of time under bolus injection and different infusion durations (dose = 50 mg/m^2).

Because binding with protein is a dynamics process, both free and bound doxorubicin concentrations vary with time. Comparing Figure 4-5 (a) and (b), it is clear that the time course of free and bound concentrations shares a similar trend, but bound doxorubicin concentration is approximately 3 times of the free doxorubicin concentration, indicating that most doxorubicin in the interstitial fluid is in bound form. Since only free form doxorubicin can be taken up by tumour cells [55, 90], the high binding rate is expected to reduce the intracellular concentration of doxorubicin.
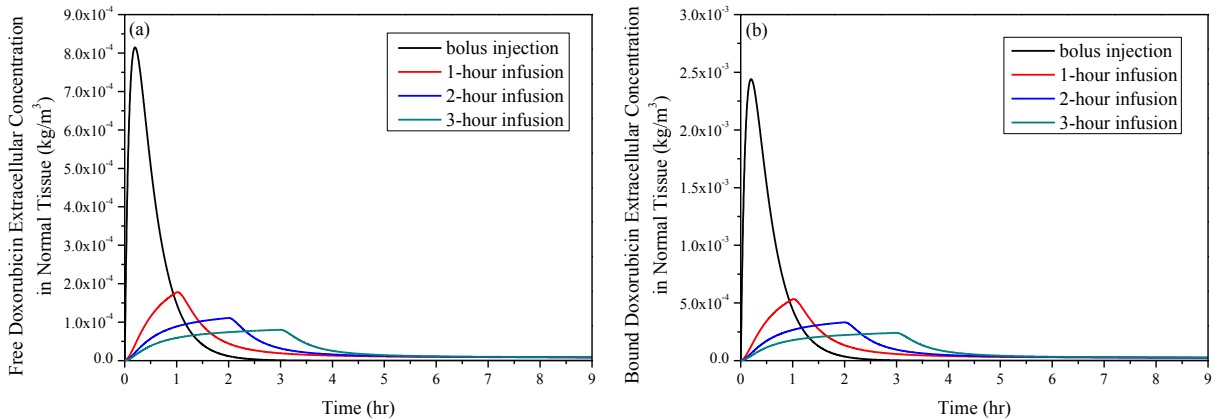
Figure 4-6. Spatial mean (a) free and (b) bound doxorubicin extracellular concentration in normal tissue as a function of time under bolus injection and different infusion durations. (dose = 50 mg/m^2).

Figure 4-7 shows the spatial distribution of free doxorubicin extracellular concentration in tumour and its surrounding normal tissue at 0.5 hour under 2-hour continuous infusion. There is a difference in drug concentration between tumour and surrounding normal tissue. Since the

properties of doxorubicin and tissues are assumed to be uniform in each region, the corresponding distribution is also uniform except near the tumour boundary where a large concentration gradient exists. This thin layer of steep concentration gradient represents the exchange of drug between tumour and normal tissue.
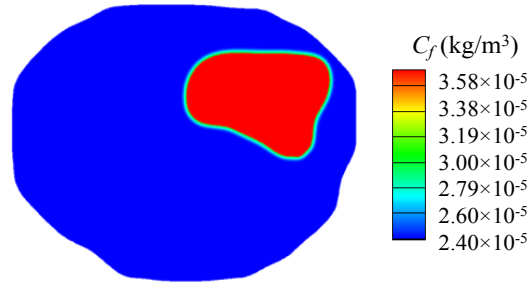
Figure 4-7. Spatial distribution of extracellular concentration of free doxorubicin in tumour and normal tissues (2-hour infusion, time = 0.5 hour).

As has already been shown in Figure 4-3, the interstitial fluid pressure in tumour is much higher than in normal tissue; this pressure difference drives interstitial fluid flow from the tumour to normal tissue, and doxorubicin is also carried by this flux. Moreover, doxorubicin diffuses from tumour where its concentration is high compared to the surrounding tissue because of the large concentration gradient in the interstitial space. The transport from tumour to normal tissue needs to be minimised in order to maintain a high level of doxorubicin concentration in tumour.
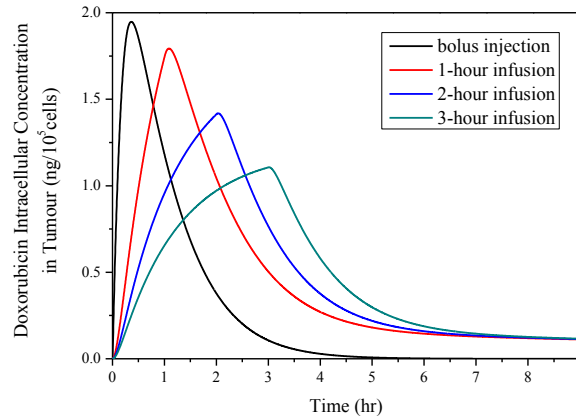
Figure 4-8. Doxorubicin intracellular concentration as a function of time, for bolus injection and continuous infusions of various durations (dose = 50 mg/m^2).

Figure 4-8 presents the intracellular doxorubicin concentration in tumour under bolus injection and continuous infusions with various infusion durations. The intracellular concentration

displays a sharp rise at the beginning until it reaches a peak, and then decreases. During the initial phase, the rate of increase in doxorubicin concentration slows down with increase of infusion duration. Compared to continuous infusions, bolus injection leads to a higher peak and a faster reduction in intracellular concentration which also remains at a much lower level after cessation of drug administration.

For continuous infusions, longer infusion durations tend to slow down the increase in intracellular concentration at the initial phase of treatment, and produce a lower peak. Here, the highest intracellular concentration is found for a 1-hour continuous infusion. Moreover, for continuous infusion with different durations, intracellular concentrations reach a very similar level after drug infusions terminate.
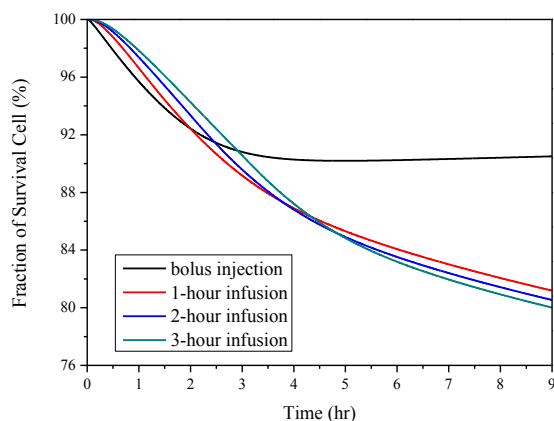
Figure 4-9. Predicated percentage tumour cell survival under bolus injection and continuous infusions of various durations (dose = 50 mg/m^2).

Figure 4-9 shows the percentage of survival tumour cells by applying the pharmacodynamics model described by Equation (3-30). As can be observed, the cytotoxic effect of bolus injection on tumour cells is significantly lower than that of continuous infusions. This is because of the rapid clearance of doxorubicin from blood (shown in Figure 4-4), resulting in a dramatic reduction in extracellular drug concentration which is reduced to approximately zero after 5~6 hours (shown in Figure 4-5). Without enough doxorubicin accumulating in tumour cells, the cell killing rate and physical degradation rate become slower than cell proliferation rate, and hence tumour cell density begins to increase after reaching the minimum value at around 5 hours after the cessation of drug administration. On the contrary, the extracellular drug concentration with continuous infusion stays at a low but non-zero level for a longer period to supply sufficient

75

doxorubicin for cell killing. This is the reason for the continuous reduction in survival fraction of tumour cells with continuous infusion in the simulation time window.

However, the effect of infusion duration seems to be insignificant for the limited range of infusion durations examined, with a difference of up to 2% between the slower (3 hours) and faster infusion (1 hour). The best therapeutic efficacy is not achieved with the infusion duration that leads to the highest intracellular concentration. Results show that 1-hour infusion leads to high cell killing rate at the beginning of treatment because of high intracellular concentration (shown in Figure 4-8). However, the killing rate slows down due to a rapid reduction in intracellular concentration. This low level of intracellular concentration sustains to the end of the simulation time window, and the therapeutic efficacy is the worst among the continuous infusion modes examined. On the contrary, although a 3-hour infusion results in a slower increase and lower peak, as shown in Figure 4-8, the intracellular concentration is at a higher level after peak time and the cytotoxic effect is better than others. This indicates that the final treatment outcome is more dependent on the intracellular concentration over the entire exposure time rather than its peak value.

4.2.2.2. Effect of Dose Level

Another controllable parameter in chemotherapy is the dose level of anticancer drugs. In current clinical use, doxorubicin dose ranges from 50 mg/m^2 to 75 mg/m^2 for a 70kg patient, hence the effect of dose on drug effectiveness is examined within this range.

Comparison is made between different doses (50, 60 and 75 mg/m^2) under a 2-hour continuous infusion, simulating treatment doses used for a 70 kg patient. Blood concentration of free doxorubicin presented in Figure 4-10 (a) shows that increasing the dose results in linear elevation of drug concentration. Since following the same pharmacokinetics, blood concentration of bound doxorubicin is believed to share the same feature. As shown in Figure 4-10 (b) and (c), extracellular concentration of doxorubicin in both free and bound forms are increased because of the close relationship between concentration in blood and in interstitial space. As a consequence, more drugs accumulate in tumour cells under a high dose administration.

Results shown in Figure 4-10 (d) show that intracellular drug concentration is not proportional to the administrated dose level. In summary, doxorubicin concentrations in all regions increase with

the dose level, since a high dose increases the amount of drug delivered to both the tumour and normal tissues. In addition, the high concentration in blood may also increase the risk of heart failure.
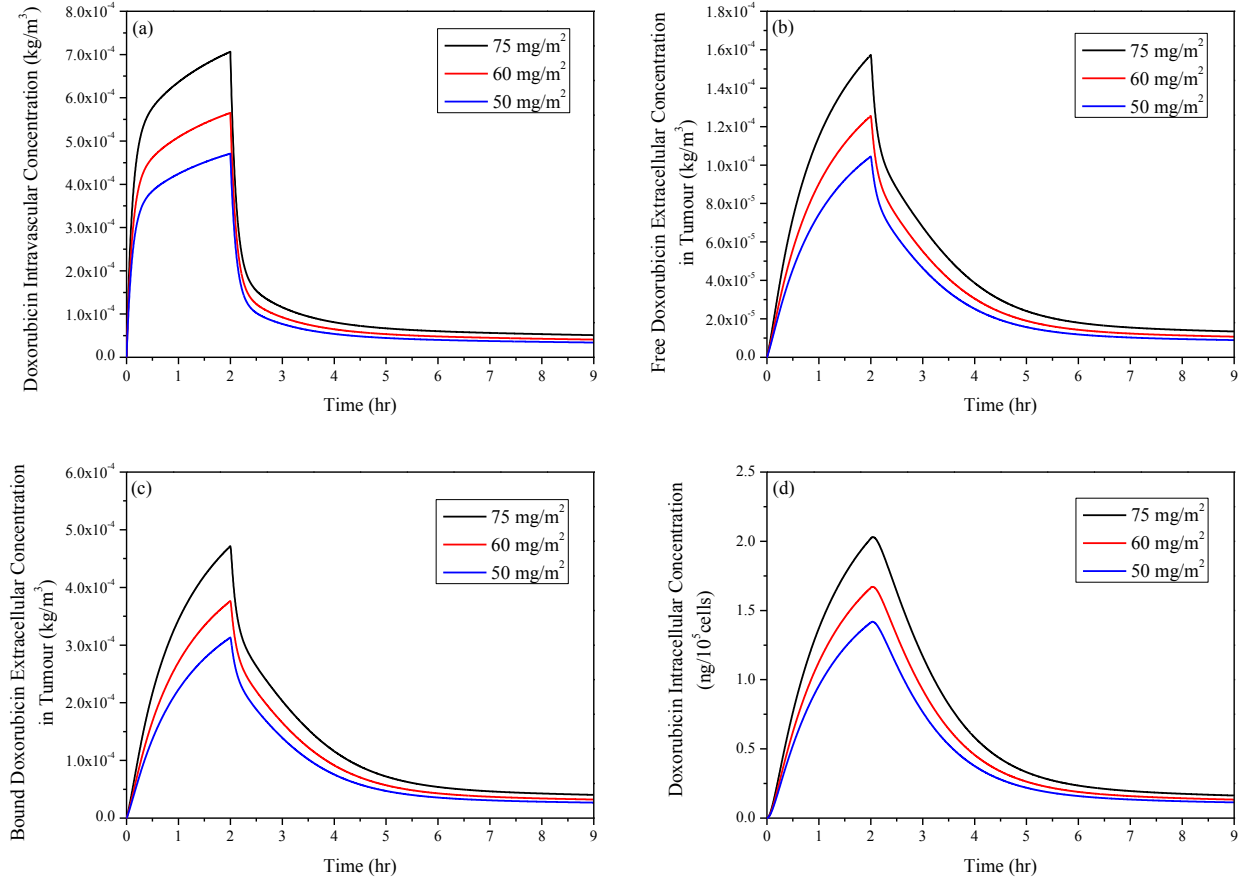
Figure 4-10. Spatial mean doxorubicin concentration in tumour as a function of time under 2-hour infusion duration.(a) doxorubicin blood concentration, (b) free doxorubicin extracellular concentration, (c) bound doxorubicin extracellular concentration, and (d) intracellular concentration.

The percentage of survival tumour cells is compared in Figure 4-11 by solving the pharmacodynamics equation based on the predicted intracellular concentration. The results show that the cytotoxic effect of doxorubicin on tumour cells increases with the dose level, with the difference between low (50 mg/m^2) and high doses (75 mg/m^2) being 2.5% at 9-hour following drug administration. Compared to the administrated dose level, this improvement in treatment outcome is not obvious.
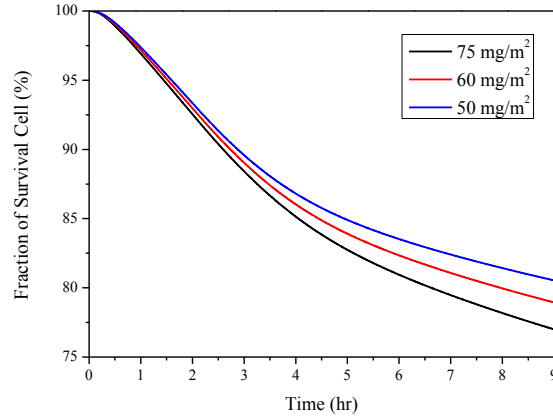
Figure 4-11. Predicated percentage of tumour cell survival under various doses.

The predicated free and bound doxorubicin concentration in the interstitial space of normal tissue with different drug dosages is compared in Figure 4-12. Results show that increasing the dose results in elevation of extracellular concentration of doxorubicin in both free and bound forms. This indicates that the risk of cell killing in normal tissue may also be increased at higher dose.
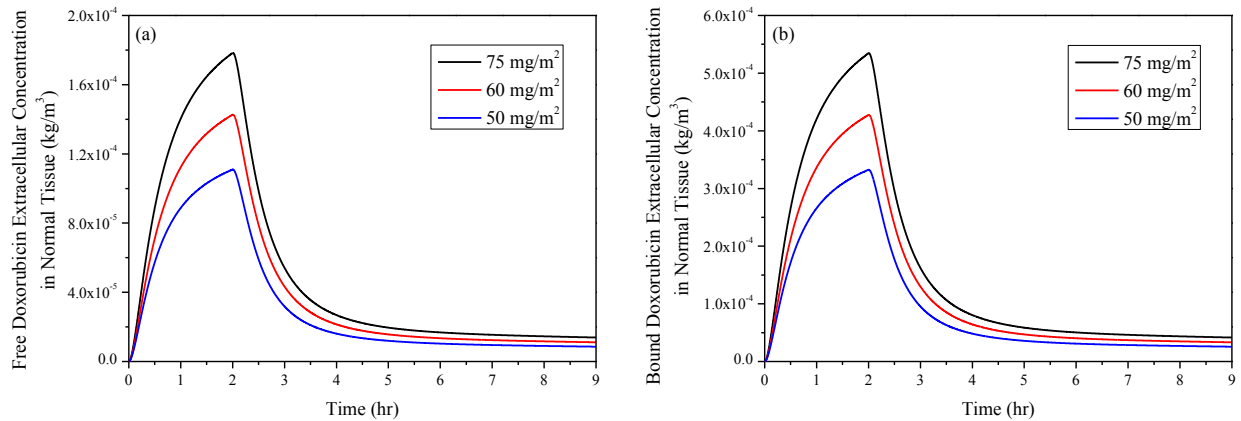
Figure 4-12. Spatial mean doxorubicin concentration in normal tissue as a function of time under 2-hour infusion duration (for a 70 kg patient). (a) free doxorubicin extracellular concentration, (b) bound doxorubicin extracellular concentration.

4.2.3. Multiple Administration Mode

Numerical studies are carried out under continuous infusion and bolus injection with multiple administrations for 2, 4 and 8 times within the first 48 hours of treatments with intervals of 24, 12 and 6 hours, respectively. The infusion duration is set as 2-hour for each of continuous infusion, and the simulation is performed for 96 hours.

4.2.3.1. Continuous Infusion

Figure 4-13 shows the predicted time course of plasma doxorubicin concentration, for a total dose of 50 mg/m^2 administrated by single and multiple 2-hour continuous infusions. Regardless of the administration mode, the drug concentration in blood reaches a peak after the end of each administration. Results show that multiple-infusion can significantly reduce the peak plasma concentration, and this reduction effect increases with the number of infusion. Administrating the same dose of doxorubicin 8-times gives a 20% lower peak concentration compared with a single administration. Hence multiple-infusion is likely to reduce the risk of heart electrophysiology dysfunction and muscle damage caused by doxorubicin. However, quantitative comparison of blood concentration after administration shows that multiple-infusion can also lead to a slightly high level of drug concentration in plasma over time.
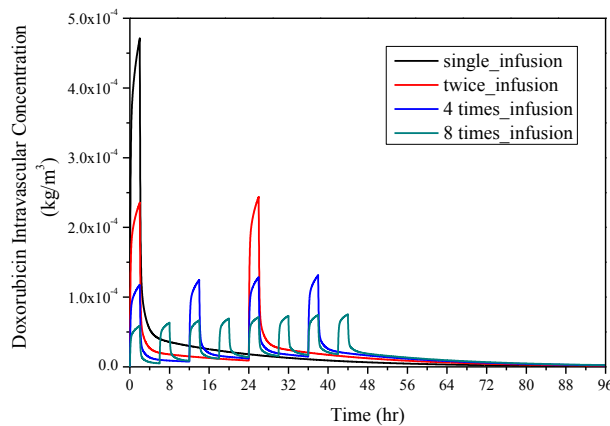
Figure 4-13. Doxorubicin intravascular concentration under single and multiple continuous infusions as a function of time (total dose = 50 mg/m^2).

Figure 4-14 shows the time course of free and bound doxorubicin concentration in the interstitial fluid for different infusion modes. During each infusion period, all forms of doxorubicin begin to accumulate in the interstitial space since doxorubicin is continuously administrated into the circulation system. Drug concentration reaches a peak value at the end of each infusion, and then falls to a lower level as time proceeds. Results show that free and bound doxorubicin concentrations share the same trend for a specific administration mode. Multiple-infusion can effectively reduce the peak extracellular concentration and lead to a slightly higher concentration level over time.
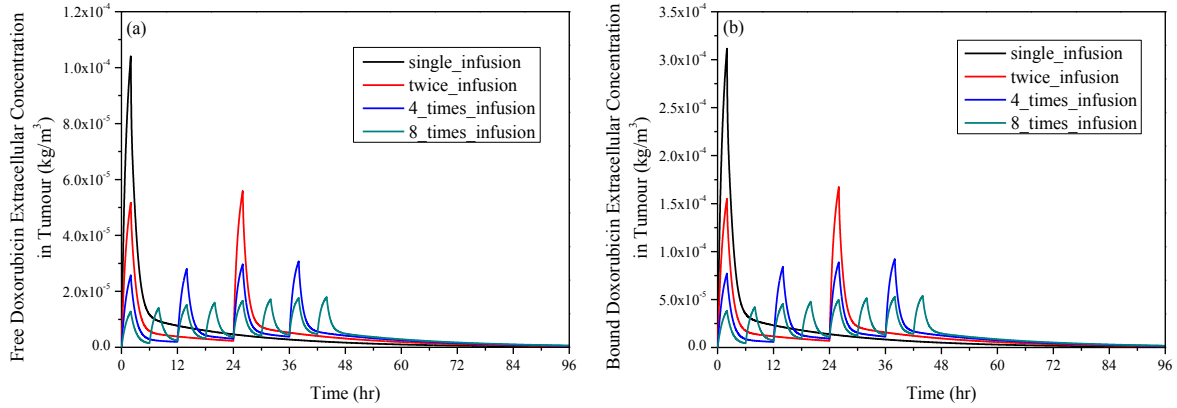
Figure 4-14. Spatial mean doxorubicin extracellular concentration as a function of time under single and multiple continuous infusion. (a) free doxorubicin, and (b) bound doxorubicin (total dose = 50 mg/m^2).

Intracellular doxorubicin concentrations in tumour with signal and multiple-infusion modes are compared in Figure 4-15. It is clear that single infusion gives the highest peak intracellular concentration, while multiple-continuous-infusions have lower but multiple peaks which help to keep a sustained level of intracellular concentration over the entire treatment period.
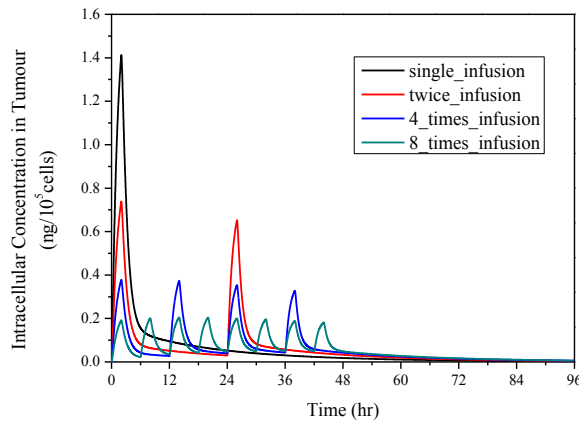
Figure 4-15. Time course of doxorubicin intracellular concentration under single and multiple continuous infusions. (total dose = 50 mg/m^2)

Figure 4-16 shows the survival fraction of tumour cells under various administration modes by applying the pharmacodynamics model described in Equation (3-30). As can be observed, single infusion is more effective at cell killing in the first 34 hours but less effective than multiple-infusions afterwards. Comparing different fractionations under the multiple-infusion mode, cell killing rate is more steady and the fraction of survival tumour cells reaches a lower level as the

number of infusions increases. Results show that the 8-times continuous infusion can improve the anticancer effectiveness by 7% when compared with a single infusion.
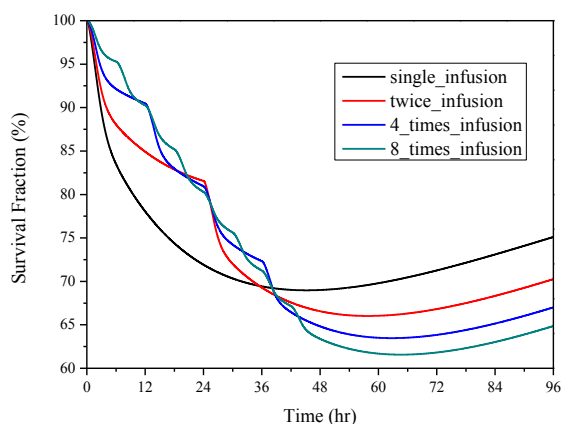
Figure 4-16. Time course of tumour survival fraction under single and multiple continuous infusions.
(dose = 50 mg/m^2)

Tumour cell density is determined by the rate of cell killing, cell proliferation and degradation rates, hence the survival fraction may increase when intracellular concentration falls below a threshold value during administration intervals. By increasing administration times while keeping the total administration dose the same, multiple-infusion mode is effective at increasing doxorubicin concentrations between administration cycles (shown in Figure 4-13, 4-14 and 4-15). Therefore, the rate of cell death (including cell killing and degradation) is faster than that of cell proliferation, and as a consequence the fraction of survival tumour cells continuous to fall for a longer period under multiple-infusion treatments than under a single administration.

Taking results shown in Figures 4-13, 4-14 and 4-15 together, it becomes clear that keeping doxorubicin at a relatively higher level for a longer period leads to a better anticancer effectiveness. The treatment outcome is related but not solely determined by the peak extra- and intra-cellular concentrations. This is because the time-scales of drug transport processes from blood to the interior of tumour cells are different. Although some of these time scales are determined by the properties of anticancer drug and tissues, the rate-limiting step is crossing the cell membrane [55]. The slow cellular influx requires the concentration to sustain at a high level for a sufficient period of time in order to let more doxorubicin accumulate in the cells.

Time course profiles of free and bound doxorubicin concentration in the interstitial space of normal tissue are presented in Figure 4-17. Results indicate that multiple-continuous-infusion lead to lower peak doxorubicin concentration but a slightly higher concentration level after administration ends. Compared with doxorubicin intravascular concentration shown in Figure 4-13, the accumulation of doxorubicin in normal tissue is found to be strongly dependent on doxorubicin concentration in blood.
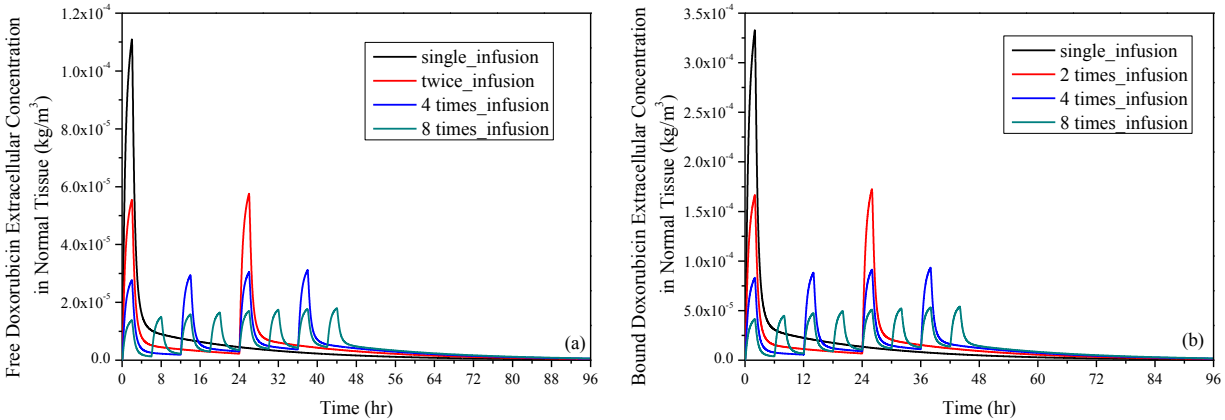
Figure 4-17. Spatial mean doxorubicin extracellular concentration in normal tissue as a function of time under single and multiple continuous infusion against time. (a) free doxorubicin, (b) bound doxorubicin (total dose = 50 mg/m^2).

Figure 4-18 compares the single infusion with a high dose and multiple-infusions with a low dose. In Figure 4-18 (a) and (c), intracellular concentration resulted by multiple-infusions with low dose is obviously low, and quantitative comparisons show that 8 times infusion with half dose can reduce the peak concentration by an order of magnitude

The survival fractions of tumour cells under different administration modes are shown in Figure 4-18 (b) and (d). Numerical results show that differences in the maximum cytotoxic effect between high drug dose single infusion and low drug dose 8 times infusion are 8% with a 50% dose and 3% with a 67% dose for multiple infusions. In addition, the recovery of tumour cells is slower with low dose 8 times infusion, as shown in Figure 4-18 (d). Consequently, multiple-continuous-infusion seems to offer improved treatment outcome overall.

82
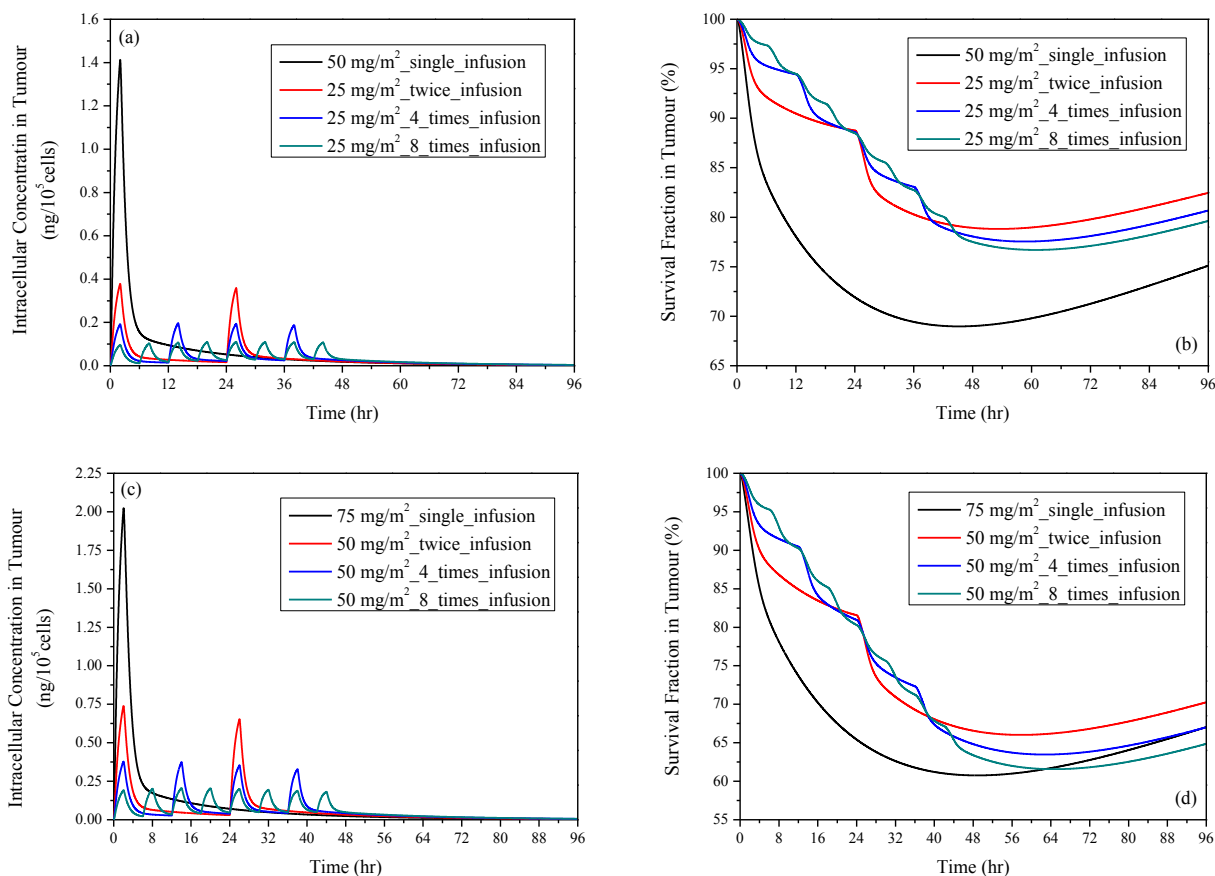
Figure 4-18. Comparison of various doses under single and multiple-infusions. (a) intracellular concentration and (b) cell survival fraction under single infusion with 50 mg/m^2 and multiple infusions with 25 mg/m^2 as a function of time ; (c) intracellular concentration and (d) cell survival fraction under single infusion with 75 mg/m^2 and multiple infusions with 50 mg/m^2 as a function of time.

4.2.3.2. Bolus Injection

The doxorubicin concentration in plasma under various bolus injection schedules are shown in Figure 4-19 (a). Since the injection duration is short enough to be ignored, peak blood concentration is reached at the beginning of each administration. Fast plasma clearance is the reason for the rapid fall of blood concentration after administration. Quantitative comparisons show that the peak intravascular concentration is inversely related to the number of injections. This means that multiple bolus injection can reduce the peak concentration in plasma, and hence may help reduce the risk of cardiotoxicity.

The free and bound doxorubicin concentration in the interstitial space is shown in Figure 4-19 (b) and (c). Because doxorubicin needs to permeate through the vasculature wall and then enter the

interstitial space, its extracellular concentration shares a similar pattern to the intravascular concentration shown in Figure 4-19 (a).
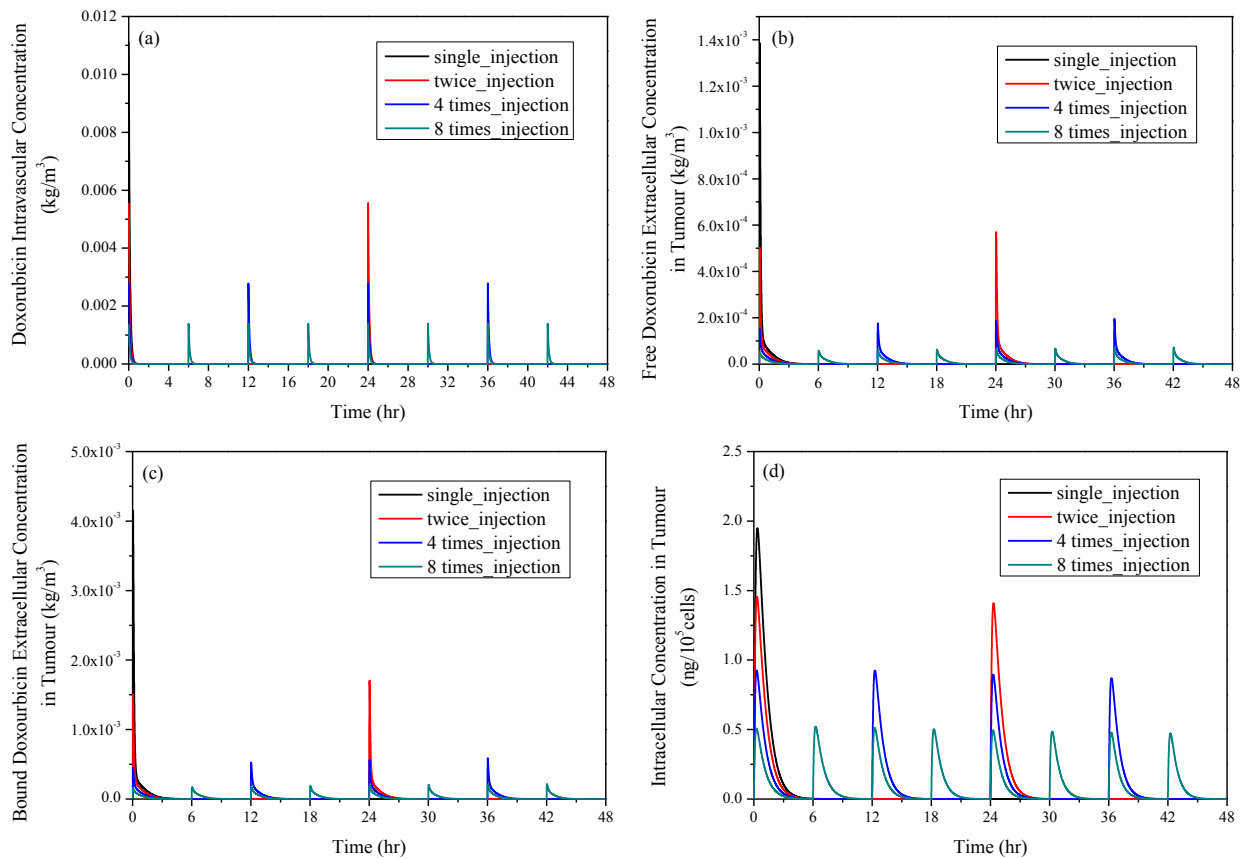
Figure 4-19. Comparison of doxorubicin concentration under single and multiple bolus injections as a function of time (total dose = 50 mg/m^2). (a) intravascular concentration, (b) free doxorubicin extracellular concentration, (c) bound doxorubicin extracellular concentration, and (d) intracellular concentration

The predicted time courses of doxorubicin intracellular concentration, for a total dose of 50 mg/m^2 administered by different bolus injection schedules, are compared in Figure 4-19 (d). Results show that single injection leads to the highest peak intracellular concentration, and the peak value decreases with the number of injections. Although sharing a similar trend to intravascular concentration, intracellular concentration takes longer to drop to its lowest level which is approximately zero. This is because the time-scale for crossing cell membrane is much longer than that of plasma clearance [55].

Figure 4-20 presents the survival fraction of tumour cell based on the predicted intracellular concentration over time. The cytotoxic effect of single bolus injection on tumour cells is

significantly lower than that of multiple injections, and the difference is up to 15% between the single and 8-times injections.
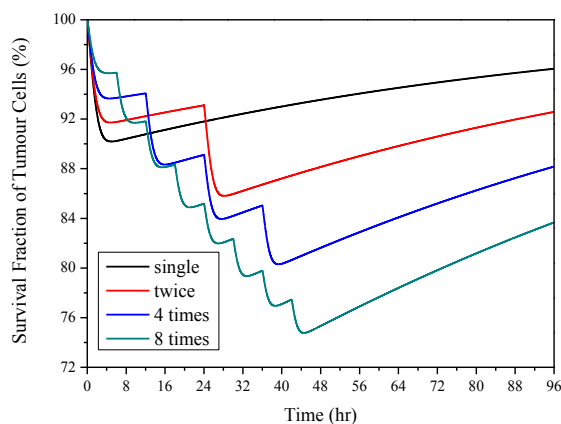
Figure 4-20. Tumour survival fraction as a function of time with single and multiple bolus injection
(total dose = 50 mg/m^2)

Free and bound doxorubicin concentration in normal tissue under different bolus injection schedules are compared in Figure 4-21. Results show that peak concentration of doxorubicin in normal tissue can be reduced by increasing the number of injections.
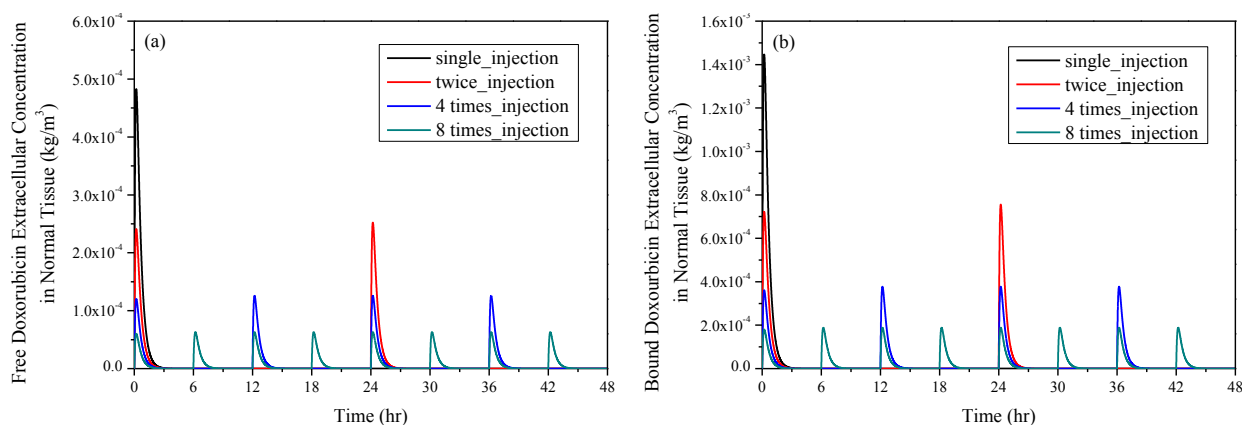
Figure 4-21. Comparison of doxorubicin concentration under single and multiple bolus injections as a function of time (total dose = 50 mg/m^2). (a) free and (b) bound doxorubicin concentration in normal tissue.

The treatment outcomes under 8-times bolus injection and a single 2-hour continuous infusion for the total dose of 50 mg/m^2 non-encapsulated doxorubicin are compared in Figure 4-22. Although multiple injections help to improve the anticancer effectiveness as already shown in

85

Figure 4-20, results obtained with 8-times bolus injection is still not as good as that with 2-hour continuous infusion for the same dose.
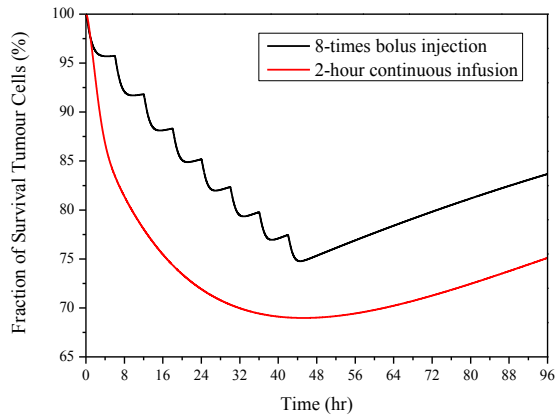
Figure 4-22. Comparison of survival fraction between single continuous infusion and 8 times bolus injection. (total dose = 50 mg/m^2)

4.2.4. Comparison of 2-D and 3-D Models

All the simulations presented so far are based on a 2-D model reconstructed from a selected MR image of a transverse section. However, a real tumour and its surrounding normal tissues are three-dimensional (3-D). Hence, it is necessary to evaluate the need for 3D simulation by quantitative comparison of results based on 2-D and 3-D models.
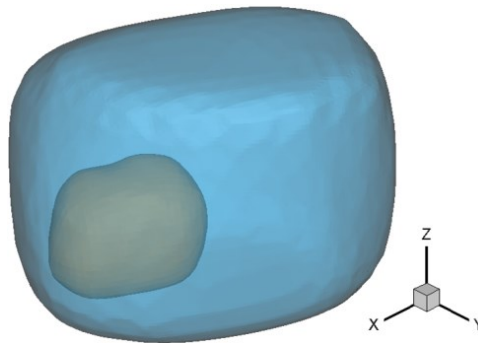
Figure 4-23. 3-D model geometry.

For this purpose, a 3-D model is reconstructed from the same series of MR images acquired from a patient with prostate tumour, and a representative MR image is already shown in Figure 4-1 (a). The reconstructed 3-D geometry is shown in Figure 4-23, where the tumour region is highlighted

in orange which is surrounded by normal prostatic tissues in pale blue. The dimension of the reconstructed 3-D model is approximately 40 mm in length, and the tumour and normal tissue volumes are 2.28×10^{-6} m^3 and 4.42×10^{-5} m^3, respectively. The final mesh consists of 757,453 tetrahedral elements which have been tested to produce grid independent solutions.

Numerical simulation has been carried out for a 2-hour continuous infusion of 50 mg/m^2 doxorubicin. Comparisons of drug concentration and drug cytotoxic effect are summarized in Figure 4-24. The time courses of free doxorubicin extracellular concentration based on the 2-D and 3-D models are compared in Figure 4-24 (a). No difference can be observed between the two models. Quantitative differences in drug concentrations and tumour cell density are summarized in Figure 4-24 (b), which shows that differences between the 2-D and 3-D models are less than 0.25%, justifying the use of 2-D models in this study. These results agree with the work of other researchers [79]. However, it is important to point out that the high level of consistence between the 2-D and 3-D models is mainly due to the fact that both drug and tissue properties are assumed to be uniform in each region. The effect of heterogeneous distribution of microvasculature in tumour will be addressed in Chapter 5.
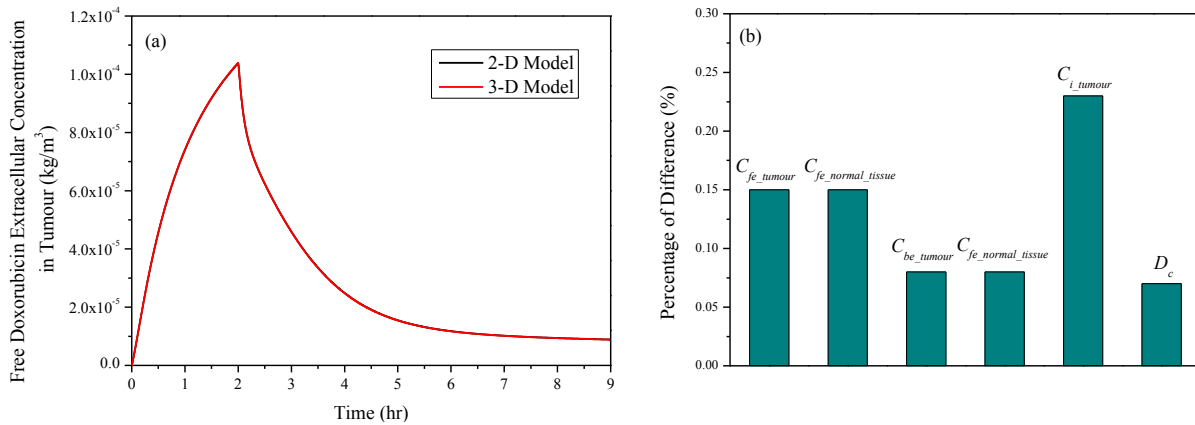
Figure 4-24. Comparison of drug concentration and cell density between 2-D and 3-D models. (a) free doxorubicin extracellular concentration in tumour as a function of time, (b) maximum percentage differences in drug concentration and tumour cell density (total dose = 50 mg/m^2)

4.3. Discussion

After intravenous infusion, anticancer drugs need to experience the following steps before reaching the interior of tumour cells: clearance from plasma, passing through the

microvasculature wall, diffusion and convection in extracellular space and crossing tumour cell membrane. The time scale for each of these transport steps is different owing to the different properties of microvasculature, interstitial fluid and the kinetics of cellular uptake. Data in the literature suggest that there is a delay between intracellular and extracellular drug concentration levels [55]. This is the reason why extracellular concentration needs to be maintained at a high level for long enough to enable cellular uptake. Simulation results in this study show that peak intracellular doxorubicin concentration is achieved 0.8~19 minutes later than the corresponding peak extracellular concentration. Comparisons between single and multiple administration methods as well as dose levels suggest that a more effective administration is more successful in maintaining high levels of extracellular doxorubicin over longer time (shown in Figure 4-5, and 4-10 (b,c)), and thereby raising intracellular levels (shown in Figure 4-8, and 4-10 (d)) and enhancing cellular uptake.

Anticancer effectiveness is usually evaluated by cell survival fraction, which can be predicted by different mathematical models. As an improvement of the AUC model [104], the peak intracellular concentration model [55, 90] was found to have better agreement to experimental data. However, this model predicts the best cell kill fraction for the entire treatment only, without giving detailed information on the dynamic variation of tumour cell density over time. Knowledge of temporal variation of cell survival is important since both extra- and intra-cellular drug concentrations change with time during a treatment period. The pharmacodynamics model employed in this study overcomes this shortcoming by providing temporal profiles of cell survival fraction. In addition, the model allows cell proliferation and degradation to be included, making it a step closer to mimicking an *in vivo* environment. With the consideration of cell proliferation and degradation in the present study, results shown in Figures 4-8, 4-10, 4-14, 4-15 and 4-16 demonstrate that sustained levels of extracellular concentration lead to higher intracellular concentration over time, which can cause more effective tumour cell killing.

Comparisons of drug concentration and survival fraction of tumour cells between 2-D and 3-D models show that the difference between the two models is negligible. However, this verdict is based on a number of assumptions. Firstly, the properties of tumour and normal tissues are assumed to be constant. These may vary with the tissue type, growth stage and individual conditions of a patient. Secondly, transport properties and vascular distribution are assumed to be

uniform, which is not true in a real tumour. All these properties will affect the way anticancer drugs are transported to tumour cells, and eventually the effectiveness of anticancer treatment. The model parameters adopted in this study correspond to average and representative values for tumour and normal tissues extracted from the literature, which may be sufficient for qualitative study, but more information would be required for detailed quantitative analysis.

4.4. Summary

In this chapter, various administration modes, schedules and dose levels are compared based on a 2-D prostate tumour model with a realistic geometry. The results show that better anticancer effectiveness is achieved with administration methods that are able to maintain a high level of extracellular concentration over the entire treatment period.

Results on single administrations show that bolus injection is much less effective in tumour cell killing than continuous infusion, the latter being not only effective in improving the cytotoxic effect of doxorubicin on tumour cells, but also in reducing peak level of doxorubicin in blood stream. Modelling results also show that rapid continuous infusion leads to faster cell killing at the beginning of the treatment, but slow infusion modes perform better over time.

Increasing drug doses can increase concentration levels in all regions of tumour, and improve the effectiveness of anticancer treatments. Whilst consideration must be given to potential side effects, which limit the dose used in clinical treatment, the highest tolerable dose gives the best result.

Multiple-administration can improve the efficacy of anticancer treatments, while significantly reducing the peak intravascular concentration and therefore lower the risk of cardiotoxicity caused by doxorubicin in blood stream. Treatment outcomes may be improved by increasing the number of administrations. The simulation results indicate that reducing the total dose while increasing the number of continuous infusions is an effective strategy to reduce plasma drug concentration, hence the associated cardiotoxicity, although at the expense of a slight reduction in predicted anticancer effectiveness.

5. Effect of Tumour Properties on Drug Delivery

The properties of tumours are decisive factors in drug transport and final treatment efficacy. Since in most chemotherapies anticancer drugs are carried via the systemic circulation, the characteristics of tumour vasculature plays a crucial role in drug delivery. On the one hand, vasculature in malignant tumours is highly abnormal and heterogeneous. A typical tumour consists of a necrotic core with no functional blood vessels in the centre, semi-necrotic regions with less capillaries and veins, and a tumour advance front which is rich in arterioles, capillaries and venules [49]. On the other hand, tumour vasculature density varies in the growth process, with less vasculature in large, advanced tumours.

In this chapter, a liver tumour model incorporating details of microvascular distribution is adopted first to examine the effect of heterogeneous vasculature distribution on drug delivery. This is followed by studies of drug transport in prostate tumours with different sizes and vasculature density.

5.1. Heterogeneous Vasculature Distribution

The effect of vasculature distribution is investigated in a liver tumour with anticancer drugs being directly administrated through intravenous infusion. The drug transport processes and their governing equations are consistent with those used in Chapter 4. The unique tumour geometry and parameters are described below.

5.1.1. Model Geometry

The geometry of a liver tumour is reconstructed from the post contrast MR images acquired from a patient using a 3.0-Tesla MR scanner (DISCOVERY MR750, GE, Schenectady, New York, USA). Multislice anatomical images of the liver were acquired in three orthogonal planes with GR sequence at three time points after systemic infusion of the tracer Gd-DTPA (gadopentetate dimeglumine, *MW*~0.57 kDa), with each image comprising 256×256 pixels. Other imaging parameters are given in Table 5-1.

Table 5-1. MR imaging parameters

Parameter	Pixel Size	Field of View	Slice Thickness	Repetition Time	Echo Time
(unit)	(mm)	(mm)	(mm)	(ms)	(ms)
	1.3	420	5.0	3.808	1.808

In order to build a 2D model of the tumour and its surrounding normal tissue, a representative transverse image is chosen, as shown in Figure 5-1 (a). The chosen section covers the maximum dimension of the tumour. Image processing is carried out by using Mimics (Materialise HQ, Leuven, Belgium), with the tumour and its sub-regions being segmented based on pixel intensities and contrast enhancement. It can be seen that the tumour is located at the corner with a maximum dimension of 41 mm and an area of $9.0 \times 10^{-4} \, \mathrm{m}^2$. The tumour is divided into 6 sub-regions based on differences in signal intensities which are correlated to vessel densities as described later. Region_1 is further divided into two regions in order to compensate for any potential boundary effect caused by the lack of surrounding normal tissue. The resulting smoothed contours of the tumour and normal tissues are imported into ANSYS ICEM CFD to generate a computational mesh. The dimensions of the reconstructed model are approximately 118.8 mm (maximum width) by 126.8 mm (maximum depth), and the area of the normal tissue is $8.7 \times 10^{-3} \, \mathrm{m}^2$. The final mesh consists of 88,594 triangular elements. This is obtained based on

mesh sensitivity tests which are carried out until the difference in predicted drug concentration between the adopted mesh and a 10-time finer mesh is less than 1%.
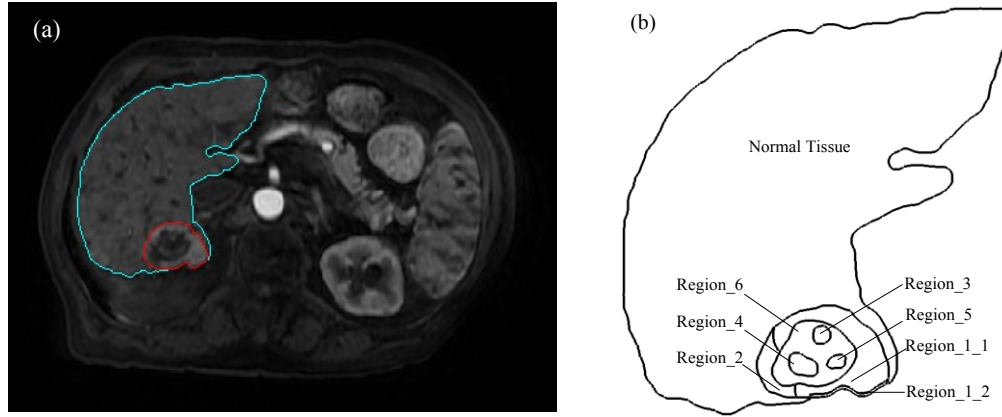
Figure 5-1. Model geometry: (a) MR image of the liver tumour (in red) and its surrounding tissue (in pule blue); (b) the reconstructed 2-D geometry.

5.1.2. Model Parameters

A large number of model parameters are required for the computational simulation; these include physical and transport properties for doxorubicin, tumour and normal tissues. Essential model parameters adopted in the present study are summarized in Tables 3-1 and 3-3. All the geometric and transport parameters are considered to be independent of time, since the growth of tumour and its surrounding normal tissue is negligible during one simulated cycle.

The parameter used to describe the density of vasculature is the surface area of blood vessels per unit volume of tumour tissue (S/V). Since Gd-DTPA is an approved contrast agent for imaging of blood vessels and inflamed or diseased tissue with leaky blood vessels, this MRI-visible tracer is first systemically administrated before MR imaging. The concentration of Gd-DTPA tracer in the interstitial fluid can be described by

$$\frac{dC_{Gd}}{dt} = P\frac{S}{V}\left(C_{p\_Gd} - C_{Gd}\right) + F_v\left(1-\sigma\right)C_{p\_Gd} \tag{5-1}$$

where t is time, P is the permeability of the tracer, S/V is the surface area of blood vessels per unit volume of tumour tissue, C_{Gd} and C_p represent the tracer concentration in the interstitial

fluid and blood, respectively, F_v is the filtration rate from the blood vessels per unit volume of tumour tissue, and σ is the osmotic reflection coefficient of the tracer ($\sigma = 0.6$ [136])

The average interstitial concentration of Gd-DTPA has been found to be proportional to the signal relative intensity enhancement [136]:

$$C_{Gd} \approx \frac{S_{Gd} - S_{Gd\_0}}{S_{Gd\_0}T_{10}r_1}$$

(5-2)

where S_{Gd} and S_{Gd_0} represent the signal with and without the tracer, Gd-DTPA. T_{10} denotes the relaxation time and r_1 is the relaxivity, both of which are constant and can be cancelled out during the evaluation of S/V.

The spatial-mean signal intensity of each tumour region at three different time points is calculated, and the relative value of surface area of blood vessel per tumour size, $(S/V)^*$, can be obtained by interpolation. The ratio of $(S/V)^*$ in each tumour region to the average value for the entire tumour region is then used to calculate values for S/V, by scaling with the standard value from the literature which is 200 cm^{-1}. The scaled values are summarized in Table 5-2 in descending order of microvasculature density.

Table 5-2. The relative and scaled values of surface area of blood vessel per tumour size (cm^{-1})

	Average	Region_1	Region_2	Region_3	Region_4	Region_5	Region_6
$(S/V)^*$	776.52	1741.73	860.84	554.73	502.23	428.69	324.48
S/V	200.00**	448.60	221.72	142.88	129.35	110.41	83.57

** baseline value from literature [49-51]

5.1.3. Numerical Methods

The mathematical equations are solved by means of a finite volume based computational fluid dynamics (CFD) code, ANSYS FLUENT, together with tailor-made routines using the User Defined Scalar (UDS) function. The second order UPWIND scheme is adopted for spatial discretization, while temporal discretization is achieved by employing the second order implicit backward Euler scheme. Regarding boundary conditions, the external boundaries are the outer surface of the normal tissue and tumour regions_1_2, where a zero relative pressure is prescribed. All variables at the internal boundaries between the tumour and normal tissue and between

different tumour regions are assumed to be continuous. The governing equations for interstitial fluid flow are solved first, and the resolved pressure and velocity fields in tumour and normal tissues are then used to solve the mass transfer equations for drug transport. A fixed time-step of 10 seconds is chosen following a time-step sensitivity test. The convergence criteria for residual tolerances are 1×10^{-5} for momentum equations and 1×10^{-8} for mass transfer equations.

5.1.4. Results

A total dose of 50 mg/m^2 non-encapsulated doxorubicin [3] is continuously infused within 2 hours [55], simulating a typical treatment for a 70 kg patient [51]. As a foundation for drug delivery, the micro-mechanical environment in the tumour is examined first. This is followed by an analysis of the concentration profiles and drug cytotoxic effect.

5.1.4.1. Interstitial Fluid Field

Interstitial fluid pressure (IFP) plays an important role in determining the transport of drug in tumours. IFP is obtained by solving the governing equations for interstitial flow for the entire tumour region and its surrounding normal tissue, subject to the boundary conditions described above and a vascular pressure of 2080 Pa. As shown in Figure 5-2, there is no discernable difference among different tumour regions, although IFP in the tumour is much higher than that in the normal tissue. The observation that IFP is not sensitive to tumour microvasculature distribution is consistent with the results of Baxter and Jain [50] who found that even the presence of a necrotic core had virtually no effect on the IFP profile, unless the necrotic core size is greater than 90% of the tumour size. This is because in regions except for a thin layer close to the outer boundary of the tumour, IFP equilibrates with the effective vascular pressure, which is given by $p_v - \sigma_p (\pi_v - \pi_i)$; refer to Chapter 3 for definition of symbols and parameter values. Based on the model parameters adopted in this study, the effective vascular pressure is 1533.88 Pa; this is reached in all tumour regions except region_1 and region_2, where the mean IFP is slightly lower. This means that there is no net filtration between the microvessels and interstitium in regions 3~6 which are surrounded by regions 1 and 2. On the other hand, the rather uniform IFP in the interior of tumour implies that pressure-induced convection of interstitial fluid is weak there, and convective drug transport in the interstitium occurs mainly within a thin layer at the tumour/normal tissue interface, where there is a steep pressure gradient.
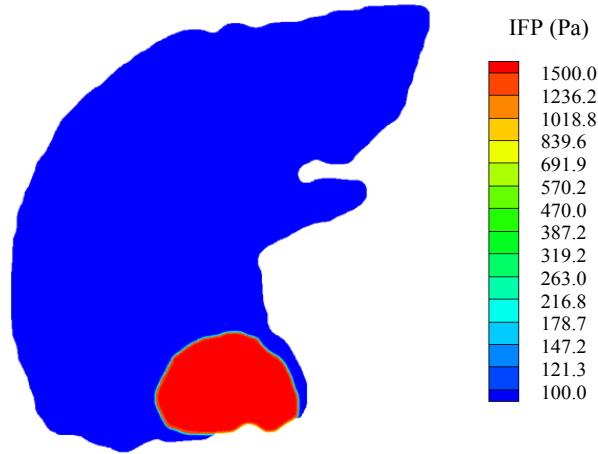
Figure 5-2. Interstitial fluid pressure distribution in tumour and normal tissues.

5.1.4.2. Doxorubicin Concentration

Figure 5-3 shows the spatial distribution of free doxorubicin at different time points in the tumour. It is clear that the extracellular concentration of doxorubicin is non-uniform, which is not surprising since the transport of drug is channelled through blood vessels, and as such, vasculature density is expected to have a strong influence on the spatial distribution of drug. Since the difference in extra- and intra-cellular concentrations between sub-regions 1_1 and 1_2 is very small, these sub-regions are combined and referred to as region_1 in the following discussion.
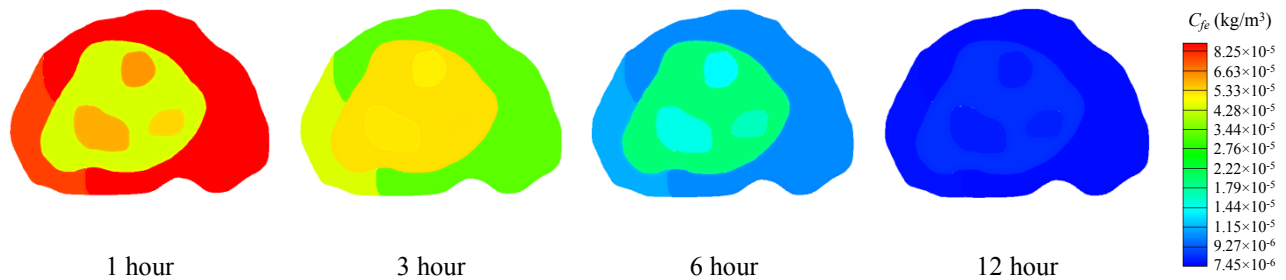
Figure 5-3. Spatial distribution of free doxorubicin extracellular concentration in tumour regions (total dose = 50 mg/m^2, infusion duration = 2 hours)

Figure 5-4 shows the variation of extracellular concentration of free and bound doxorubicin in the liver tumour and each of its sub-regions of different vessel densities. In all regions, the predicted concentration increases during the infusion period, when doxorubicin is administrated continuously into the circulatory system. After the end of administration, both free and bound

doxorubicin concentrations start falling immediately. There are obvious differences in the drug concentrations in the different tumour regions until at approximately 12 hours, when uniform doxorubicin concentrations are reached in all tumour regions (also demonstrated in Figure 5-3). The rate of change of doxorubicin concentration is slower in regions with low vessel density (*e.g.* region_6), owing to reduced drug exchange between plasma and interstitial fluid as a result of sparse vasculature.
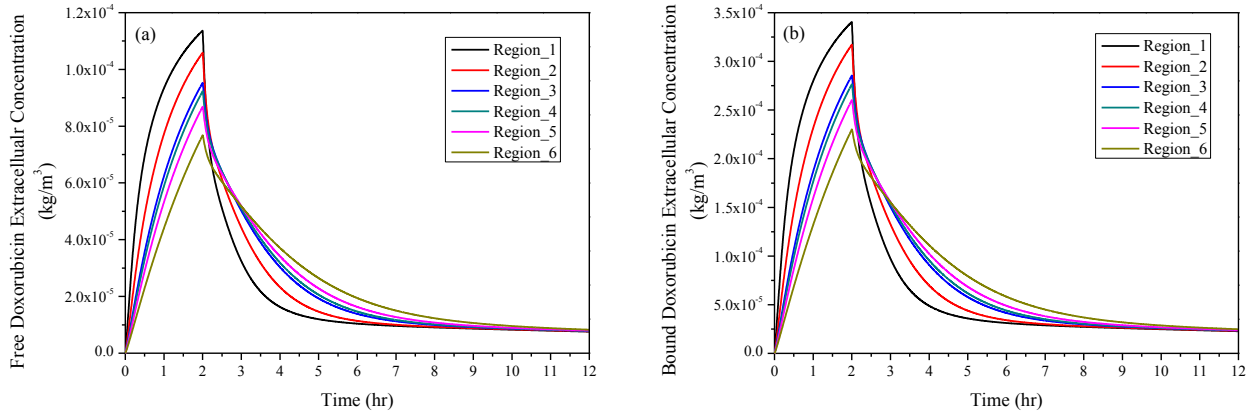
Figure 5-4. Spatial mean doxorubicin extracellular concentration in tumour as a function of time. (a) Free doxorubicin, and (b) bound doxorubicin. (total dose = 50 mg/m^2, infusion duration = 2 hours)

Although vascular densities vary in the different tumour regions, the results in each tumour region show that nearly 75% doxorubicin is in bound form, and both free and bound drugs share a similar time course, confirming that the mechanism of binding with protein is independent of vasculature distribution.
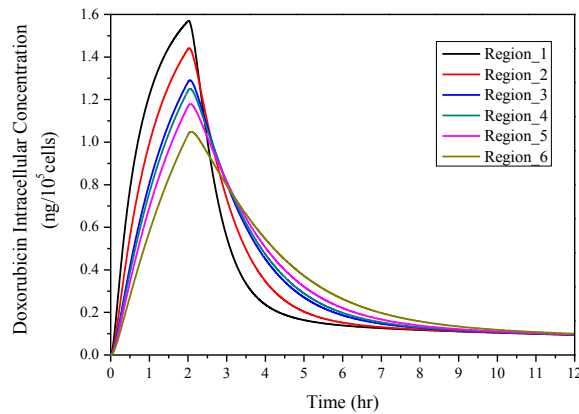
Figure 5-5. Spatial mean of doxorubicin intracellular concentration in tumour regions as a function of time. (total dose = 50 mg/m^2, infusion duration = 2 hours)

Intracellular concentration also displays a non-uniform pattern among the tumour regions of different vessel densities. As shown in Figure 5-5, the rate of change of intracellular concentration is slower and peak concentration is lower in poorly vascularised regions, similar to the pattern observed for extracellular concentration. This is because cellular uptake follows the process of transvascular transport and migration in interstitial space, therefore, the intracellular concentration profile is strongly dependent on the concentration in extracellular space. The highest peak is observed in the region with the densest microvasculature, and results in Figure 5-5 indicate that the peak value increases monotonically with vascular density.

5.1.4.3. Doxorubicin Cytotoxic Effect

The predicted anticancer effectiveness, assessed based on the variation in the percentage of tumour cells (Figure 5-6), suggests that cell killing is more effective in well-vascularised regions in the first few hours, but the trend is reversed thereafter. However, the difference among the various regions is small, with the maximum difference being 3% between region_1 (high vessel density) and region_6 (low vessel density) at 12-hour following drug administration.
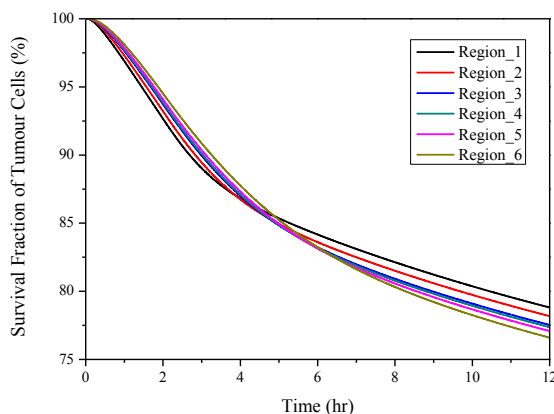
Figure 5-6. Spatial mean percentage of tumour cells in tumour regions as a function of time (total dose = 50 mg/m^2, infusion duration = 2 hours).

The spatial distributions of survival cell fraction in the tumour regions at different time points are shown in Figure 5-7. As a result of the non-uniform distribution of extracellular concentration (see Figures 5-3 and 5-4), different treatment outcomes are found in different tumour regions.

97
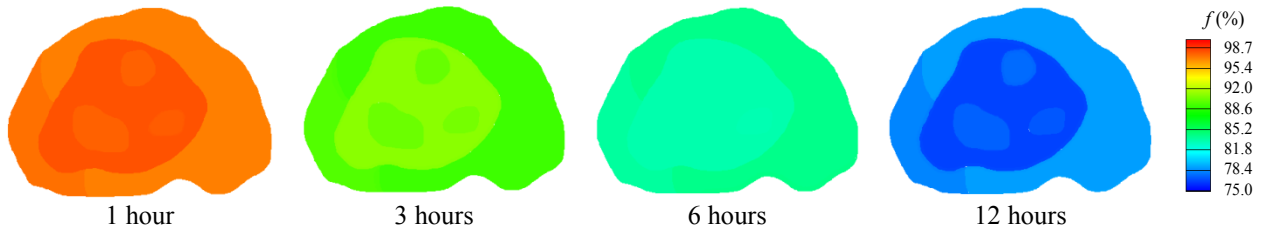
Figure 5-7. Spatial distribution of survival cell fraction in tumour regions.
(total dose = 50 mg/m^2, infusion duration = 2 hours)

5.1.4.4. Comparison of Various Administration Schedules

Comparisons between different doses (25, 50 and 75 mg/m^2) for a 2-hour continuous infusion confirm that the qualitative trend presented above is not altered by changes in dose level. As shown in Figure 5-8, the maximum differences in free doxorubicin extra- and intra-cellular concentrations among tumour regions increase proportionally with an increase in drug dose.
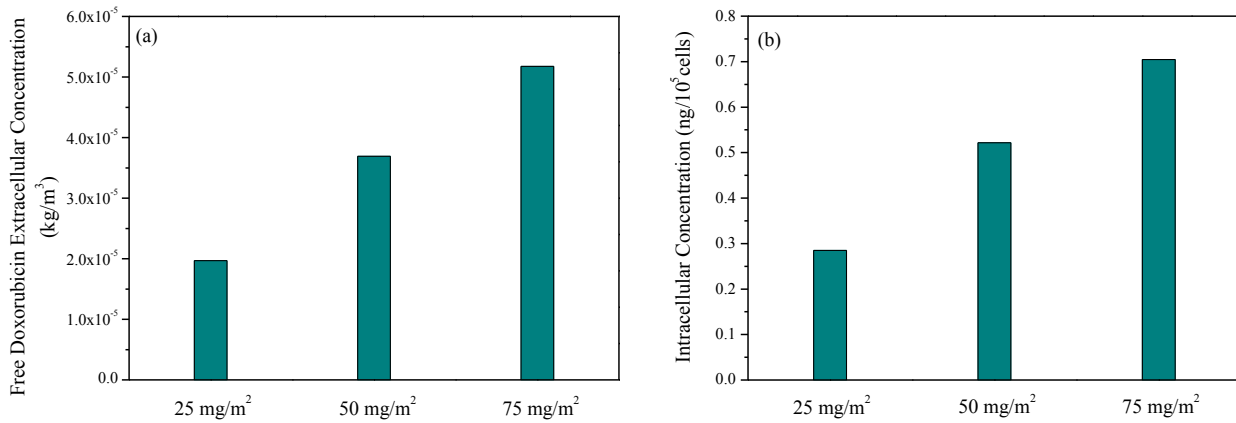
Figure 5-8. Maximum difference among tumour regions over treatment with various doses. (a) free doxorubicin extracellular concentration and (b) intracellular concentration (infusion duration = 2 hours)

Comparisons are also made between different infusion durations (1-hour, 2-hour and 4-hour) for a 50 mg/m^2 continuous infusion, and the qualitative tread among tumour regions is not altered by this parameter. The maximum differences in free doxorubicin extra- and intra-cellular concentration among tumour regions, shown in Figure 5-9, indicate that prolonging the infusion duration may help to reduce the difference in both extra- and intra-cellular concentration among tumour regions.
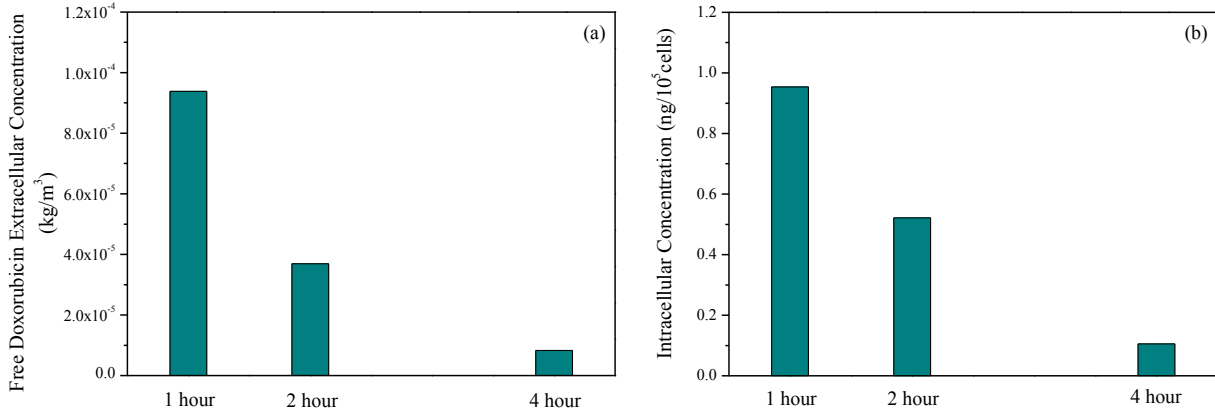
Figure 5-9. Maximum difference among tumour regions over treatment with various infusion durations. (a) free doxorubicin extracellular concentration and (b) intracellular concentration (total dose = 50 mg/m^2)

5.2. Tumour Size

The effect of tumour size is investigated using three prostate tumours under free form drug delivery. The drug transport processes and their governing equations are consistent with those adopted in Chapter 4. The unique tumour geometry and parameters are described below.

5.2.1. Model Geometry

Three prostate tumour models are reconstructed from images acquired from patients using a 3.0-Tesla MR scanner (DISCOVERY MR750, GE, Schenectady, New York, USA). Multislice anatomical images of the prostate were acquired in three orthogonal planes with echo-planer (EP) sequence, with each image comprising 256 by 256 pixels. Other imaging parameters are given in Table 5-3.

Table 5-3. MR imaging parameters

	Pixel Size (mm)	Field of View (cm)	Slice Thickness (mm)	Repetition Time (ms)	Echo Time (ms)
case_1				3675	85.7
case_2	1.250	32.0	7.000	4000	84.4
case_3				4000	91.5

An example of the MR images has been shown previously in Figure 4-1. Transverse images are processed using image analysis software Mimics (Materialise HQ, Leuven, Belgium), and the tumours are segmented from its surrounding normal tissues based on signal intensity values. The

resulting smoothed surfaces of the tumour and normal tissues are imported into ANSYS ICEM CFD to generate computational mesh for the entire volume. The dimension of the reconstructed models shown in Figure 5-10 is approximately 40~50 mm in length for three cases. The final mesh consists of 1,173,908, 1,163,374 and 1,474,027 tetrahedral elements for case 1, 2 and 3, respectively. These meshes have been tested to produce grid independent solutions.

tumour   normal tissue
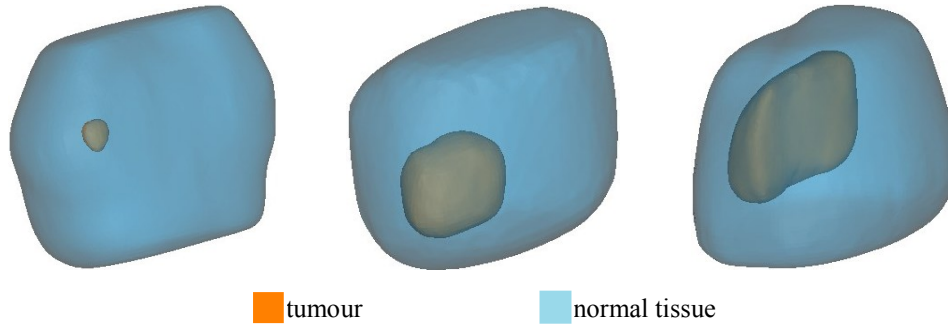
Figure 5-10. Model geometry: (a) case_1; (b) case_2; (c) case_3

5.2.2. Model Parameters

Since the time window of simulations is smaller than the growth of tumour, all the geometric and transport parameters are considered to be independent of time. Baseline values for all model parameters are summarized in Tables 3-1 and 3-3. The tumour size dependent parameter is the surface area of blood vessels per unit volume of tumour tissue (S/V), which reflects the microvasculature density.
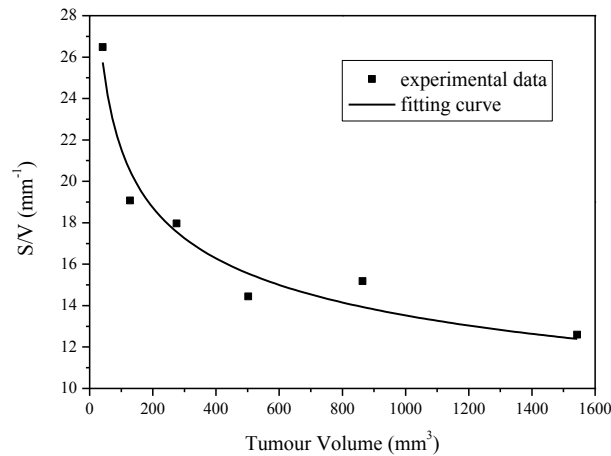
Figure 5-11. Estimation of blood vessel surface area to tissue volume ratio of tumours with various tumour sizes (experimental data extracted from [116]). For the best fitted curve using equation $y=ax^b$ (a = 54.68, b = -0.2021).

Pappenheimer measured S/V normal tissue and found this to be 70 cm^{-1} [117]; this value was adopted by Baxter and Jain [49, 50, 88] in their series of works. Hilmas and Gillette [116] measured this ratio in tumours with different volumes and at different growth stages by using morphometric methods. By using non-linear least squares curve-fitting technique, the relationship between S/V and tumour size is obtained (shown in Figure 5-11), and the S/V value for each prostate tumour is then calculated based on its own size; all the values obtained are summarized in Table 5-4.

Table 5-4. Tumour size and the blood vessel surface area to tissue volume ratio in each model

	Tumour size (mm^3)	S/V (mm^{-1})
case_1	45.46	25.28
case_2	2277.97	11.46
case_3	7118.84	9.10

The numerical method and boundary conditions are consistent with previous studies in this Chapter.

5.2.3. Results

A numerical simulation has been carried out for continuous infusion of 50 mg/m^2 [3] non-encapsulated doxorubicin in 2 hours [55], which corresponds to a standard treatment for a patient of 70 kg body weight [51]. The obtained interstitial fluid field is presented first as this provides the microenvironment for drug delivery. This is followed by comparisons of doxorubicin concentration in the three prostate tumours to investigate the effect of tumour size on drug delivery. Finally, predicted treatment outcomes based on survival fractions of tumour cells calculated from the pharmacodynamics model are compared.

5.2.3.1. Interstitial Fluid Field

Because of abnormalities in tumour, such as vasculature, cellular matrix and the components of interstitial fluid, tumour interstitial fluid pressure (IFP) has been found to be higher than that in normal tissues [49, 50, 88, 89]. Predicted IFP contours at a representative cross-section for each of the three tumours are shown in Figure 5-12. IFP is uniformly high in the entire tumour except in a thin layer close to the tumour boundary. Owing to the low pressure in normal tissue, a sharp

pressure gradient can be found near the boundary between tumour and the surrounding normal tissue.
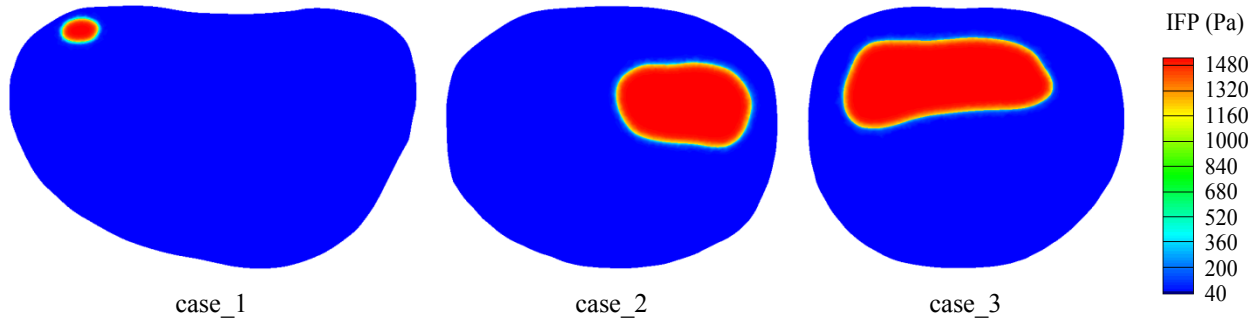
Figure 5-12. Interstitial fluid pressure distribution in tumour and normal tissue

The predicted spatial mean IFP and spatial mean transvascular flux per tumour volume in each tumour are shown in Figure 5-13 (a) and (b), respectively. It can be clearly observed that spatial mean IFP varies with tumour size, with higher IFP in larger tumour. Since IFP in tumour centre are at the same for all three models (at 1533.88 Pa), the observed variation of mean IFP with tumour size is caused by the thin layer with a sharp IFP gradient near the tumour boundary as shown in Figure 5-12. It has been reported in a parameter sensitivity study that IFP gradient is steeper in larger tumour [49], which would result in a higher spatial mean IFP. This is consistent with the finding presented here.
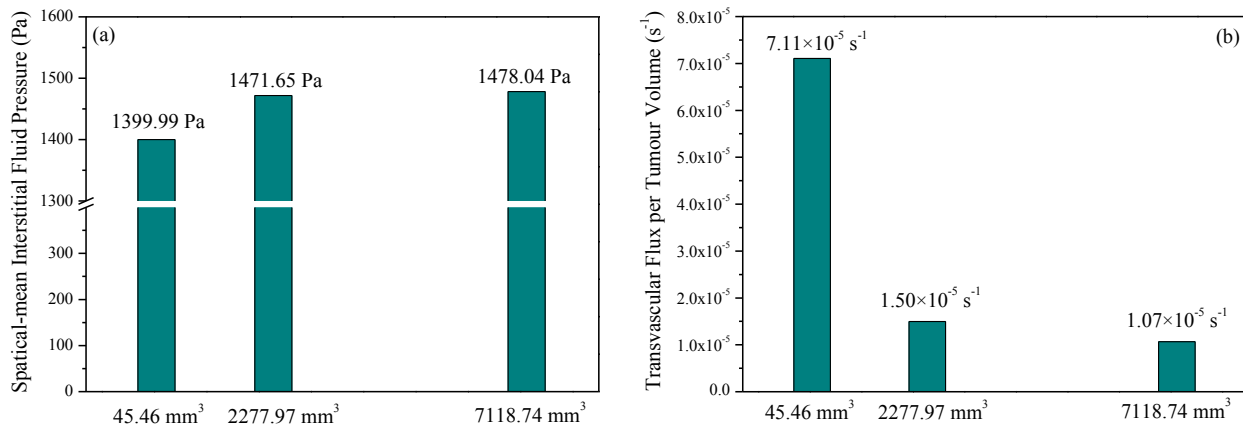
Figure 5-13. The spatial mean interstitial fluid pressure and transvacular flux per tumour volume as a function of tumour size

The transvascular flux per tumour volume from blood to interstitium (F_v) is governed by Equation (3-2), which is recalled here:

$$F_v = K_v \frac{S}{V}\left[p_v - p_i - \sigma(\pi_v - \pi_i)\right] \tag{3-2}$$

As shown in Figure 5-13 (b), the spatial mean transvascular flux per tumour volume from vasculature is higher in small tumour. This is because: (1) the driving force is high in small tumour owing to the low value of spatial mean interstitial fluid pressure and uniform intravascular pressure; (2) higher *S/V* in small tumour improves this exchange. However, referring to the spatial distribution of IFP in Figure 5-12, the transvascular flux mainly occurs in the thin layer at tumour/normal tissue interface owing to the equilibrium between IFP and effective vascular pressure within tumour centre. Results also show that spatial mean IFP and transvascular flux per tumour volume are non-linearly related to tumour volume.

5.2.3.2. Doxorubicin Concentration

Intravascular concentrations of free and bound doxorubicin are shown in Figure 5-14. Doxorubicin in blood circulation system keeps increasing in the 2-hour infusion period and reaches the peak at the end of administration. This is followed by a rapid fall, after which there is a gradual and slow reduction of doxorubicin concentration as time proceeds. Quantitative comparison shows that 75% doxorubicin is bound with proteins in blood stream.
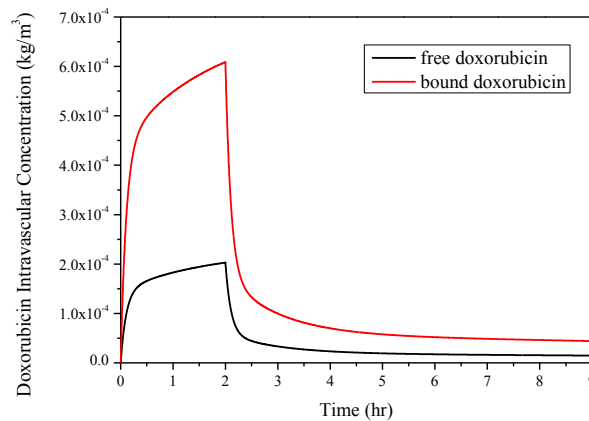
Figure 5-14. Free and bound doxorubicin concentration in blood after administration as a function of time. (infusion duration=2 hours, total dose=50mg/m^2)

Free and bound doxorubicin extracellular concentration in tumour and its holding normal tissue are shown in Figure 5-15. Regardless of the tumour size, both free and bound doxorubicin concentrations in tumour and normal tissue increase rapidly during the initial period after administration, reach their peaks and then fall to a low level after the end of infusion. The rate of change in doxorubicin concentration slows down with the increase in tumour size. This is because S/V is lower in larger tumour, leading to less drug exchange between blood and tumour interstitium. As shown in Figure 5-15 (c) and (d), variation of tumour size has no obvious influence on drug concentration in normal tissue.
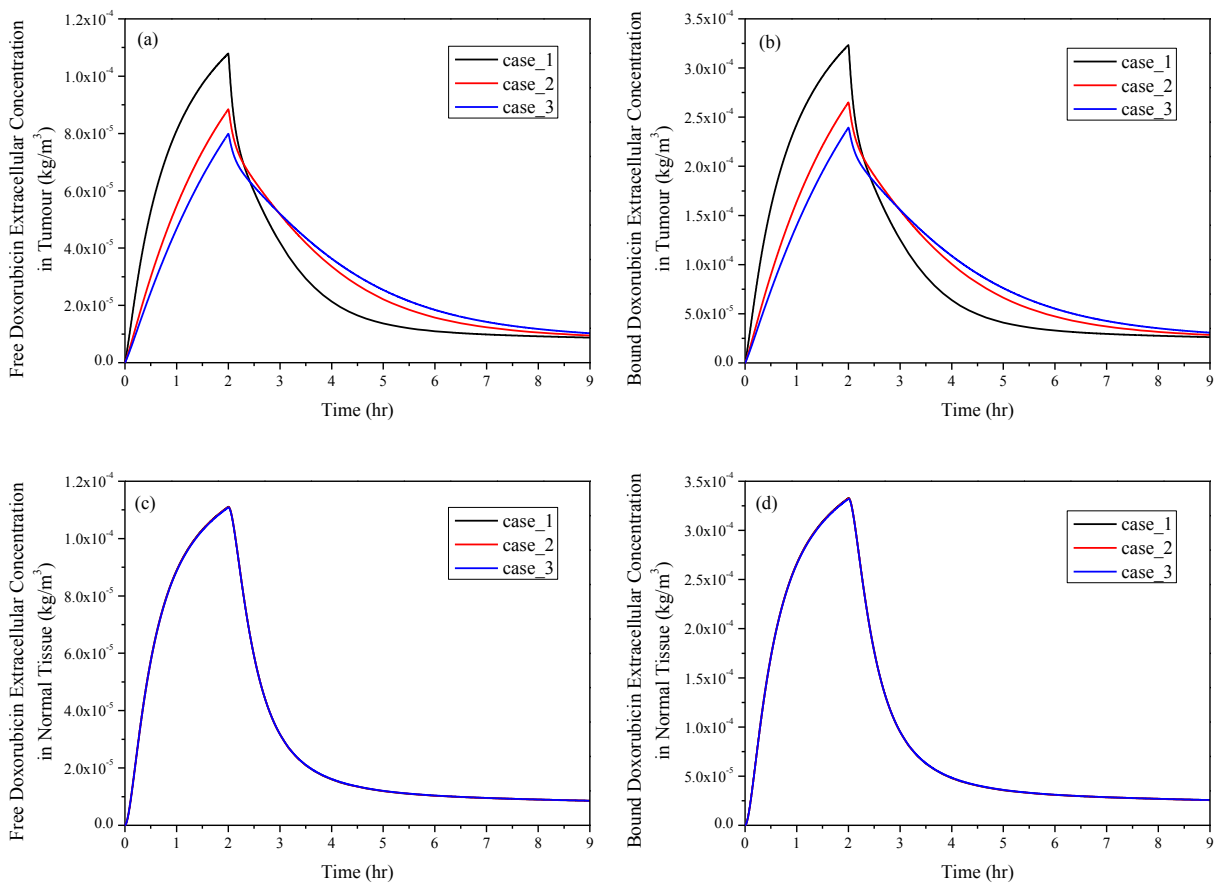
Figure 5-15. Spatial mean doxorubicin extracellular concentration as a function of time under 2-hour continuous infusion, dose=50mg/m². (a) Free and (b) bound doxorubicin in tumour, (c) bound and (d) bound doxorubicin in normal tissue

Figure 5-16 shows the amount of drug exchange between vasculature and interstitial fluid by convection in each tumour. Compared with the blood concentration in Figure 5-14, doxorubicin exchange by convection follows the same pattern. This means that blood concentration has a

direct influence on transvascular transport of doxorubicin by convection. Result in Figure 5-16 also shows that transvascular transport in small tumour is higher than in large tumour.
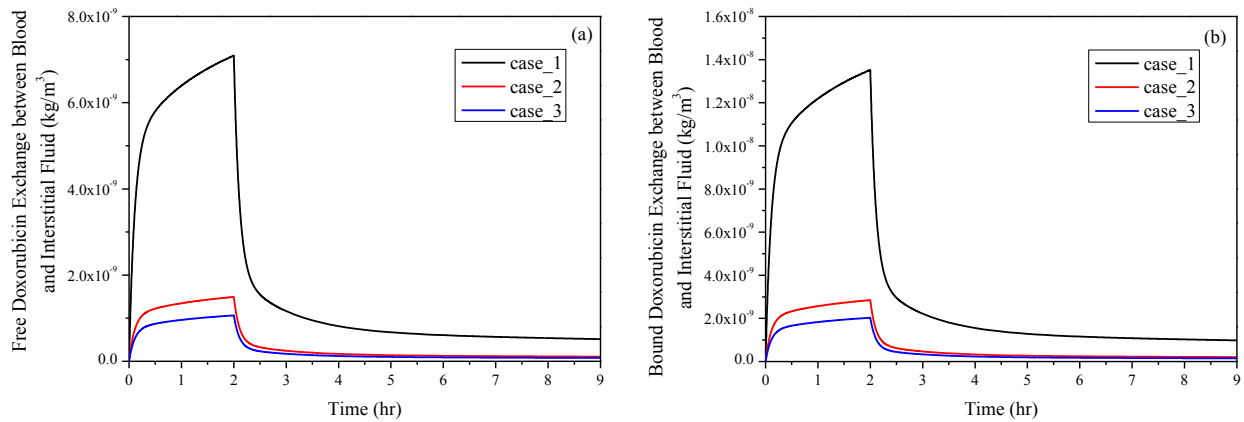
Figure 5-16. Doxorubicin exchange between blood vasculature and interstitial fluid by convection as a function of time. (a) free and (b) doxorubicin exchange (2-hour infusion, total dose =50 mg/m^2)

Regardless of the tumour size, transvascular transport of doxorubicin by diffusion shown in Figure 5-17 experiences the following stages: (1) increasing rapidly until reaching the peak, and then decreasing slowly to a positive level at the end of administration; (2) dropping sharply to a negative level in a few minutes and then returning very slowly to zero.
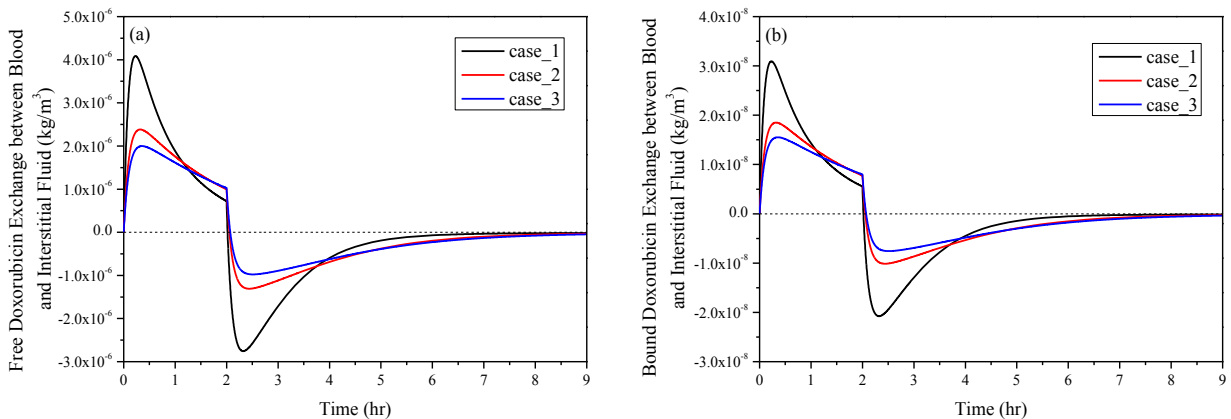
Figure 5-17. Doxorubicin exchange between blood vasculature and interstitial fluid as a function of time in each tumour. (a) free and (b) bound doxorubicin exchange by diffusion owing to concentration gradient (2-hour infusion, total dose = 50 mg/m^2)

Because the initial value of doxorubicin extracellular concentration is zero, the rapid increase in intravascular concentration results in a large concentration gradient between blood and the

interstitial fluid after administration begins, therefore, transvascular transport by diffusion increases rapidly to its peak. Since the increase of blood concentration slows down, the gradient becomes small and leads to a reduction in diffusive transport. However, it is still positive until the end of drug administration, after which blood concentration drops rapidly and no more doxorubicin is supplied. As a consequence, the concentration gradient reduces to zero quickly. Since doxorubicin is washed out quickly, its extracellular concentration becomes higher than blood concentration, causing the exchange to reverse owing to a negative concentration gradient. Afterwards, the negative gradient becomes smaller as the extracellular concentration decreases, causing the diffusive transport to return to zero gradually.

As shown in Figures 5-14 and 5-15, most of doxorubicin is in bound form in blood plasma and interstitial fluid. However, comparison of trans-vascular exchange of free and bound doxorubicin presented in Figures 5-16 and 5-17 indicates that transvascular exchange mainly depends on free doxorubicin. This can be attributed to the small osmotic reflection coefficient and high permeability of free doxorubicin, which ease the transvascular process. Results also show that the rate of change slows down as the tumour size increases. This is because the sparse microvasculature in large tumour reduces drug exchange between blood and interstitial fluid in tumour.

Comparisons are made between spatial mean convection exchange and diffusion exchange by applying the same administration method to case_2. The result in Figure 5-18 shows that diffusion exchange is up to 1000 fold higher than convection during the infusion period. This means that diffusion dominants the drug transport process in the initial hours of anticancer treatment. After the end of administration, diffusive transport driven by concentration difference weakens but is still dominant, resulting in continued reduction in extracellular concentration. It is worth noting that transvascular transport by convection mainly occurs in a thin layer at the interface between tumour and normal tissue. On the contrary, transvascular transport by diffusion takes place in the entire tumour and normal tissue owing to the concentration gradient across microvasculature walls.
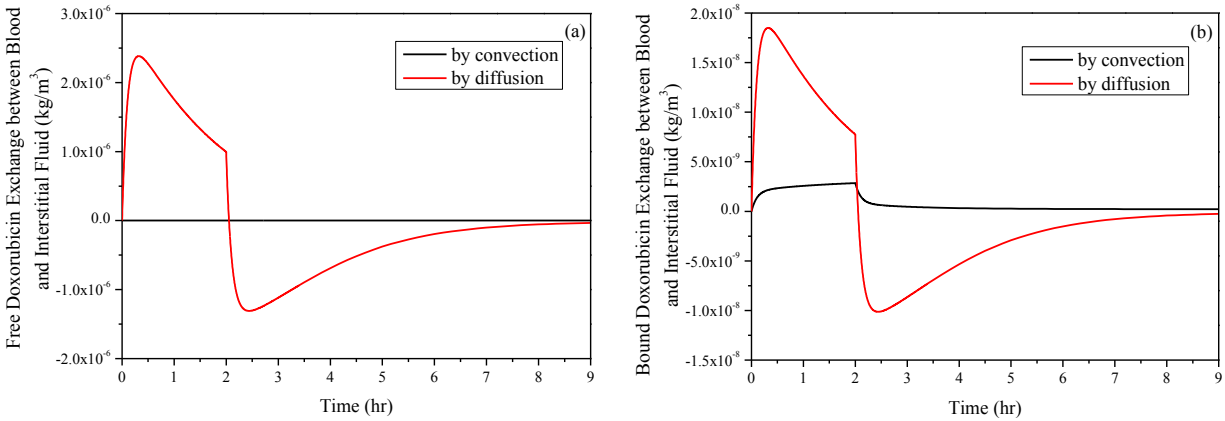
Figure 5-18. Comparison of (a) free and (b) bound doxorubicin exchange between blood and interstitial fluid by convection and diffusion in case_2 (2-hour infusion, total dose = 50mg/m^2)

Figure 5-19 presents the intracellular doxorubicin concentration in the tree tumours for 2-hour direct infusion. Given that intracellular concentration depends on the free doxorubicin extracellular concentration in tumour, intracellular concentration increases rapidly to its peak and before falling off. The computational model predicts that a small tumour with denser microvasculature has more rapid changing rates and higher peaks. However, intracellular concentration in a large tumour sustains at a slightly higher level over time.
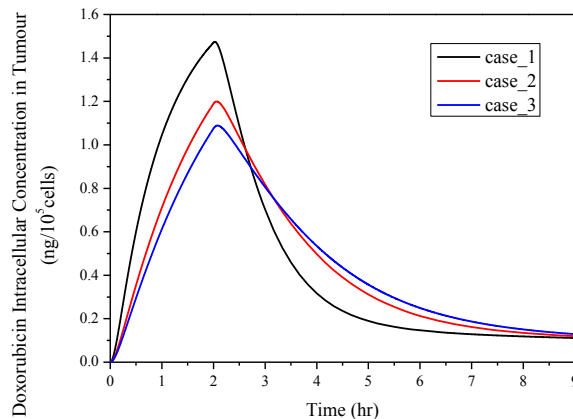
Figure 5-19. Temporal profiles of predicated intracellular concentration in tumours with different sizes (2-hour infusion, total dose = 50 mg/m^2)

5.2.3.3. Doxorubicin Cytotoxic Effect

Figure 5-20 presents the fraction of survival tumour cells by applying the pharmacodynamics model described by Equation (3-30). In small tumours with a denser vasculature, more tumour

cells can be killed in the first few hours after administration begins. However, the drug cytotoxic effect in small tumours becomes worse as time proceeds. This is because the intracellular concentration in small tumours increases rapidly to a higher peak value, but also decreases faster to a low level (shown in Figure 5-19). This fast reduction leads to insufficient cell killing in the later hours of a treatment in small tumours. As can be observed, differences in cytotoxic effectiveness are limited, with a difference of up to 3.2% between case_1 (small tumour) and case_3 (large tumour) in the simulation duration.
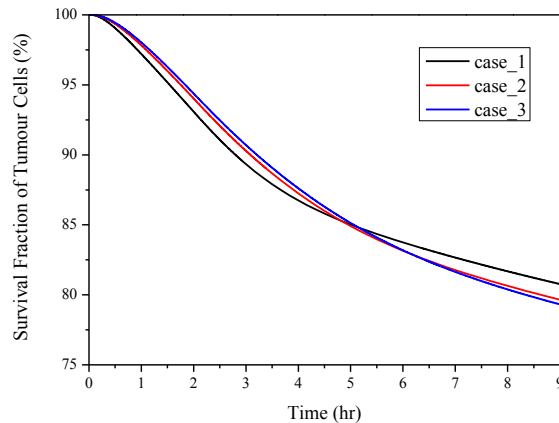
Figure 5-20. Survival cell fraction of tumour as a function of time in three tumours with different sizes (2-hour infusion, total dose = 50 mg/m^2)

5.3. Discussion

Results from the mathematical model show that IFP is uniform within a tumour except for the tumour boundary because IFP in the tumour interior reaches equilibrium with the effective vascular pressure, implying that there is no net filtration between the blood vessels and tumour interstitium. Therefore, convective transvacular transport of drug only occurs within a thin layer at the tumour/normal tissue interface, where there is a steep pressure gradient, and hence transvascular transport mainly replies on diffusion driven by concentration gradient across microvasculature wall.

After administration, doxorubicin accumulates faster in tumour regions with denser vasculature to achieve a higher peak. This is because the rate of transvascular transport is higher than that in tumour regions with sparser microvasculature. Similarly, doxorubicin is rapidly drained back to blood lumen after the end of administrations in these regions owing to the fast plasma clearance

and reverse concentration gradient, resulting in a quick reduction of concentration. Similar results have been found when examining the effect of tumour size with different microvasculature density. The rate of change of concentration is faster in small tumours with dense microvasculature, where the anticancer efficacy is reduced.

Results demonstrate that vasculature in tumour is a crucial factor in drug delivery. Nevertheless, the mathematical model employed here involves a number of assumptions. First, the tumour vascular network is treated as a distributed source term in the governing equations instead of being modelled explicitly. As a result, the effects of intravascular transport and geometric features of tumour vasculature are not included. While this may be an over-simplification, it is practical given the lack of information on realistic tumour vasculature geometry and the complexity in direct modelling of blood flow in a vascular network coupled with interstitial drug transport. Second, all the tumour regions are assumed to be perfused via microvasculature in the studied liver tumour model. Drug transport in tumour regions without functional blood vessels, such as necrotic cores, is not investigated. Third, a 2D tumour model is used instead of a full 3D model. Based on the comparisons between 2D and 3D models of a prostate tumour discussed in Chapter 4, the 3D effect on spatial-mean parameters, such as intracellular drug concentration and tumour cell density, is negligible. This is consistent with the work of Teo et al [79] who found qualitatively similar results between their 2D and 3D models of a brain tumour.

Other assumptions include: (1) signal intensities of tracer Gd-DTPA in post-contrast MR images are used to calculate vascular density, with the tracer concentration in the plasma being assumed to be proportional to the relative change in signal intensity. This could be improved by measuring the intravascular concentration of Gd-DTPA directly in MR imaging [136]. (2) uniform transport properties and uniform tumour cell density are assumed in each tumour region. (3) the intratumoural formation of new blood vessels is a dynamic and complex process involving several cellular and subcellular events in *vivo* [137], and the administered doxorubicin can inhibit angiogenesis rather than cytotoxic effect on tumour cells in doxorubicin-insensitive tumour models [138-140]. Changes in blood vessels are expected to directly affect drug concentration in interstitial fluid and cell killing. However, since these variations usually take place in days [137, 138] which are much longer than the simulated time window, the

vasculature-related parameters are assumed to be constant in this series of work, but their time-varying nature needs to be considered when long simulations are carried out.

5.4. Summary

The effects of vasculature-related microenvironment in tumour have been investigated. Modelling of a liver tumour with heterogeneous vasculature distribution shows that the tumour interstitial fluid pressure is insensitive to the distribution of blood vessels. Even in parts of the tumour that is not well surrounded by holding normal tissue, the pressure gradient there is still limited to a thin layer with a negligible impact on the tumour interior. Better anticancer effectiveness is achieved in regions with low vasculature density, owing to the reduced loss of drugs to the plasma.

Modelling of three prostate tumours with different sizes under direct continuous infusion demonstrates the nonlinear relationships between spatial-mean interstitial fluid pressure and tumour volume, as well as between transvascular flux per tumour volume and tumour volume. During the infusion period, transvascular drug exchange mainly depends on diffusion, owing to the concentration gradient of free drug between blood and interstitial fluid.

6. Thermo-Sensitive Liposome-Mediated Drug Delivery to Solid Tumour

Thermo-sensitive liposome-mediated drug delivery is a promising method to reduce the risk of side effects in anticancer treatment. For well-designed thermo-sensitive liposomes (TSL) that are stable in blood, encapsulated drugs cannot be released until local temperature is raised above the phase transition temperature of the liposome membrane. Among several heating methods that are currently available, high intensity focused ultrasound (HIFU) is favoured for its non-invasive nature and accuracy when used under the guidance of MRI. In the focus region of HIFU, both tumour and blood are heated directly by the absorbed acoustic power, whereas temperature elevation in the surrounding region is achieved via heat transfer through convection and conduction.

In this chapter, the acoustic model for HIFU described in Chapter 3 is firstly validated by comparison with experimental data. Subsequently, the coupled bioheat transfer and drug transport models are used to investigate TSL-mediated drug delivery to a realistic 2-D prostate tumour. Finally, a comparison of temperature profiles between 2-D and 3-D tumour models is presented.

6.1. Acoustic Model for High Intensity Focused Ultrasound

Given that temperature elevation and the following drug release are consequences of absorption of ultrasound energy in tissue and blood, the acoustic pressure generated by HIFU is an essential input to the simulation of TSL-mediated drug delivery. The acoustic HIFU model described in Chapter 3 is applied to a standard test case for which experimental measurements are available.
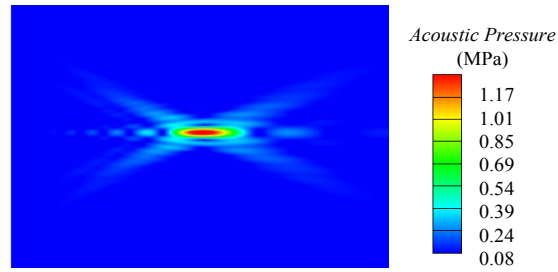
Figure 6-1. Spatial distribution of acoustic pressure

The test case is for a single element HIFU transducer with a 120-mm focal length and 120-mm aperture. The transducer with a fixed frequency of 1.33 MHz is driven by a continuous wave to generate 1.45 MPa at the focus point, with a corresponding intensity of 141.78 W/cm^2. Moving the transducer along the beam and its orthogonal directions, the acoustic pressure in water was measured by a chosen 0.4 mm hydrophone in Solovchuk's experiment [114]. The validation study of acoustic pressure is based on a square geometry (8cm×5.5cm) with the focus region located in the centre. The spatial distribution of acoustic pressure is shown in Figure 6-1.
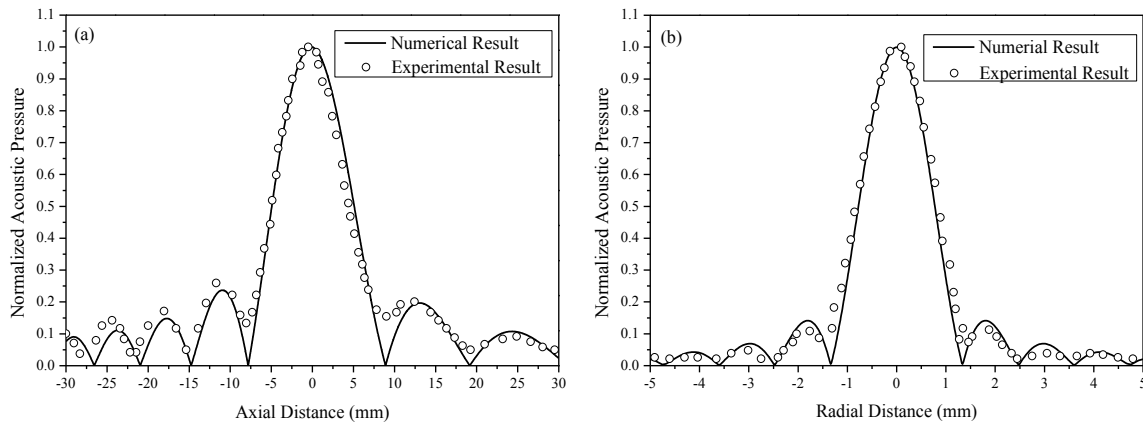
Figure 6-2. Measured and computed acoustic pressure profiles at 1.33 MHz and 1.45 MPa pressure at the focal point. (a) along axis and (b) radial distance. Experimental data are extracted from [114].

Normalized by the pressure at the focal point, acoustic pressure along the axial and radial distance in the focus plane is shown in Figure 6-2. Results show that the predicted acoustic profiles agree well with the experimental data, demonstrating the validity of the HIFU model for prediction of acoustic profiles in biological media [114].

6.2. Thermo-Sensitive Liposome-Mediated Delivery

The combined HIFU, bioheat transfer and drug transport models are applied to a prostate tumour, which is heated simultaneously with the administration of TSL encapsulated doxorubicin. By solving the governing equations described in Chapter 3, spatial and temporal distributions of temperature and drug concentration in blood, tumour and normal tissues are obtained. The expected therapeutic efficacy is evaluated by tumour cell survival fraction.

6.2.1. Model Description

The mathematical model for TSL-mediated drug delivery consists of two parts: bioheat transfer model and drug transport model. The former covers acoustic energy generated by a single element ultrasound transducer, heat absorption by blood, tumour and normal tissues, as well as heat transfer between these compartments; while the later describes the transport of encapsulated, free and bound doxorubicin in blood, extracellular space of tumour and surrounding normal tissues, as well as cellular uptake of the drug.

6.2.1.1. Model Geometry

A 2-D model of prostate tumour is reconstructed from MR images; the same model has been used in Chapter 4. As shown in Figure 6-3, two focus regions are chosen in order to achieve adequate coverage of the tumour [76, 77].
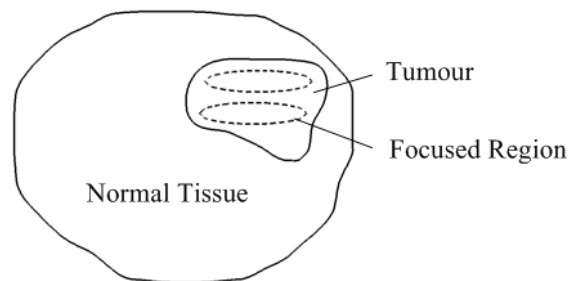
Figure 6-3. Model geometry and locations of focus regions.

ANSYS ICEM CFD is used to generate the computational mesh. The final mesh consists of 64,966 triangular elements. This is obtained based on mesh independence tests which show that the difference in predicted drug concentration between the adopted mesh and a 10 times finer mesh is less than 1%.

6.2.1.2. Model Parameters

Parameters describing the basic physical and transport properties of doxorubicin, tumour and normal tissue have been given in Tables 3-1, 3-2 and 3-3 in the preceding chapter. Additional parameters required for the acoustic and bioheat transfer models are summarised in Table 6-1. Since temperature elevations in response to HIFU heating may influence some of the properties used in the drug transport model, temperature dependence of these properties is also considered.

Table 6-1. Acoustic and thermal properties

Symbol	Description	Unit	Value			Source
			Blood	Tumour	Normal Tissue	
v_a	ultrasound speed	m/s	1540	1550	1550	[74]
ρ	density	kg/m^3	1060	1000	1055	[74]
c	specific heat	J/kg/K	3770	3800	3600	[74]
k	thermal conductivity	W/m/K	0.53	0.552	0.512	[74]
α	absorption coefficient		1.5 f	9 f	9 f	[74]
w_{b0}	perfusion rate of blood flow at 37°C	s^{-1}	-	0.002	0.018	[45]
R	universal gas constant	J/mol/K	-	8.314	8.314	[141]
ΔE	activation energy	J/mol	-	6.67×10^5	6.67×10^5	[141]
A_f	frequency factor	s^{-1}	-	1.98×10^{106}	1.98×10^{106}	[141]

* f represents ultrasound frequency

HIFU Transducer

The acoustic source is a single-element, spherically focused transducer, and its parameters are summarized in Table 6-2. The local acoustic intensity and peak negative pressure are set as 120 W/cm^2 and 1.98 MPa, respectively.

Table 6-2. HIFU transducer parameters

Parameter (unit)	Inside diameter (mm)	Outside diameter (mm)	Focal length (mm)	Frequency (MHz)
	20.0	70.0	62.64	1.10

Temperature controller

In TSL-mediated drug delivery, it is desirable to keep the tumour temperature within a narrow hyperthermia range which should not exceed 43°C to avoid vascular shut down [142]. The phase transition temperature of liposome strongly depends on its formulation, and a typical temperature is 42°C based on experimental studies [69, 143]. In order to achieve the target temperature range, a feedback system with an appropriate temperature control mechanism is required. In the present study, a temperature controller is incorporated, which is designed to adjust the applied ultrasound power according to the maximum temperature in the heated region (T_{max}). The transducer power is determined by

$$P(t) = k_{cp}\left[T_{t\,\arg\,et} - T_{\max}(t)\right] + k_{ci}\sum\left[T_{t\,\arg\,et} - T_{\max}(t)\right] \tag{6-1}$$

where k_{cp} and k_{ci} are Proportional-Integral (PI) control parameters, which are set as 5 and 0.006 respectively, based on values in the literature [72] and previous studies.

Permeability

(1) Free & bound doxorubicin

Dalmark and Strom [144] measured the permeability of free doxorubicin at various temperatures, and found that the logarithmic value of permeability is proportional to temperature. Based on their data, a linear relationship was found between fold increase in logarithmic value of permeability and temperature, as given by Equation (6-2), and the best fitting line is shown in Figure 6-4.

$$\log P = z_1 T + z_2 \tag{6-2}$$

where z_1 and z_2 are fitted parameters which are 0.07 and 2.43, respectively.

Hence the fold increase in permeability is

$$P_1 \Big/ P_2 = 10^{z_1(T_1 - T_2)} \tag{6-3}$$

The permeability of bound doxorubicin is assumed to follow the same relation.
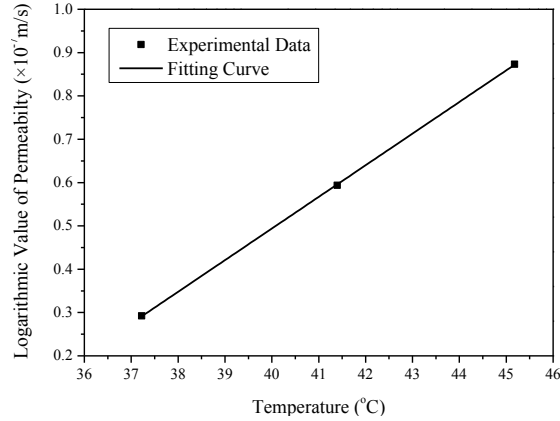
Figure 6-4. Permeability of free doxorubicin as a function of temperature. Curve fitting parameters z_1=0.07 and z_2=-2.43. Experimental data extracted from [144].

(2) Liposome Encapsulated Doxorubicin

For a baseline temperature of 34°C, extracellular concentrations of TSL doxorubicin were found to have increased by 76-fold and 38-fold upon heating to 45°C and 42°C, respectively [145]. Based on these experimental data [145], a relationship between fold increase in permeability and temperature can be obtained by curve fitting, and the best fitting curve is given by Equation (6-4) and shown in Figure 6-5.

$$m_p = m_{p0} + m_{p11}e^{(T-T_0)/m_{p12}} + m_{p21}e^{(T-T_0)/m_{p21}} \qquad (6\text{-}4)$$

where T and T_0 represent temporal temperature and body temperature, respectively, and the other terms in Equation (6-4) are curve fitting parameters.
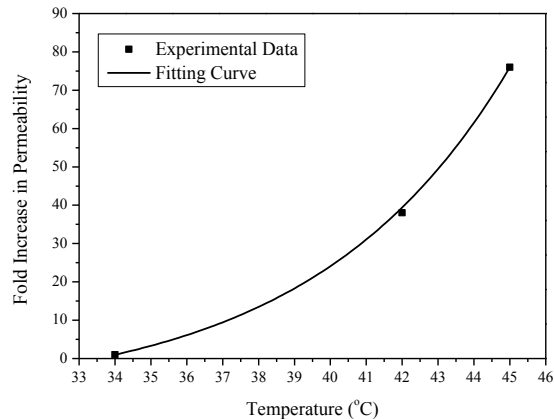
Figure 6-5. Fold increase in permeability of liposome-mediated doxorubicin as a function of temperature. Curve fitting parameters: m_{p0}=-10.54, T_o=34, m_{p11}=5.76, m_{p21}=5.78, m_{p12}=5.44, and m_{p22}=5.46. Experimental data of [145] are adopted.

116

Diffusivity

According to the Stokes-Einstein equation (Equation 3-48), the fold increase in diffusivity as a function of temperature is

$$\frac{D_1}{D_2} = \frac{T_1^* \mu_2}{T_2^* \mu_1} \tag{6-5}$$

where *D* and strands for diffusivity, and μ is the viscosity of solvent. Subscripts 1 and 2 correspond to conditions 1 and 2, respectively. Owing to the lack of relevant data, viscosity values in Equation (6-5) are assumed to be those of water [146], whose dependence on temperature is given by Equation (6-6), with the best fitting result shown in Figure 6-6.

$$m_d = \exp\left(m_{d1} + m_{d2}T + m_{d3}T^2\right) \tag{6-6}$$

where *T* is temporal temperature, and the other terms are parameters used in curve fitting.
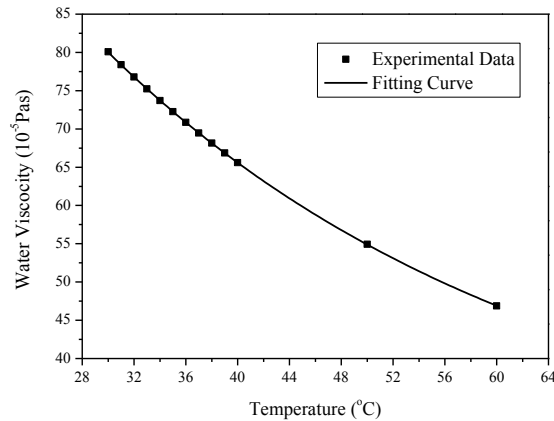
Figure 6-6. Viscosity of water as a function of temperature. Curve fitting parameter m_{d1}=5.10 m_{d2}=-0.03 m_{d3}=1.04×10^{-4} Experimental data extracted from [146]

Rate of Transmembrane Transport

The transmembrane parameter was determined by El-Kareh and Secomb [55] by curve fitting to data obtained from *in vitro* experiments [101]. It has been suggested that increased cellular uptake of doxorubicin with heating will lead to improved outcome when the drug is administrated simultaneously with hyperthermia [55]. Based on data in [147], there is a 2.2-fold increase at 42°C. Here, the fold increase at temperature *T* is obtained by linear interpolation.

$$k_{tv} = 0.24T - 7.88 \tag{6-7}$$

Perfusion rate

Blood perfusion rate (w) also depends on temperature [141] by the following relation:

$$w = w_0 DS \tag{6-8}$$

where w_0 represents the time dependent perfusion at 37°C, and DS is the degree of vascular stasis with a value between 0 and 1.

$$DS = \exp\left(-\int_0^t A_f e^{-\Delta E / RT^*(t)} d\tau\right) \tag{6-9}$$

where T^* is the absolute temperature as a function of time t, R is the universal gas constant, and A_f and ΔE represent the frequency factor and the activation energy, respectively.

Plasma Pharmacokinetics of Encapsulated Doxorubicin

After intravenous administration, liposome-encapsulated doxorubicin begins to circulate to all over the body in circulatory system. Because of the continuous clearance in blood stream and drug release triggered by environmental temperature, the intravascular concentration of encapsulated doxorubicin (C_{lp}) is governed by [13]:

$$\frac{dC_{lp}}{dt} = -CL_{lp}C_{lp} - k_{rel}C_{lp} \tag{6-10}$$

where CL_{lp} and k_{rel} refer to the clearance rate and drug release rate, respectively. The initial concentration of encapsulated doxorubicin is 0.0191 kg/m^3, corresponding to a total dose of 50 mg/m^2 in literature [62].

Drug Release Rate from Liposome Encapsulation

TSL is designed to release its contents rapidly upon heating [65]. The exact release rate varies according to the composition of liposome, its preparation procedure and heating temperature [69]. The relation between percentage release and exposure time is found to follow the first-order kinetics expressed as [148]:

$$\%R(t) = R_c\left(1 - e^{-k_{rel}t}\right) \tag{6-11}$$

where *%R(t)* is the percentage of drug released at exposure time t, R_c is the total percentage of drug released at a given heating temperature. This equation is used to fit experimental data obtained in the range of 37~42˚C [143], and curve fitting for drug release at 37 ^{o}C and 42°C is shown in Figure 6-7.
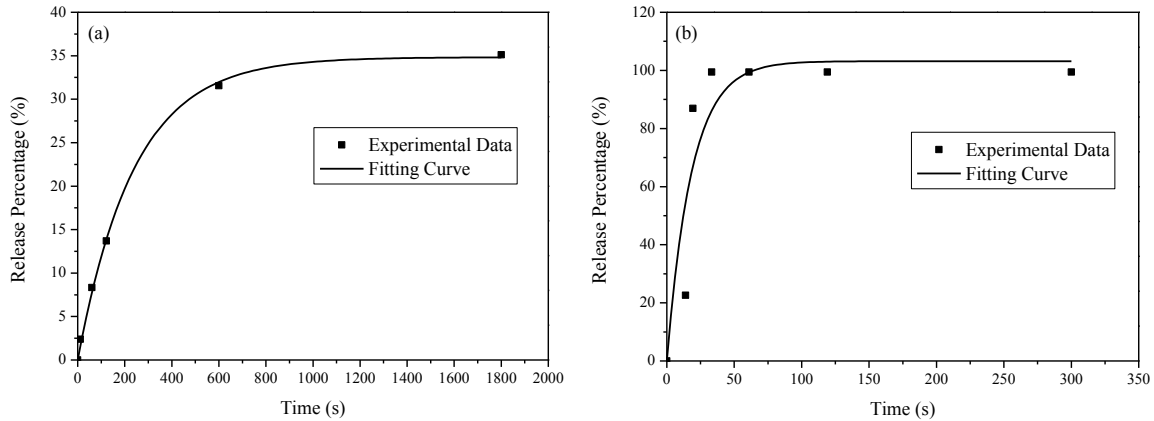
Figure 6-7. Drug release at (a) 37°C and (b) 42°C. Experimental data extracted from [143].

Note that the TSL formulation used in [143] still allows some drug to be slowly released at 37 ^{o}C, although release at 42°C is much faster. From the best fitting results, release rates at different temperatures in the range of 37~42˚C are summarized in Table 6-3. Linear interpolation is performed to obtain release rate at temperatures between the listed temperature points, and the release rate is assumed to be constant when temperature exceeds 42˚C.

Table 6-3. Release rates at various temperatures

T (^{o}C)	37	38	39	40	41	42
k_{rel} (s^{-1})	0.00417	0.00545	0.01492	0.02815	0.04250	0.05409

6.2.1.3. Numerical Methods

The mathematical models are implemented into a finite-volume based computational fluid dynamics (CFD) code, ANSYS FLUENT. The User Defined Scalar (UDS) function is used to code bioheat transfer model, mass transfer equations governing the drug transport and pharmacodynamics. The momentum, drug transport and heat transfer equations are discretised by using the 2nd order UPWIND scheme, and the SIMPLEC algorithm is employed for pressure-velocity coupling. The convergence is controlled by setting residual tolerances of the momentum

119

equation, drug transport equations and bioheat transfer equations to be 1×10^{-5}, 1×10^{-8} and 1×10^{-10}, respectively. As shown in Figure 6-8, interstitial fluid equations are solved first to obtain a steady-state solution in the entire computational domain. The obtained pressure and velocity are then introduced at time zero for the simulation of bioheat transfer, drug transport and cellular uptake. The 2nd order implicit backward Euler scheme is employed to perform the temporal discretization. A fixed time step size of 0.1 second is chosen after time-step sensitivity tests.
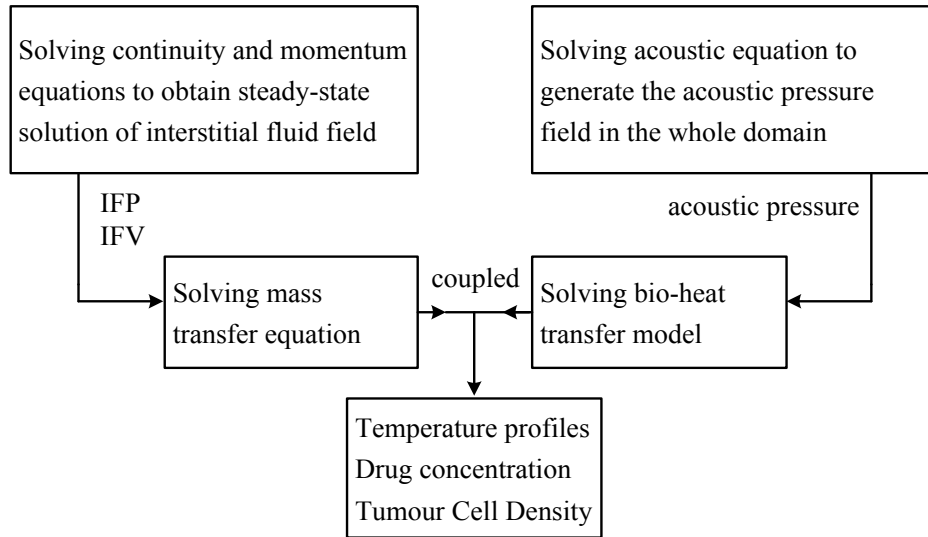
Figure 6-8. Numerical Procedure

Given the time scale of modelling is much shorter than that of tumour growth, all the boundaries of the tumour and normal tissue are assumed to be fixed. The interface between tumour and normal tissue is treated as an internal boundary, where all variables are continuous. The relative pressure and temperature at the surface of normal tissue is specified to be 0 Pa and 37°C, with zero flux of drug.

6.2.2. Results and Discussion

A coupled mathematical model is used to examine the interplays among the various steps involved in the delivery of TSL-mediated chemotherapy. Basic features of the interstitial fluid field are the same as those discussed in Chapters 4 and 5, which will not be repeated here. Results presented below are focused on spatial and temporal distributions of temperature and drug concentration in blood, tumour and normal tissue.

6.2.2.1. Temperature Profile

For clinical application, HIFU heating for 30~60 minutes after administration of TSL are recommended [142]. In an experimental study [149], 10 minutes HIFU heating which was interleaved with a 5 minutes cooling down period was repeated 3 times. Therefore, simulations have been carried out for TSL-mediated drug delivery with simultaneously HIFU heating for durations of 10 minutes, 30 minutes and 60 minutes, respectively. Results are compared with a control case without heating. The two focused regions presented in Figure 6-3 are heated sequentially during the treatment, and the sonication duration for each region is 1 second, which is chosen based on previous studies.

The time course of temperature with 10 minutes heating is shown in Figure 6-9. Variations of maximum and spatial-mean temperature in blood, tumour and normal tissues have a similar pattern in response to the heating schedule. The maximum temperature in tumour reaches the target value of 42^oC rapidly, and is then maintained at this level owing to the temperature control mode governed by Equation (6-1) until the heating period ends. This is followed by a fall in temperature during the cooling down stage. The lower temperature in blood is because the continuous perfusion of blood is effective in removing heat from the focus region, and this forced convection via blood is the main mechanism of heat transfer in tumour and normal tissues. Results show that temperatures fall back to body temperature within 20 minutes after the cessation of heating.
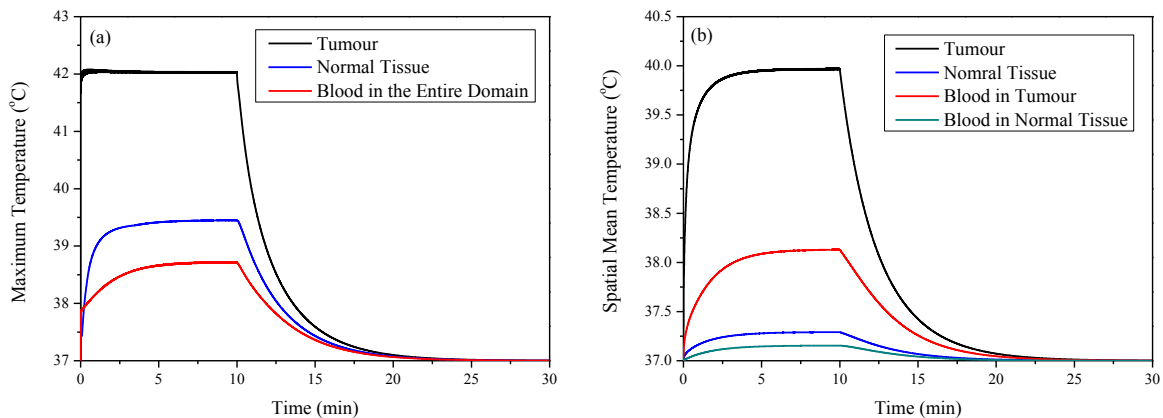
Figure 6-9. Variations of temperature in tumour, blood and normal tissue as a function of time for 10 minutes heating. (a) Maximum and (b) spatial-mean temperature.

Since the focus regions for direct heating are located inside the tumour (shown in Figure 6-3), temperature in tumour increases faster and is higher than in normal tissues, whereas, temperature elevation in normal tissues depends on heat transfer from tumour, which in turn causes heat loss hence reduction in tumour temperature. However, since heat is continuously carried away by the circulating blood, blood temperature in the tumour region is always lower than tumour temperature. The large difference in spatial-mean temperature between tumour and normal tissues (shown in Figure 6-9 (b)) indicates that the release of doxorubicin mainly occurs in the tumour region, thereby achieving localised treatment and reducing the risk of side effects. Since blood in the tumour region is directly heated by HIFU, its mean temperature is higher than that in the surrounding normal tissue.

Spatial distributions of temperature in tissues and blood at 10 minutes after heating are shown in Figure 6-10. It is clear that the highest temperature is located in the focus regions where tumour and blood are directly heated by HIFU. Temperature elevation in the surrounding regions is a consequence of convective and conductive heat transfer from the focus regions, and temperature in normal tissues is mostly around 37°C, lower than in the tumour. This temperature distribution can successfully enhance doxorubicin release in tumour.
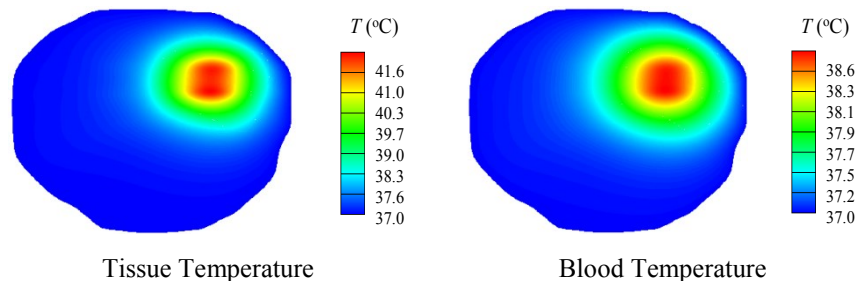
Figure 6-10. Spatial distribution of temperature in (a) tissue and (b) blood at 10min after heating starts.

Figure 6-10 (a) also shows that tissue temperature varies gradually from tumour to normal tissue, owing to similar thermal properties of tumour and normal tissues summarized in Table 6-1. The temperature distribution in blood shown in Figure 6-10 (b) has a similar pattern to tissue temperature but with a narrower range, so that the intravascular release of doxorubicin is much higher in HIFU focus regions than in the periphery.

Temporal variations of temperature for 30 and 60 minutes heating are shown in Figure 6-11.

Identical shapes can be found in each compartment for a given heating duration. The spatial mean temperature of tumour tissue remains at 40°C, which is lower than the most effective release temperature.
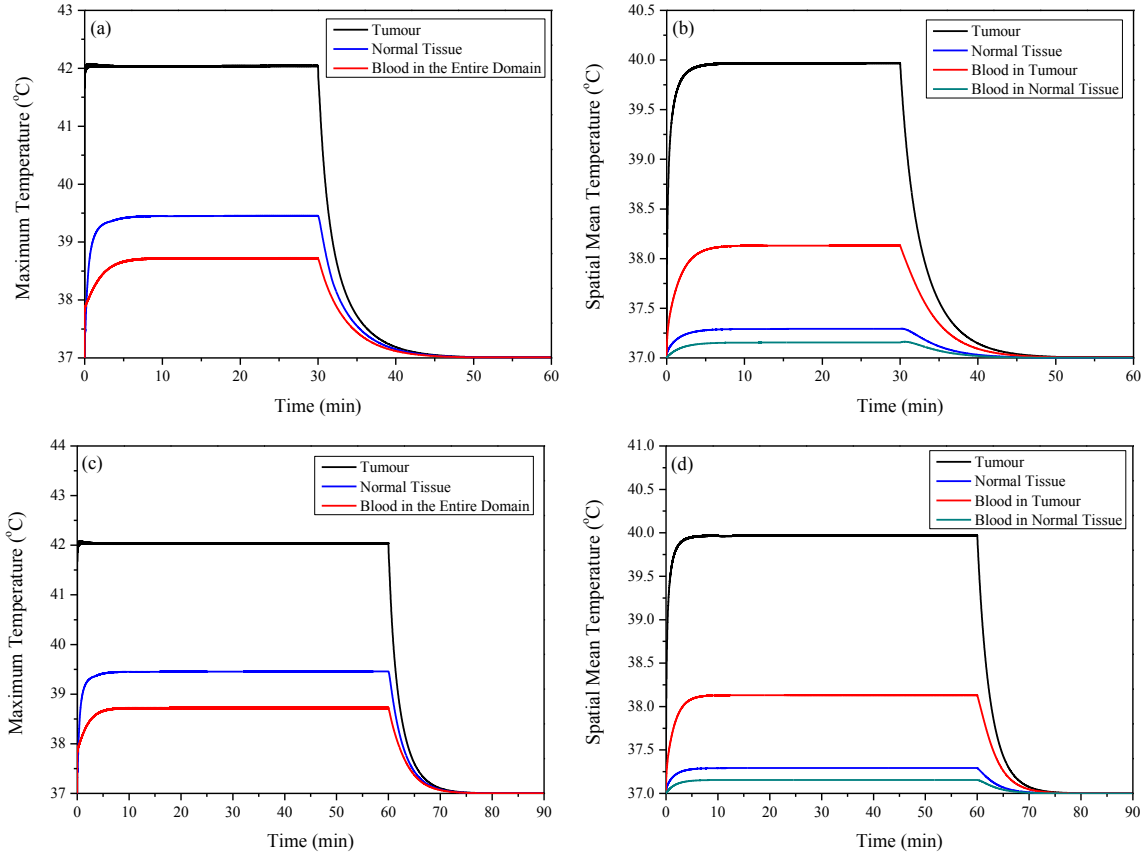
Figure 6-11. Variations of temperature in tumour, blood and normal tissue as a function of time for various heating durations. (a) Maximum and (b) spatial-mean temperature for 30 minutes heating; (c) Maximum and (d) spatial-mean temperature for 60 minutes heating.

6.2.2.2. Drug Concentration

Doxorubicin is initially encapsulated in TSL which are administrated intravenously and carried by the blood stream into the tumour and its surrounding normal tissue. The release of doxorubicin from TSL is triggered by elevated temperature upon HIFU heating. Therefore, the concentration of encapsulated and released doxorubicin in blood should be examined when evaluating its anticancer efficacy. The time courses of encapsulated doxorubicin intravascular concentration with various heating durations are compared in Figure 6-12. Because of the short administration period which can be ignored in comparison with the heating duration, drug

concentration achieves its peak at the very beginning of treatment. Owing to rapid clearance in the circulatory system and increased release as temperature rises, the intravascular concentration of encapsulated doxorubicin falls continuously until it drops to 0.
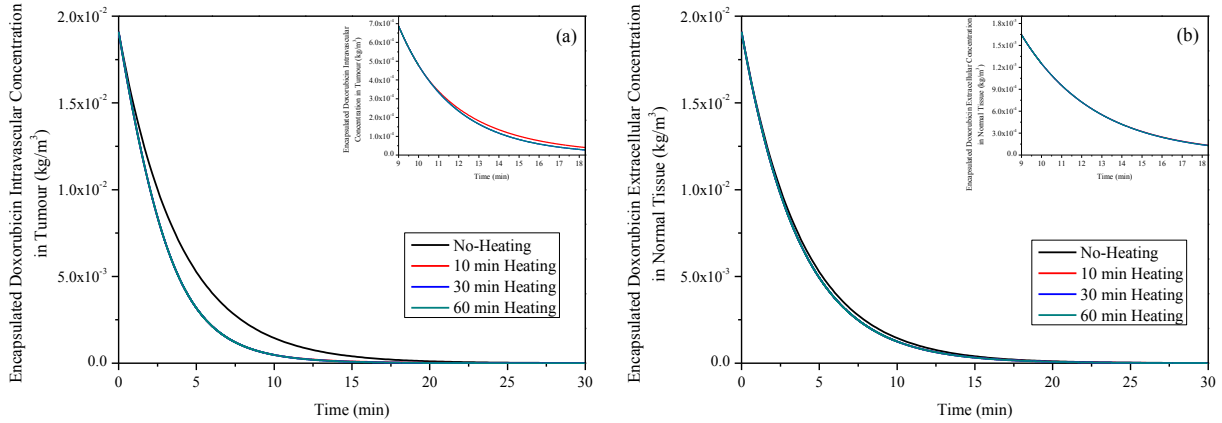
Figure 6-12. Spatial-mean concentration of encapsulated doxorubicin in blood stream as a function of time (dose = 50 mg/m^2). (a) in tumour, and (b) in normal tissue.

Compared with the control case without HIFU heating, encapsulated doxorubicin concentration in tumour (Figure 6-12 (a)) reduces faster upon HIFU heating, owing to enhanced release rate in response to temperature raise. It appears that encapsulated doxorubicin concentration drops to almost zero after about 20 minutes, and the duration of heating (10, 30 and 60 mins) has little effect on encapsulated doxorubicin concentration in tumour. Since normal tissue temperature is approximately 2~3 degrees lower than tumour temperature during HIFU heating, the effect of heating on encapsulated doxorubicin concentration in normal tissue is trivial (Figure 6-12 (b)).
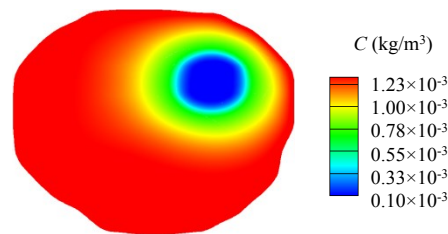
Figure 6-13. Encapsulated doxorubicin concentration in blood at 10 min after heating

The spatial distribution of encapsulated doxorubicin concentration in blood is shown in Figure 6-13 at 10 minutes after heating; it clearly demonstrates that there is little encapsulated doxorubicin left in and around HIFU focus regions.

The time courses of encapsulated doxorubicin concentration in tumour extracellular space are presented in Figure 6-14 (a) for various heating durations. Compared with the case without heating, encapsulated doxorubicin accumulates faster in the extracellular space of the tumour as soon as HIFU heating begins. This is attributed to enhanced vascular permeability in response to temperature elevation. However, the peak concentration is lower and occurs earlier in treatments with hyperthermia. The effect of the heating duration can only be noticed after heating ends.
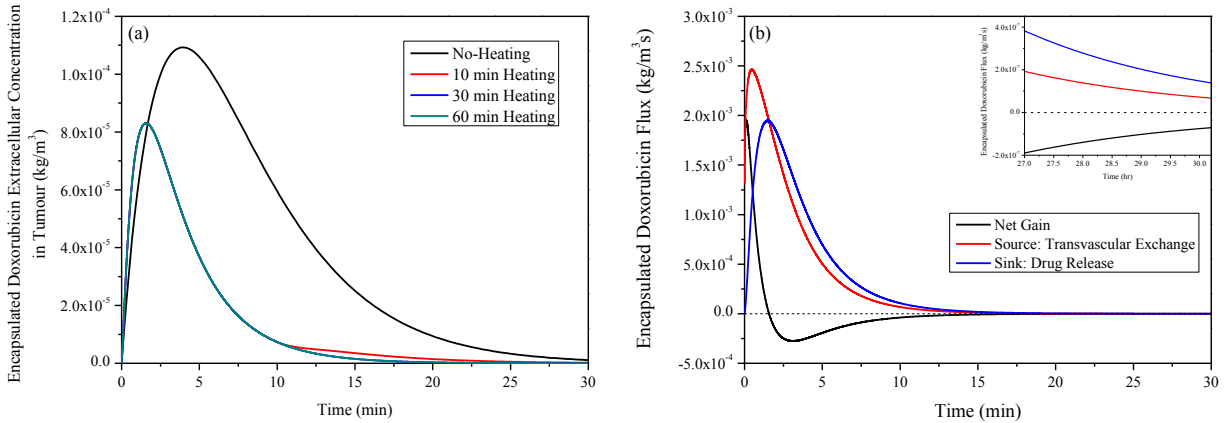
Figure 6-14. Spatial-mean concentration (a) and flux (b) of encapsulated doxorubicin in tumour extracellular space as a function of time.

Encapsulated doxorubicin concentration in tumour extracellular space depends on the balance between the source term which accounts for drug transport from blood vessels, and the sink term which is related to drug release from TSL. The time courses of each term and net grain in the 60-minute heating period are presented in Figure 6-14 (b). The source term reaches its peak very rapidly and then falls off as the intravascular concentration reduces. As a result of increased extracellular concentration and enhanced release rate, the sink term increases initially until it catches up with the source term at around 2 minutes after treatment begins, leading to zero followed by negative net gain. As a consequence, encapsulated doxorubicin extracellular concentration starts to fall, which in turn causes the sink term to decrease and finally reaching zero concentration.

Similar patterns can be found in normal tissues as shown in Figure 6-15. Quantitative comparison shows that encapsulated doxorubicin concentration in normal tissues is 3 orders of magnitude lower than that in tumour, indicating that TSL-mediated drug delivery could effectively avoid liposome accumulation in normal tissue.
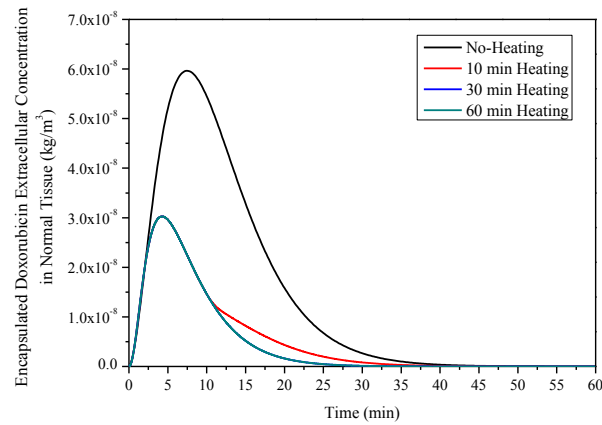
Figure 6-15. Spatial-mean concentration of encapsulated doxorubicin in extracellular space of normal tissue as a function of time.

The spatial concentration of encapsulated doxorubicin in extracellular space at different time points is presented in Figure 6-16. Since blood vessel walls in tumour are leakier with larger pores than those in normal tissue [110, 150], TSL particles are designed in a size range that allows them to pass through the vessel walls in tumour only, thereby achieving effective accumulation in the extracellular space. As shown in Figure 6-16, encapsulated doxorubicin mainly accumulates in tumour, and drugs in normal tissue (shown in Figure 6-15) come from tumour by migration in the extracellular space.
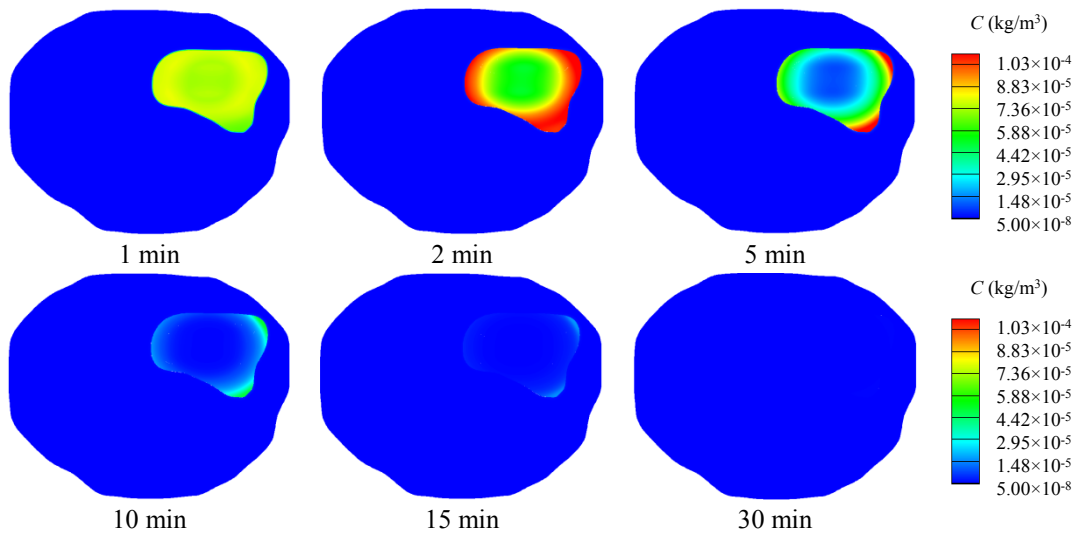
Figure 6-16. Spatial distribution of encapsulated doxorubicin extracellular concentration in tumour and surrounding normal tissues at various time points with 60 minutes heating.

126

Encapsulated doxorubicin concentration in the tumour is highly heterogeneous upon HIFU heating. Tumour centre has lower concentration than in periphery with time proceeds, owing to the fast release of doxorubicin enhanced by HIFU heating in and around the focus regions. Because of the reduction of encapsulated doxorubicin concentration in the blood stream, the corresponding extracellular concentration decreases in the entire tumour and finally becomes to uniform at 30 minutes when the temperature falls back to 37 $^{\circ}$C.
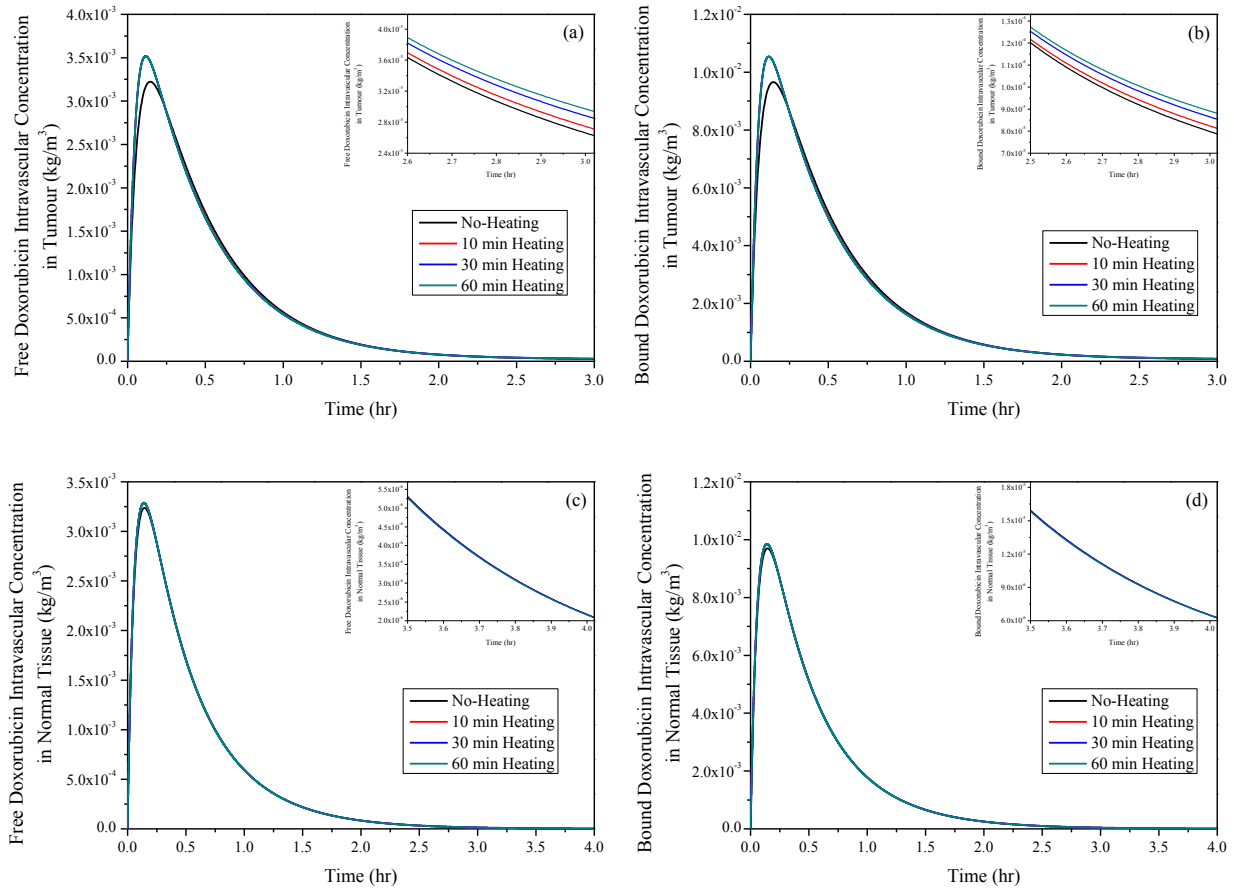
Figure 6-17. Doxorubicin extracellular concentration with various heating duration as a function of time. (a) free and (b) doxorubicin concentration in tumour, and (c) free and (d) doxorubicin concentration in normal tissue.

The time courses of free and bound doxorubicin intravascular concentration in tumour and its surrounding normal tissue are shown in Figure 6-17. Doxorubicin is released from TSL upon heating, leading to an increase in intravascular concentration of drug in free and bound forms. However, drug concentrations fall after reaching their peaks owing to the reduction of encapsulated doxorubicin in blood. The predicted results show that hyperthermia is capable of

enhancing drug release and thereby increasing the concentration in blood in the tumour region, whereas heating makes little difference to intravascular concentration in normal tissue.
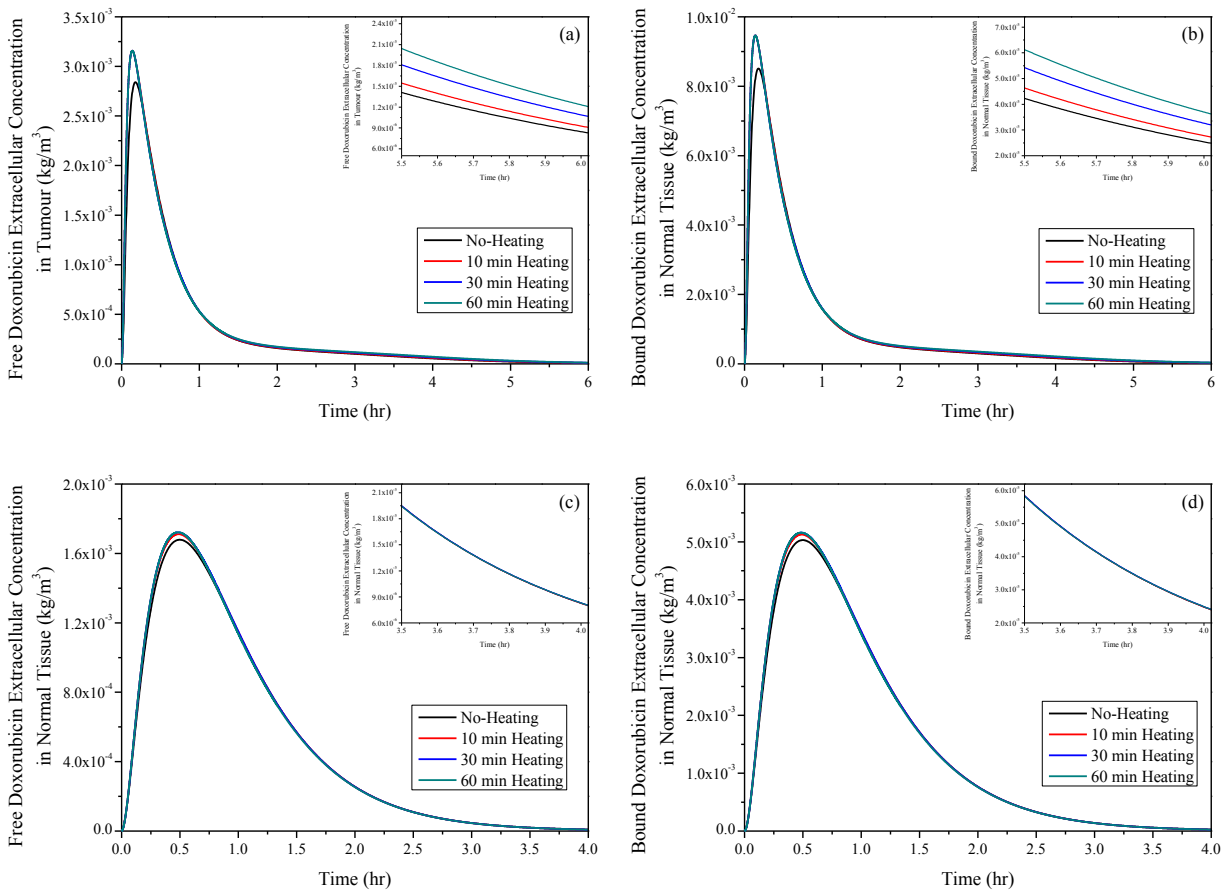
Figure 6-18. Doxorubicin extracellular concentration with various heating duration as a function of time. (a) free and (b) doxorubicin concentration in tumour, and (c) free and (d) doxorubicin concentration in normal tissue

Temporal profiles of free and bound doxorubicin concentration in tumour extracellular space and its surrounding normal tissue are compared in Figure 6-18 between HIFU heating and no-heating. Regardless of the heating duration, both free and bound doxorubicin concentrations increase rapidly during the initial period following drug administration. Doxorubicin concentrations in tumour interstitial space increase faster and reach a much higher peak upon heating. Although doxorubicin concentration drops to a low level as time proceeds, longer heating duration is able to maintain a slightly higher concentration. Comparing doxorubicin extracellular concentrations in Figures 6-18 with the concentration in blood in Figure 6-17, the concentration curves have

identical shapes for a given heating duration. This means that drug concentration in blood has a direct influence on the extracellular concentration for both free and bound doxorubicin.

Comparisons show that doxorubicin concentration in both free and bound forms in tumour is increased by up to 11.26 % upon heating, owing to enhanced drug release, whereas the influence of HIFU heating on doxorubicin concentration in normal tissue is trivial. On the one hand, encapsulated doxorubicin concentration in extracellular space of normal tissue is limited (shown in Figure 6-15 and 6-16), hence less free doxorubicin that can be released. On the other hand, although there is a large amount of encapsulated doxorubicin in blood, drug release in most regions of normal tissue is not enhanced as the temperature is close to 37°C.

Spatial distributions of doxorubicin intratumoural concentration and survival fraction of tumour cells at 10 minutes after administration are displayed in Figure 6-19. It is clear that doxorubicin concentration and survival tumour cells are non-uniform, which is not surprising since the tumour and drug transport properties are enhanced by temperature rise, and as such, the position of HIFU focus regions is expected to have a strong influence on the spatial distribution of drug and cell killing.

Free Doxorubicin Intravascular Concentration

Free Doxorubicin Extracellular Concentration

Intracellular Concentration in Tumour

Bound Doxorubicin Intravascular Concentration

Bound Doxorubicin Extracellular Concentration

Survival Fraction of Tumour Cells
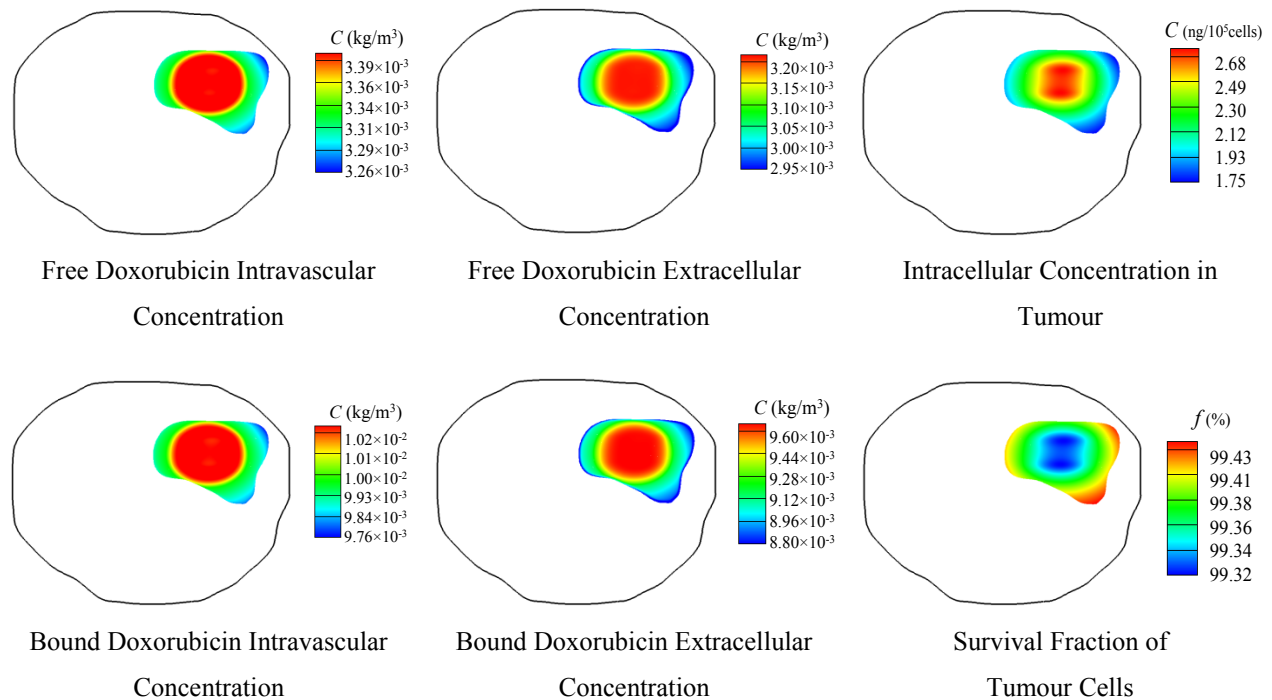
Figure 6-19. Spatial distribution of doxorubicin concentration and cell survival fraction in tumour at 10 minutes.

Intracellular concentration is the highest in tumour centre where HIFU focus regions are located, and it decreases radially towards tumour periphery with the lowest level at the right and bottom corners. As a consequence, cell killing is most effective in the tumour centre, while the cytotoxic effect is insufficient at the right and bottom corners which are the furthest from the HIFU focus regions. Therefore, the heterogeneous enhancement presented in Figure 6-19 demonstrate that TSL-mediated drug delivery with HIFU heating is capable of improving treatment efficacy in designated tumour regions, and careful selection of focus regions may help achieve desired therapeutic effect in the entire tumour.

Temporal profiles of intracellular concentration with various heating durations are presented in Figure 6-20. The intracellular concentration displays a sharp rise at the beginning until it reaches a peak, and then decreases. Compared with the case with no-heating, the rate of increase in intracellular concentration improves upon heating. Increasing heating duration results in higher peaks and higher intracellular concentration levels over time.
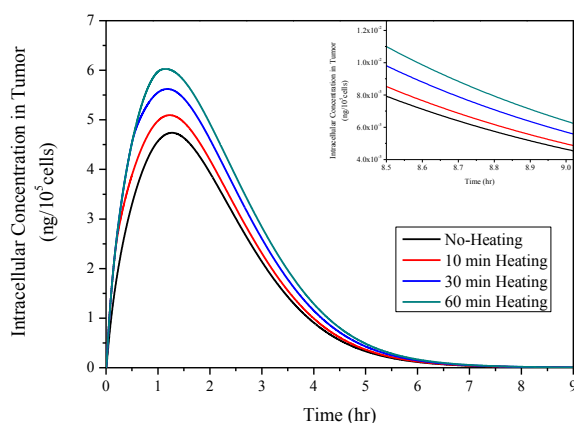
Figure 6-20. Doxorubicin intracellular concentration with heating and no-heating as a function of time.

6.2.2.3. Doxorubicin Cytotoxic Effect

The anticancer effectiveness is evaluated by calculating changes in the percentage of tumour cells using a pharmacodynamics model detailed in Chapter 3. As can be seen from Figure 6-21, the percentage of tumour cells starts to fall immediately after drug administration. There is a rapid cell killing phase in the first few hours after heating in all treatments, but the duration of this phase depends strongly on the heating duration. This is followed by a slower cell killing phase which lasts for approximately 2 hours (6~8 hours after administration). With further

reduction in the intracellular concentration, the rate of cell killing and physiological degradation is overtaken by that of cell proliferation, and as a result, the percentage of tumour cells begins to increase. Results in Figure 6-20 suggest that anticancer effectiveness can be improved by modifying the heating duration.
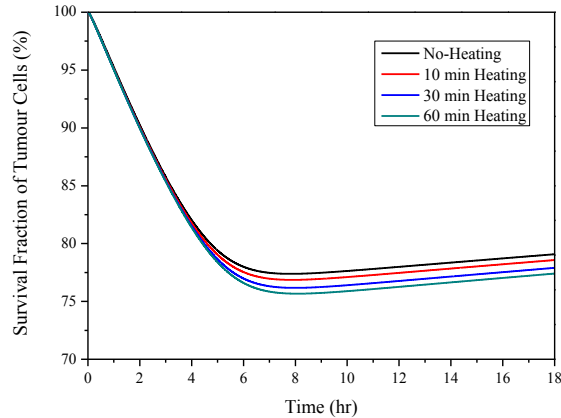
Figure 6-21. Survival cell fraction in treatment with various heating duration as a function of time.

Relative to the control case with no-heating, improvement in the intracellular concentration and cell killing with various heating durations are compared in Figure 6-22 (a) and (b), respectively. Results show that improvements in intracellular concentration and cell killing are non-linearly related to heating duration. This may be attributed to the fast reduction of encapsulated doxorubicin concentration in blood and the non-linear relationship of drug transport described in Chapter 3.
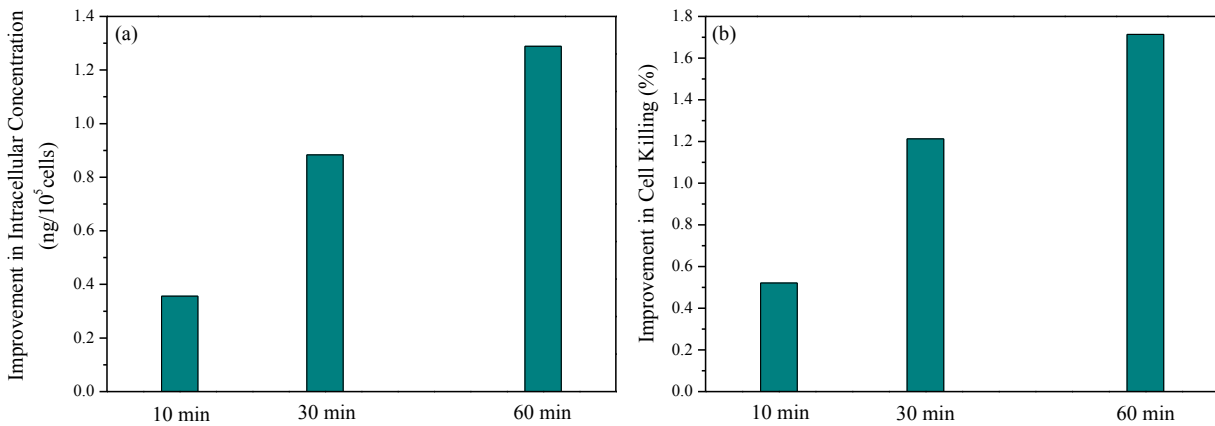
Figure 6-22. Improvement by HIFU heating. (a) intracellular concentration, and (b) cell killing

Although simulation results presented so far demonstrate that TSL drug delivery with HIFU introduced hyperthermia can improve the cytotoxic effect of doxorubicin, the gain in quantitative terms is quite small when compared to the control case. Possible reasons are given below.

(1) Unstable liposome. The simulated TSL formulation [143] is unstable at body temperature. Ideally, TSL should be designed to release its contents upon hyperthermia only, with no release at physiological temperature. However, this is difficult to achieve *in vivo*. Undesirable release at 37 ^{o}C can reduce the intravascular concentration of encapsulated doxorubicin and thereby resulting in high concentration of free doxorubicin in blood. As a consequence, less doxorubicin can be released upon hyperthermia. High concentration of doxorubicin in blood and normal tissue may increase the risk of side effects, such as cardiotoxicity. Therefore, further improvement in liposome formulation to prevent drug release at body temperature is essential to future clinical application of TSL-mediated chemotherapy.

(2) Non-optimal focus region. Tumour cell killing is mostly enhanced in HIFU focus regions. The rate of doxorubicin release is insufficient in the rest of the tumour as the local temperature is lower than 42 ^{o}C, at which drug releases is most effective. Therefore, heating strategy needs to be optimised in order to generate a uniform temperature profile close to the desired temperature within tumour; these include careful design of the number and location of focus regions, heating duration and HIFU scanning method.

6.3. Comparison of 2-D and 3-D Models

All the numerical results on TSL-mediated drug delivery presented so far are based on a 2-D model reconstructed from a selected MR image of a transverse section. However, a real tumour and its surrounding normal tissues are 3-D, and the acoustic pressure as well as the resultant temperature field are highly heterogeneous upon HIFU heating. Hence, it is necessary to evaluate the need for 3-D simulation by quantitative comparison of results based on 2-D and 3-D models.

For this purpose, the 3-D model shown in Figure 4-23 is adopted with an improved mesh to meet the requirement of simulation on acoustic profiles upon HIFU heating, and the final mesh consists of 4,161,964 tetrahedral elements which have been tested to produce grid independent solutions.

Numerical simulation has been carried out with only one focus region located in the tumour centre. Comparison of the maximum temperature within the tumour is shown in Figure 6-23. No difference can be observed between the 2-D and 3-D models owing to the temperature control mode described in Equation (6-1).
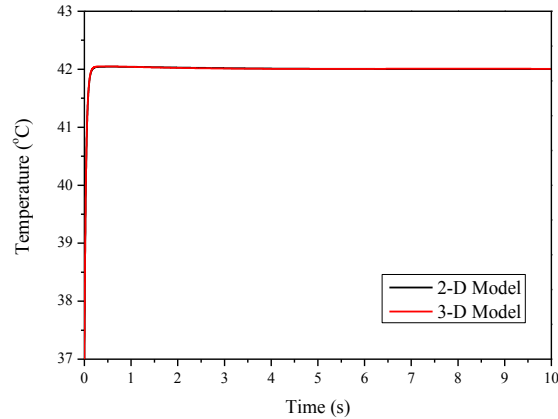
Figure 6-23. Comparison of maximum temperature of tumour in 2-D and 3-D model.

Temporal profiles of spatial-mean temperature of tissues and blood based on the 2-D and 3-D models are compared in Figure 6-24 and Figure 6-25, respectively. The predicted temperature is higher in 2-D model. This over-prediction is attributed to the acoustic pressure distribution which is highly non-uniform. The focus region to tumour size ratio is 0.17 (mm^2/mm^2) in the 2-D and 0.03 (mm^3/mm^3) in 3-D models. Since the focus region covers more tumour regions in the 2-D model, the predicted temperature rises faster than in the 3-D model. Therefore, the predicted drug release and cell killing are expected to be more effective in 2-D model simulations.
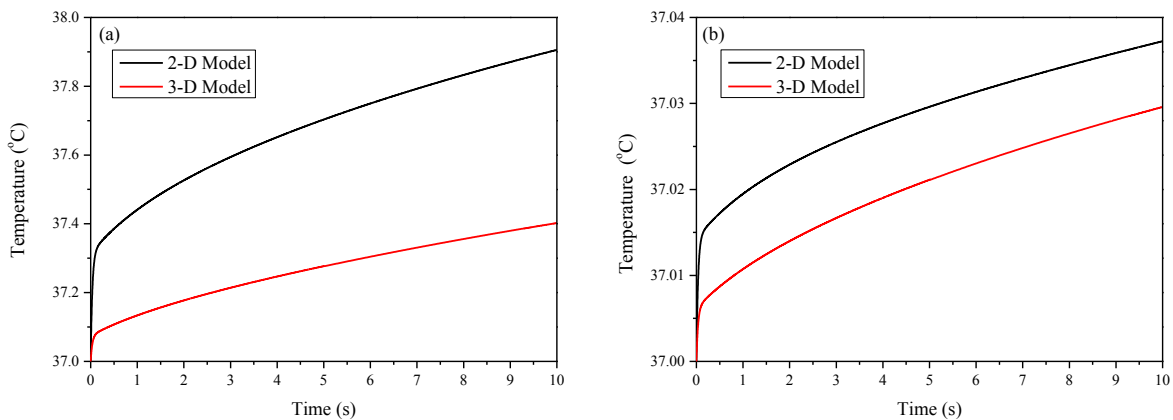
Figure 6-24. Comparison of spatial mean temperature in 2-D and 3-D model. (a) tumour and (b) normal temperature.

133
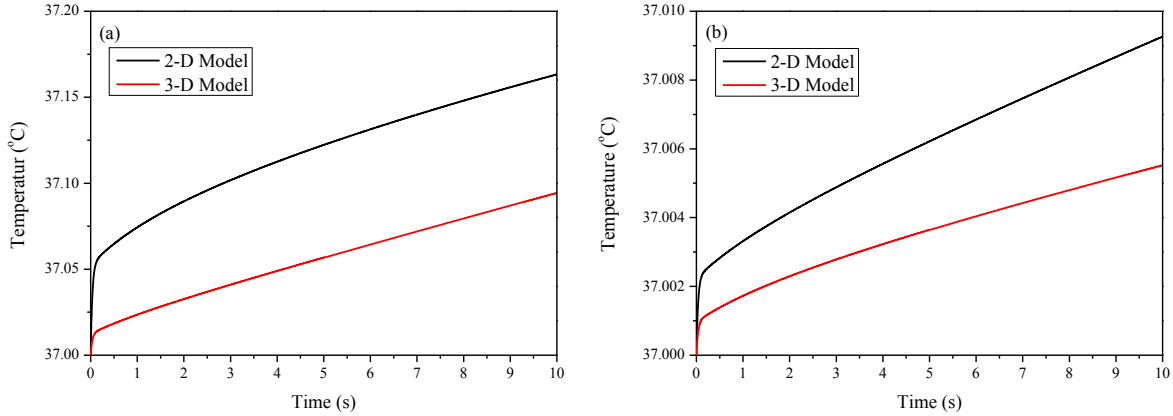
Figure 6-25. Comparison of spatial mean temperature in 2-D and 3-D model. (a) blood temperature in tumour, and (b) blood temperature in normal tissue.

By incorporating bioheat transfer and drug transport in a realistic tumour model, the presents study has provided insights into TSL-mediated drug delivery to solid tumours. Nevertheless, the mathematical model employed here involves a number of assumptions.

First, physical complexities including cavitation and the non-linear progression of ultrasound are ignored. It has been shown that the effects of these complexities are minor for a local intensity in the range of 100~1000 W/cm^2 and the peak negative pressure in the range of 1~4 MPa [151, 152]. Given that the simulated transducer parameters (acoustic intensity is 120 W/cm^2, peak negative pressure is 1.98 MPa) are within the specified ranges, these physical complexities are not considered to be important at the conditions examined here.

Second, the influence of temperature elevation on tumour properties is complicated. Hence not all variations, such as temperature-dependent change in plasma clearance, are included in the current model. Detailed descriptions and mathematical models are required in the future studies in order to examine these effects.

Third, focus regions are ideally positioned in the tumour, without considering movement trajectory of ultrasound transducer, vascular distribution and other micro-environment in tumour. Moreover, only 3 heating durations have been studied. In order to have a more comprehensive investigation, complex heating strategies should be simulated. These include release mode, duration/timing of heating and various release rates.

134

6.4. Summary

In this chapter, thermo-sensitive liposome-mediated drug delivery with various heating durations are compared based on a 2-D prostate tumour model with a realistic geometry. The results indicate that thermo-sensitive liposome-mediated drug delivery is a possible method to achieve localised treatment in cancer therapy. Heating duration is a controllable parameter to improve the efficacy of anticancer treatment.

7.   Conclusion

In this chapter, main conclusions and limitations of the present study are summarized. This is followed by suggestions for further works in anticancer drug delivery research.

7.1. Main Conclusion

In this thesis, a mathematical model comprising drug transport and bioheat transfer is presented to simulate the delivery of anticancer drugs, either in their free form or encapsulated in thermo-sensitive liposomes. Anticancer efficacy of the delivered drugs is predicted based on a pharmacodynamics model. Model parameters describing physiological and biological properties of tissue and drugs are derived from experimental data in the literature. The model has been applied to realistic tumours reconstructed from MRI in order to (a) understand the transport steps of non-encapsulated drugs (Chapter 4), (b) elucidate the effects of tumour properties (Chapter 5), and (c) examine the coupled effect of heat transfer and drug transports under thermo-sensitive liposome-mediated delivery (Chapter 6).

The main findings are as follows:

(1) Better anticancer efficacy is achieved with administration methods that are able to maintain a high level of extracellular concentration over the entire treatment period.

In direct delivery of non-encapsulated drugs, continuous infusion is much more effective than bolus injection in improving the cytotoxic effect of doxorubicin on tumour cells and reducing peak levels of doxorubicin in blood stream. Although rapid continuous infusion with a high peak intracellular concentration leads to faster cell killing at the beginning of the treatment, slow infusion modes give better overall treatment efficacy.

Increasing drug dose can increase concentration levels in the entire tumour and thereby improving doxorubicin cytotoxicity. Whilst consideration must be given to the limitation on doses used in clinical treatment owing to potential side effects, which are caused by doxorubicin in the circulatory system and normal tissues, the highest tolerable dose gives the best therapeutic efficacy.

Multiple-administration can improve the efficacy of anticancer treatments, while significantly reducing the peak intravascular concentration, thereby lowering the risk of cardiotoxicity caused by doxorubicin in blood stream. Treatment outcomes may be improved by increasing the number of administrations. Although there is a slight reduction in predicted anticancer

effectiveness, reducing the total dose while increasing the number of continuous infusions is effective in reducing drug concentration in blood.

(2) Interstitial fluid pressure is not shown to be sensitive to microvasculature density in the interior of tumour, implying that drug transport by pressure-induced convection is weak except in a thin layer close to the interface of tumour/normal tissue. However, better anticancer effectiveness is achieved in tumour regions with relatively low but non-zero microvasculature density, owing to reduced loss of drugs back to the circulatory system.

(3) Spatial-mean transvascular transport is strong in small tumour which is well-vascularised, owing to the low spatial-mean interstitial fluid pressure and dense microvasculature. However, anticancer effectiveness is compromised in small tumour as a result of enhanced reverse diffusion of drug to the blood circulation.

(4) Thermo-sensitive liposome-mediated drug delivery with hyperthermia induced by high intensity focused ultrasound is effective in releasing encapsulated anticancer drugs within targeted regions, thereby achieving localised treatment. Heating duration is an important factor in determining the efficacy of anticancer treatment. Increasing heating duration to 1 hours is beneficial in help maintain higher concentration of anticancer drugs and improve predicted treatment efficacy.

(5) Under the assumption of homogeneous and uniform tissue and drug transport properties, 2-D models of tumours without explicit representation of microvasculature provide comparable results to corresponding 3-D models as far as spatial-averaged parameters are concerned. Nevertheless, 3-D model is preferred for comprehensive details about spatial distributions of drug concentration and cell killing, especially when heterogeneous microvasculature density and heat transfer upon HIFU heating are considered.

7.2. Limitations

The mathematical models described in Chapter 3 involve a number of assumptions which relate to descriptions of tumour properties, drug transport and HIFU heating. Details of these are given below.

7.2.1. Tumour Property

In the present study, tumour properties except for cell density are considered to be time-independent. In reality, tumour growth is a dynamic process which requires variations of tumour properties with time. The effect of this assumption is considered to be minor for simulations with a time window of a few hours only. However, variations of tumour properties should be considered when simulating treatment over a very long time period.

Except for the tumour microvasculature density studied in Chapter 5, tumour properties are assumed to be homogeneous. However, these properties are likely to be heterogeneous and non-uniform, which will affect the transport of anticancer drugs to tumour cells, and eventually the effectiveness of an anticancer treatment.

The present study can be regarded as a qualitative investigation for predictions of trends since all model parameters, apart from tumour geometry, correspond to average and representative values extracted from the literature. More information is required for type-specific and patient-specific studies.

7.2.2. Drug Transport Model

Tumour vascular network is treated as a source term in the governing equations instead of being modelled explicitly. As a consequence, the effect of intravascular transport and geometric features of tumour vasculature are not included. While this assumption may be an over-simplification, it is practical given the lack of information on realistic tumour vasculature geometry and the complexity in direct modelling of blood flow in a vascular network coupled with interstitial drug transport.

Furthermore, only the effect of intratumoural microenvironment on drug transport is considered. However, anticancer drugs may in turn alter the intratumoural microenvironment. For example, drugs such as doxorubicin also attack blood vessels [138] by reducing microvasculature density in tumour. This effect can be incorporated by using a more detailed description with a two-way interaction.

Drug efflux from cells depends on the transmembrane protein, P-Glycoprotein (P-gp), which is capable of effectively reducing intracellular concentration of structurally unrelated cytotoxic

agents [153], such as doxorubicin [154] and cisplatin [155]. In the present study, this efflux is included without considering variations of P-gp concentration over time [99]. This limitation can be overcome by employing an improved transmembrane model.

7.2.3. HIFU Heating Model

The proposed HIFU heating model is a first step towards developing a comprehensive numerical platform for thermo-sensitive liposome-mediated drug delivery system. The employed transducer only consists of one element. However, transducers with a few hundreds of elements are required and have been adopted in clinical use [156]. Moreover, sonication is controlled by a binary feedback loop with a modified algorithm [157] based on the adjustment of the ultrasound phase generated by each element.

7.3. Suggestions for Future Work

The long term goal of computational investigations of drug delivery to solid tumour is to develop an experiment-assisted computational modelling framework spanning across multiple spatial and time-scales to advance the understanding of drug transport process and provide guidance for improvement in anticancer treatments. Therefore, several possible modelling tasks have been identified and these are described below to give an overall idea about how to expand the modelling work described in this thesis.

7.3.1. Realistic Blood Vessel Geometry

The morphological feature of blood vessels in tumour is significantly different from those in normal tissue, leading to highly abnormal organization and connection between vessels [20, 21]. Experimental [158] and numerical [102] studies showed that not all the tumour cells could be exposed to sufficient drugs during treatment. Real micro-vasculature networks reconstructed from advanced imaging techniques may help to examine the effect of blood vessel geometric features on drug delivery and the resultant cytotoxic effect. Modelling of blood flow can then be coupled with intravascular drug transport. Such a model can provide spatial-temporal profiles of drug concentration and cytotoxic effect to gain more insights into the effect of tumour-specific blood vessel network on anticancer effectiveness in different types of tumours.

7.3.2. Nutrient Transport

Tumour growth needs nutrient which is also carried by the circulating blood. Highly proliferating tumour cells and insufficient supply of nutrient, such as oxygen and glucose, may result in hypoxia in localised tumour regions, and cause tumour cell arrest. Given that many anticancer drugs (*e.g.* doxorubicin) act on proliferating cells because their working mechanism is to stop cell duplication by interacting with DNA [3], treatment efficacy may be compromised in regions with insufficient supply of oxygen and other nutrients. On the other hand, arrested tumour cells can re-proliferate after nutrition in the surrounding environment is restored, or tumour cells may die from nutrition shortage, resulting in the formation of necrotic core. It is important to point out that blood supply is closely related to the distribution of functional microvasculature. Therefore, it would make the model more realistic by incorporating nutrient transport, especially when heterogeneous distribution of microvasculature is considered.

7.3.3. Model Validation

The present study serves to provide predictions of qualitative trends, hence detailed model validations are not included except for the HIFU acoustic model. This limitation is attributed to both the numerical model and experiments. On the one hand, not all model parameters are available for a specified tumour, especially when considering the unique condition of each patient; on the other hand, important results, such as intracellular concentration and cell density, cannot be directly measured *in vivo*. Animal experiments may help to provide comparable data for validation. Advanced optical methods, such as high-performance liquid chromatography, can potentially be used to obtain *in vivo* data for validations in the future.

7.3.4. Type / Patient-Specific Tumour

The properties of tumour and normal tissue vary with tissue type, growth stage and individual conditions of a patient [41, 45]. These variations may influence drug transport processes and eventually the anticancer efficacy. Numerical study can be used to predict these differences and provide suggestions in order to optimize treatments. However, detailed type-specific and patient-specific information is required.

7.3.5. Chemotherapy Drugs

Since different anticancer drugs can be combined in clinical use [3, 159, 160], it would be useful to simulate drug transport and cell killing for different combinations of drugs. Most of chemotherapy drugs experience similar transport processes in delivery to tumour cells, including: transport within/through blood vessels, migration in interstitial space and cell uptake. Besides doxorubicin, the basic mathematical model presented here can be applied to various drugs, such as 5-fluorouracid, BCNU, cisplatin, Methotrexate and antibody (*e.g.* Fab and IgG). Necessary modifications should be made in terms of drug-specific properties and behaviour. For instance, 5-fluorouracid and cisplatin do not easily bind with proteins [17].

7.3.6. HIFU Heating Strategy

Heating strategy is essential in thermo-sensitive liposome-mediated drug delivery systems. Further computational studies should be carried out to design an optimal heating strategy that aims to generate a uniform temperature distribution within designated tumour regions in order to improve local treatment efficacy while reducing side effects to normal organs. HIFU scanning method of multiple-element transducer can be designed to maintain tumour temperature above the phase transition temperature of liposome while minimising heating of untargeted regions. Moreover, the predicted anticancer efficacy can be influenced by a number of factors which should be optimised for the treatment of different types of tumours; these include release mode (intra- and extra-vascular triggered release), duration and timing of heating and release rate of chemotherapy drugs.

In summary, a mathematical model for drug delivery in free and encapsulated forms has been developed in order to provide qualitative and mechanistic understanding of anticancer drug transport and cytotoxicity in solid tumours. The developed numerical platform can serve as a foundation for further comprehensive investigations on anticancer drug delivery.

Appendix: Publications during the Project

Journal papers

[1] Wenbo Zhan, Xiao Yun Xu, 2013, A mathematical model for thermosensitive liposomal delivery of Doxorubicin to solid tumour., *J Drug Deliv*, Vol:2013, ISSN:2090-3014

[2] Wenbo Zhan, Wladyslaw Gedroyc, Xiao Yun Xu, 2014, Mathematical Modelling of Drug Transport and Uptake in a Realistic Model of Solid Tumour. *Protein Pept Lett*, Vol: 21, Issue No.11, 2014: 1146-56.

[3] Wenbo Zhan, Wladyslaw Gedroyc, Xiao Yun Xu, 2014. Effect of Heterogeneous Microvasculature Distribution on Drug Delivery to Solid Tumour. *Journal of Physics: D*. 47, 2014: 475401

Conference Presentations

[1] Wenbo Zhan, Wladyslaw Gedroyc, Xiao Yun Xu. Computational Study of Drug Transport in Realistic Models of Solid Tumour. *AIChE Annual Conference*, Pittsburgh, US, 2012

[2] Wenbo Zhan, Wladyslaw Gedroyc, Xiao Yun Xu. Computational Study of Drug Transport in Realistic Models of Solid Tumour. *Mathways into Cancer II*, Carmona, Sevilla, Spain, 2013

[3] Wenbo Zhan, Xiao Yun Xu. Simulation of HIFU Heating in Solid Tumour: Comparison of Different Temperature Control Modes. *3rd International Conference on Computational Methods for Thermal Problems*, Lake Bled, Slovenia, 2014

Appendix: Nomenclature

Symbols

A_1	parameter of pharmacokinetic model for doxorubicin
A_2	parameter of pharmacokinetic model for doxorubicin
A_3	parameter of pharmacokinetic model for doxorubicin
A_f	frequency factor
b	chord from the ultrasound transducer centre to the radiator boundary
c	specific heat
C_{be}	bound doxorubicin concentration in interstitial fluid
C_{bp}	bound doxorubicin concentration in blood plasma
C_{fe}	Free doxorubicin concentration in the interstitial fluid
C_{fp}	free doxorubicin concentration in blood plasma
C_{Gd}	tracer concentration in the interstitial fluid
C_i	intracellular doxorubicin concentration
CL_{bp}	plasma clearance of bound doxorubicin
C_{le}	liposome encapsulated drug concentration in the interstitial fluid
CL_{fp}	plasma clearance of free doxorubicin
C_{p_Gd}	tracer concentration in blood
C_v	doxorubicin concentration in blood plasma
d	distance from a point on the radiator to a field point
D_{be}	diffusion coefficient of the bound doxorubicin-protein
Dc	tumour cell density
D_d	drug dose
D_{fe}	diffusion coefficient of free doxorubicin
D_l	diffusion coefficient of liposomes
DS	degree of vascular stasis
D_W	diffusion coefficient in water
EC_{50}	drug concentration producing 50% of f_{max}
F_{be}	bound doxorubic gain from blood vessels

F_{fl}	doxorubicin loss of doxorubicin to the lymphatic vessels per unit volume of tissue
F_{fp}	doxorubicin gained from the blood capillaries in tumour and normal tissues
F_{fp}	free doxorubicin gained from the capillaries in tumour and normal tissues
F_{ll}	loss of liposomes through the lymphatic vessels per unit volume of tissue
F_{lp}	liposomes gained from the capillaries in tumour and normal tissues
F_{ly}	interstitial fluid absorption rate by the lymphatics per unit volume of tumour tissue
f_{max}	cell-kill rate constant
F_v	interstitial fluid loss from blood vessels per unit volume of tumour tissue
h	depth of the concave surface
I_a	ultraound intensity
k	thermal conductivity
k_a	doxorubicin-protein binding rate
k_{ac}	acoustic velocity potential
k_B	Boltzmann's constant
k_{ci}	PI control parameter
k_{cp}	PI control parameter
k_d	doxorubicin-protein dissociation rate
k_e	michaelis constant for transmembrane transport
k_g	cell physiological degradation rate
k_i	michaelis constant for transmembrane transport
K_{ly}	hydraulic conductivity of the lymphatic wall
k_p	cell proliferation rate constant
k_{rel}	release rate of doxorubicin from liposome
K_v	hydraulic conductivity of the microvascular wall
m_d	inceased fold of diffusivity
m_p	inceased fold of permeability
m_{tv}	inceased fold of transmembrane rate
MW	molecular weight
P	permeability
p_a	acoustic pressure
P_{be}	permeability of vessel wall to bound doxorubicin

Pe_f	trans-capillary Peclet number
P_{fe}	permeability of vasculature wall to free doxorubicin
p_i	interstitial fluid pressures
p_{ly}	intra-lymphatic pressure
p_v	vascular pressures
q	ultrasound power deposition
r	radius of spherical particle
R	universal gas constant
s	percentage of bound doxorubicin
S/V	surface area of blood vessels per unit volume of tumour tissue
$(S/V)^*$	relative value of surface area of blood vessel per tumour size
S_b	net rate of doxorubicin gained from association/dissociation with bound doxorubicin-protein
S_{Gd}	MRI signal with tracer
S_{Gd_0}	MRI signal without tracer
S_i	net rate of doxorubicin gained from the surrounding environment
S_l	net rate of liposomes gained from the surrounding environment
S_{lp}	liposomes gained from plasma
S_{ly}/V	surface area of lymphatic vessels per unit volume of tumour tissue
S_r	released drug in the interstitial fluid
S_u	influx/efflux from tumour cells
S_v	net rate of doxorubicin gained from the blood/lymphatic vessels
T	temperature
T^*	absolute temperature
T_0	body temperature
t	time
t_d	infusion duration
Tn	normal body temperature
u_0	velocity constant
v_a	speed of ultrasound
V_B	plasma volume

V_{max}	rate of trans-membrane transport
V_T	tumour volume
W	diagonal matrix
w	perfusion rate of blood flow
w_0	perfusion rate of blood flow at body temperature
ΔE	activation energy

Tensor

$\boldsymbol{C}$	matrix of the inertial loss term
$\boldsymbol{F}$	Darcian resistance to fluid flow through porous media
$\boldsymbol{I}$	unit tensor
$\boldsymbol{u}$	normal velocity of a slightly curved radiating surface
$\boldsymbol{v}$	velocity of the interstitial fluid

Greek Letter

α	ultrasound absorption coefficient
α_1	compartment clearance rate of doxorubicin
α_2	compartment clearance rate of doxorubicin
α_3	compartment clearance rate of doxorubicin
ε	cellular efflux function
ζ	cellular uptake function
κ	permeability of the interstitial space
λ	wave length of ultrasound
μ	dynamic viscosity of interstitial fluid
π_i	osmotic pressure of interstitial fluid
π_v	osmotic pressure of the plasma
ρ	density
σ	osmotic reflection coefficient
σ_d	osmotic reflection coefficient for the drug molecules

σ_T	average osmotic reflection coefficient for plasma protein
τ	stress tensor
φ	tumour fraction extracellular space
Ψ	acoustic velocity potential
ω	angular frequency of ultrasound transducer

Abbreviation

BSA	body surface area
BSNC	bis-chloroethylnitrosourea
CFD	computational fluid dynamics
FVM	finite volume method
Gd-DTPA	gadopentetate dimeglumine
HIFU	high intensity focused ultrasound
IFP	interstitial fluid pressure
IFV	interstitial fluid velocity
MRI	magnetic resonance image
MW	molecular weight
PEG	polyethylene glycol
PDT	photodynamic therapy
P-gp	P-Glycoprotein
TSL	thermo-sensitive liposome
UDS	user defined scalar

Bibliography

1. King, R.J.B. and M.W. Robins, *Cancer biology*. 3rd ed. 2006, Harlow: Pearson/Prentice Hall. xvii, 292 p.

2. Weinberg, R.A., *The biology of cancer*. 2007, New York: Garland Science. xix, 844 p.

3. Goodman, L.S., et al., *Goodman & Gilman's the pharmacological basis of therapeutics*. 11th ed. 2005, New York: McGraw-Hill. 2021 p.

4. Kennedy, J.E., *High-intensity focused ultrasound in the treatment of solid tumours.* Nature reviews cancer, 2005. **5**(4): p. 321-327.

5. Braathen, L.R., et al., *Guidelines on the use of photodynamic therapy for nonmelanoma skin cancer: an international consensus.* Journal of the American Academy of Dermatology, 2007. **56**(1): p. 125-143.

6. Morgan, R.A., et al., *Cancer regression and neurologic toxicity following anti-MAGE-A3 TCR gene therapy.* Journal of immunotherapy (Hagerstown, Md.: 1997), 2013. **36**(2): p. 133-51.

7. Sarkar, S., et al., *Chemoprevention gene therapy (CGT) of pancreatic cancer using perillyl alcohol and a novel chimeric serotype cancer terminator virus.* Current molecular medicine, 2014. **14**(1): p. 125-140.

8. Sclafani, F., et al., *TP53 mutational status and cetuximab benefit in rectal cancer: 5-year results of the EXPERT-C trial.* Journal of the National Cancer Institute, 2014. **106**(7): p. 121.

9. Aryal, M., et al., *Multiple treatments with liposomal doxorubicin and ultrasound-induced disruption of blood–tumor and blood–brain barriers improve outcomes in a rat glioma model.* Journal of Controlled Release, 2013. **169**(1): p. 103-111.

10. Allen, T.M. and P.R. Cullis, *Liposomal drug delivery systems: from concept to clinical applications.* Advanced drug delivery reviews, 2013. **65**(1): p. 36-48.

11. Bangham, A. and R. Horne, *Negative staining of phospholipids and their structural modification by surface-active agents as observed in the electron microscope.* Journal of molecular biology, 1964. **8**(5): p. 660-IN10.

12. Zhang, X., et al., *Towards an understanding of the release behavior of temperature-sensitive liposomes: a possible explanation of the "pseudoequilibrium" release behavior at the phase transition temperature.* Journal of liposome research, 2013. **23**(3): p. 167-173.

13. Gasselhuber, A., et al., *Targeted drug delivery by high intensity focused ultrasound mediated hyperthermia combined with temperature-sensitive liposomes: computational modelling and preliminary in vivovalidation.* Int J Hyperthermia, 2012. **28**(4): p. 337-48.

14. Au, J.L., et al., *Determinants of drug delivery and transport to solid tumors.* J Control Release, 2001. **74**(1-3): p. 31-46.

15. Jain, R.K., *Transport of molecules in the tumor interstitium: a review.* Cancer Res, 1987. **47**(12): p. 3039-51.

16. Skinner, S.A., G.M. Frydman, and P.E. O'Brien, *Microvascular structure of benign and malignant tumors of the colon in humans.* Dig Dis Sci, 1995. **40**(2): p. 373-84.

17. Jang, S.H., et al., *Drug delivery and transport to solid tumors.* Pharm Res, 2003. **20**(9): p. 1337-50.

18. Clark, E.R. and E.L. Clark, *Microscopic observations on the growth of blood capillaries in the living mammal.* American journal of anatomy, 1939. **64**(2): p. 251-301.

19. Cliff, W.J., *Kinetics of Wound Healing in Rabbit Ear Chambers, a Time Lapse Cinemicroscopic Study.* Q J Exp Physiol Cogn Med Sci, 1965. **50**: p. 79-89.

20. Dreher, M.R., et al., *Tumor vascular permeability, accumulation, and penetration of macromolecular drug carriers.* Journal of the National Cancer Institute, 2006. **98**(5): p. 335-344.

21. Less, J.R., et al., *Microvascular architecture in a mammary carcinoma: branching patterns and vessel dimensions.* Cancer Res, 1991. **51**(1): p. 265-73.

22. Less, J.R., et al., *Geometric resistance and microvascular network architecture of human colorectal carcinoma.* Microcirculation, 1997. **4**(1): p. 25-33.

23. Skinner, S.A., P.J. Tutton, and P.E. O'Brien, *Microvascular architecture of experimental colon tumors in the rat.* Cancer Res, 1990. **50**(8): p. 2411-7.

24. Yamaura, H. and H. Sato, *Quantitative studies on the developing vascular system of rat hepatoma.* J Natl Cancer Inst, 1974. **53**(5): p. 1229-40.

25. Wu, N.Z., et al., *Increased microvascular permeability contributes to preferential accumulation of Stealth liposomes in tumor tissue.* Cancer Res, 1993. **53**(16): p. 3765-70.

26. Yuan, F., et al., *Microvascular permeability and interstitial penetration of sterically stabilized (stealth) liposomes in a human tumor xenograft.* Cancer Res, 1994. **54**(13): p. 3352-6.

27. Chang, Y.S., et al., *Mosaic blood vessels in tumors: frequency of cancer cells in contact with flowing blood.* Proceedings of the National Academy of Sciences, 2000. **97**(26): p. 14608-14613.

28. di Tomaso, E., et al., *Mosaic tumor vessels: cellular basis and ultrastructure of focal regions lacking endothelial cell markers.* Cancer research, 2005. **65**(13): p. 5740-5749.

29. McDonald, D.M. and P.L. Choyke, *Imaging of angiogenesis: from microscope to clinic.* Nat Med, 2003. **9**(6): p. 713-25.

30. Heuser, L.S. and F.N. Miller, *Differential macromolecular leakage from the vasculature of tumors.* Cancer, 1986. **57**(3): p. 461-4.

31. Winkler, F., et al., *Kinetics of vascular normalization by VEGFR2 blockade governs brain tumor response to radiation: role of oxygenation, angiopoietin-1, and matrix metalloproteinases.* Cancer Cell, 2004. **6**(6): p. 553-63.

32. Hobbs, S.K., et al., *Regulation of transport pathways in tumor vessels: role of tumor type and microenvironment.* Proc Natl Acad Sci U S A, 1998. **95**(8): p. 4607-12.

33. Yuan, F., et al., *Vascular permeability and microcirculation of gliomas and mammary carcinomas transplanted in rat and mouse cranial windows.* Cancer Res, 1994. **54**(17): p. 4564-8.

34. Bundgaard, M., *Transport pathways in capillaries-in search of pores.* Annual review of physiology, 1980. **42**(1): p. 325-336.

35. Firrell, J.C., G.P. Lewis, and L.J. Youlten, *Vascular permeability to macromolecules in rabbit paw and skeletal muscle: a lymphatic study with a mathematical interpretation of transport processes.* Microvasc Res, 1982. **23**(3): p. 294-310.

36. Simionescu, N., M. Simionescu, and G.E. Palade, *Open junctions in the endothelium of the postcapillary venules of the diaphragm.* J Cell Biol, 1978. **79**(1): p. 27-44.

37. Lum, H. and A.B. Malik, *Regulation of vascular endothelial barrier function.* Am J Physiol, 1994. **267**(3 Pt 1): p. L223-41.

38. Seymour, L.W., *Passive tumor targeting of soluble macromolecules and drug conjugates.* Critical reviews in therapeutic drug carrier systems, 1991. **9**(2): p. 135-187.

39. Endrich, B., et al., *Tissue perfusion inhomogeneity during early tumor growth in rats.* J Natl Cancer Inst, 1979. **62**(2): p. 387-95.

40. Jain, R.K., *Transport of molecules across tumor vasculature.* Cancer and Metastasis Reviews, 1987. **6**(4): p. 559-593.

41. Rubin, P. and G. Casarett, *Microcirculation of tumors part I: anatomy, function, and necrosis.* Clinical radiology, 1966. **17**(3): p. 220-229.

42. Jain, R.K., *Determinants of tumor blood flow: a review.* Cancer Res, 1988. **48**(10): p. 2641-58.

43. Peters, W., et al., *Microcirculatory studies in rat mammary carcinoma. I. Transparent chamber method, development of microvasculature, and pressures in tumor vessels.* Journal of the National Cancer Institute, 1980. **65**(3): p. 631-642.

44. Hori, K., et al., *Characterization of heterogeneous distribution of tumor blood flow in the rat.* Cancer Science, 1991. **82**(1): p. 109-117.

45.   Vaupel, P., F. Kallinowski, and P. Okunieff, *Blood flow, oxygen and nutrient supply, and metabolic microenvironment of human tumors: a review.* Cancer research, 1989. **49**(23): p. 6449-6465.

46.   Saltzman, W.M., *Drug delivery: engineering principles for drug therapy.* 2001: Oxford University Press.

47.   Maeda, H., et al., *Tumor vascular permeability and the EPR effect in macromolecular therapeutics: a review.* J Control Release, 2000. **65**(1-2): p. 271-84.

48.   Boucher, Y. and R.K. Jain, *Microvascular pressure is the principal driving force for interstitial hypertension in solid tumors: implications for vascular collapse.* Cancer research, 1992. **52**(18): p. 5110-5114.

49.   Baxter, L.T. and R.K. Jain, *Transport of fluid and macromolecules in tumors. I. Role of interstitial pressure and convection.* Microvasc Res, 1989. **37**(1): p. 77-104.

50.   Baxter, L.T. and R.K. Jain, *Transport of fluid and macromolecules in tumors. II. Role of heterogeneous perfusion and lymphatics.* Microvasc Res, 1990. **40**(2): p. 246-63.

51.   Goh, Y.M., H.L. Kong, and C.H. Wang, *Simulation of the delivery of doxorubicin to hepatoma.* Pharm Res, 2001. **18**(6): p. 761-70.

52.   Cusack, B.J., et al., *Doxorubicin and doxorubicinol pharmacokinetics and tissue concentrations following bolus injection and continuous infusion of doxorubicin in the rabbit.* Cancer chemotherapy and pharmacology, 1993. **32**(1): p. 53-58.

53.   Legha, S.S., et al., *Reduction of doxorubicin cardiotoxicity by prolonged continuous intravenous infusion.* Annals of Internal Medicine, 1982. **96**(2): p. 133-139.

54.   Hortobagyi, G., et al., *Decreased cardiac toxicity of doxorubicin administered by continuous intravenous infusion in combination chemotherapy for metastatic breast carcinoma.* Cancer, 1989. **63**(1): p. 37-45.

55.   El-Kareh, A.W. and T.W. Secomb, *A mathematical model for comparison of bolus injection, continuous infusion, and liposomal delivery of doxorubicin to tumor cells.* Neoplasia, 2000. **2**(4): p. 325-38.

56.   Gabizon, A.A., *Pegylated liposomal doxorubicin: metamorphosis of an old drug into a new form of chemotherapy.* Cancer Invest, 2001. **19**(4): p. 424-36.

57.   Soundararajan, A., et al., *[(186)Re]Liposomal doxorubicin (Doxil): in vitro stability, pharmacokinetics, imaging and biodistribution in a head and neck squamous cell carcinoma xenograft model.* Nucl Med Biol, 2009. **36**(5): p. 515-24.

58.   Bangham, A., M.M. Standish, and J. Watkins, *Diffusion of univalent ions across the lamellae of swollen phospholipids.* Journal of molecular biology, 1965. **13**(1): p. 238-IN27.

59.   Litzinger, D.C., et al., *Effect of liposome size on the circulation time and intraorgan distribution of amphipathic poly (ethylene glycol)-containing liposomes.* Biochimica et Biophysica Acta (BBA)-Biomembranes, 1994. **1190**(1): p. 99-107.

60.   Liu, D., A. Mori, and L. Huang, *Role of liposome size and RES blockade in controlling biodistribution and tumor uptake of GM$_1$-containing liposomes.* Biochimica et Biophysica Acta (BBA)-Biomembranes, 1992. **1104**(1): p. 95-101.

61.   Gabizon, A., H. Shmeeda, and Y. Barenholz, *Pharmacokinetics of pegylated liposomal Doxorubicin: review of animal and human studies.* Clin Pharmacokinet, 2003. **42**(5): p. 419-36.

62.   Gabizon, A., et al., *Prolonged circulation time and enhanced accumulation in malignant exudates of doxorubicin encapsulated in polyethylene-glycol coated liposomes.* Cancer Res, 1994. **54**(4): p. 987-92.

63.   Vaage, J., et al., *Tissue distribution and therapeutic effect of intravenous free or encapsulated liposomal doxorubicin on human prostate carcinoma xenografts.* Cancer, 1994. **73**(5): p. 1478-1484.

64.   Batist, G., et al., *Reduced cardiotoxicity and preserved antitumor efficacy of liposome-encapsulated doxorubicin and cyclophosphamide compared with conventional doxorubicin and cyclophosphamide in a randomized, multicenter trial of metastatic breast cancer.* Journal of Clinical Oncology, 2001. **19**(5): p. 1444-1454.

65.   Zou, Y., et al., *Enhanced therapeutic effect against liver W256 carcinosarcoma with temperature-sensitive liposomal adriamycin administered into the hepatic artery.* Cancer Res, 1993. **53**(13): p. 3046-51.

66.   Gaber, M.H., et al., *Thermosensitive sterically stabilized liposomes: formulation and in vitro studies on mechanism of doxorubicin release by bovine serum and human plasma.* Pharm Res, 1995. **12**(10): p. 1407-16.

67.   Unezaki, S., et al., *Enhanced delivery and antitumor activity of doxorubicin using long-circulating thermosensitive liposomes containing amphipathic polyethylene glycol in combination with local hyperthermia.* Pharm Res, 1994. **11**(8): p. 1180-5.

68.   Lindner, L.H., et al., *Novel temperature-sensitive liposomes with prolonged circulation time.* Clin Cancer Res, 2004. **10**(6): p. 2168-78.

69.   Tagami, T., M.J. Ernsting, and S.D. Li, *Optimization of a novel and improved thermosensitive liposome formulated with DPPC and a Brij surfactant using a robust in vitro system.* J Control Release, 2011. **154**(3): p. 290-7.

70.   de Smet, M., et al., *Magnetic resonance imaging of high intensity focused ultrasound mediated drug delivery from temperature-sensitive liposomes: an in vivo proof-of-concept study.* J Control Release, 2011. **150**(1): p. 102-10.

71.   Hynynen, K., *MRIgHIFU: A tool for image‑guided therapeutics.* Journal of Magnetic Resonance Imaging, 2011. **34**(3): p. 482-493.

72.   Staruch, R., R. Chopra, and K. Hynynen, *Localised drug release using MRI-controlled focused ultrasound hyperthermia.* International Journal of Hyperthermia, 2010. **27**(2): p. 156-171.

73.   Staruch, R.M., et al., *Enhanced drug delivery in rabbit VX2 tumours using thermosensitive liposomes and MRI-controlled focused ultrasound hyperthermia.* International Journal of Hyperthermia, 2012. **28**(8): p. 776-787.

74.   Sheu, T.W.H., et al., *On an acoustics–thermal–fluid coupling model for the prediction of temperature elevation in liver tumor.* International Journal of Heat and Mass Transfer, 2011. **54**(17): p. 4117-4126.

75.   Qiao, S., et al., *Effects of different parameters in the fast scanning method for HIFU treatment.* Medical physics, 2012. **39**: p. 5795.

76.   Lin, W.-L., R.B. Roemer, and K. Hynynen, *Theoretical and experimental evaluation of a temperature controller for scanned focused ultrasound hyperthermia.* Medical physics, 1990. **17**: p. 615.

77.   Mougenot, C., et al., *Three‑dimensional spatial and temporal temperature control with MR thermometry‑guided focused ultrasound (MRgHIFU).* Magnetic Resonance in Medicine, 2009. **61**(3): p. 603-614.

78.   Wang, C.-H. and J. Li, *Three-dimensional simulation of IgG delivery to tumors.* Chemical Engineering Science, 1998. **53**(20): p. 3579-3600.

79.   Teo, C.S., et al., *Transient interstitial fluid flow in brain tumors: Effect on drug delivery.* Chemical Engineering Science, 2005. **60**(17): p. 4803-4821.

80.   Tzafriri, A.R., et al., *Mathematical modeling and optimization of drug delivery from intratumorally injected microspheres.* Clin Cancer Res, 2005. **11**(2 Pt 1): p. 826-34.

81.   Weinberg, B.D., et al., *Model simulation and experimental validation of intratumoral chemotherapy using multiple polymer implants.* Medical & biological engineering & computing, 2008. **46**(10): p. 1039-1049.

82.   Kuenen, B.C., et al., *Dose-finding and pharmacokinetic study of cisplatin, gemcitabine, and SU5416 in patients with solid tumors.* Journal of clinical oncology, 2002. **20**(6): p. 1657-1667.

83.   Wihlm, J., et al., *Pharmacokinetic profile of high-dose doxorubicin administered during a 6 h intravenous infusion in breast cancer patients].* Bulletin du cancer, 1997. **84**(6): p. 603.

84.   Stoller, R.G., et al., *Use of plasma pharmacokinetics to predict and prevent methotrexate toxicity.* New England Journal of Medicine, 1977. **297**(12): p. 630-634.

85. Robert, J., et al., *Pharmacokinetics of adriamycin in patients with breast cancer: correlation between pharmacokinetic parameters and clinical short-term response.* European Journal of Cancer and Clinical Oncology, 1982. **18**(8): p. 739-745.

86. Greene, R.F., et al., *Plasma pharmacokinetics of adriamycin and adriamycinol: implications for the design of in vitro experiments and treatment protocols.* Cancer Res, 1983. **43**(7): p. 3417-21.

87. Deen, W.M., *Hindered transport of large molecules in liquid-filled pores.* AIChE Journal, 1987. **33**(9): p. 1409-1425.

88. Baxter, L.T. and R.K. Jain, *Transport of fluid and macromolecules in tumors. III. Role of binding and metabolism.* Microvasc Res, 1991. **41**(1): p. 5-23.

89. Baxter, L.T. and R.K. Jain, *Transport of fluid and macromolecules in tumors. IV. A microscopic model of the perivascular distribution.* Microvasc Res, 1991. **41**(2): p. 252-72.

90. Eikenberry, S., *A tumor cord model for doxorubicin delivery and dose optimization in solid tumors.* Theor Biol Med Model, 2009. **6**: p. 16.

91. Netti, P.A., et al., *Time-dependent behavior of interstitial fluid pressure in solid tumors: implications for drug delivery.* Cancer Research, 1995. **55**(22): p. 5451-5458.

92. Erlichman, C. and D. Vidgen, *Cytotoxicity of adriamycin in MGH-U1 cells grown as monolayer cultures, spheroids, and xenografts in immune-deprived mice.* Cancer research, 1984. **44**(11): p. 5369-5375.

93. Nederman, T. and J. Carlsson, *Penetration and binding of vinblastine and 5-fluorouracil in cellular spheroids.* Cancer chemotherapy and pharmacology, 1984. **13**(2): p. 131-135.

94. Nederman, T., J. Carlsson, and K. Kuoppa, *Penetration of substances into tumour tissue. Model studies using saccharides, thymidine and thymidine-5'-triphosphate in cellular spheroids.* Cancer chemotherapy and pharmacology, 1987. **22**(1): p. 21-25.

95. Nicholson, K., M. Bibby, and R. Phillips, *Influence of drug exposure parameters on the activity of paclitaxel in multicellular spheroids.* European Journal of Cancer, 1997. **33**(8): p. 1291-1298.

96. West, G.W., R. Weichselbaum, and J.B. Little, *Limited penetration of methotrexate into human osteosarcoma spheroids as a proposed model for solid tumor resistance to adjuvant chemotherapy.* Cancer research, 1980. **40**(10): p. 3665-3668.

97. Erlanson, M., E. Daniel-Szolgay, and J. Carlsson, *Relations between the penetration, binding and average concentration of cytostatic drugs in human tumour spheroids.* Cancer chemotherapy and pharmacology, 1992. **29**(5): p. 343-353.

98. Dordal, M.S., et al., *Flow cytometric assessment of the cellular pharmacokinetics of fluorescent drugs.* Cytometry, 1995. **20**(4): p. 307-314.

99. Luu, K.T. and J.A. Uchizono, *P-glycoprotein induction and tumor cell-kill dynamics in response to differential doxorubicin dosing strategies: a theoretical pharmacodynamic model.* Pharmaceutical research, 2005. **22**(5): p. 710-715.

100. Friedman, M.H., *Principles and models of biological transport.* 2008: Springer.

101. Kerr, D.J., et al., *Comparative intracellular uptake of adriamycin and 4'-deoxydoxorubicin by non-small cell lung tumor cells in culture and its relationship to cell survival.* Biochem Pharmacol, 1986. **35**(16): p. 2817-23.

102. Liu, C., J. Krishnan, and X.Y. Xu, *Investigating the effects of ABC transporter-based acquired drug resistance mechanisms at the cellular and tissue scale.* Integrative Biology, 2013.

103. Doroshow, J.H., *Anthracyclines and anthracenediones.* Cancer Chemotherapy and Biotherapy: Principles and Practice. 2nd ed. Philadelphia, Pa: Lippincott-Raven, 1996: p. 409-434.

104. Ozawa, S., et al., *Cell killing action of cell cycle phase-non-specific antitumor agents is dependent on concentration--time product.* Cancer Chemother Pharmacol, 1988. **21**(3): p. 185-90.

105. Eichholtz-Wirth, H., *Dependence of the cytostatic effect of adriamycin on drug concenration and exposure time in vitro.* Br J Cancer, 1980. **41**(6): p. 886-91.

106. Gewirtz, D., *A critical evaluation of the mechanisms of action proposed for the antitumor effects of the anthracycline antibiotics adriamycin and daunorubicin.* Biochemical pharmacology, 1999. **57**(7): p. 727-741.

107. El-Kareh, A.W. and T.W. Secomb, *A mathematical model for cisplatin cellular pharmacodynamics.* Neoplasia (New York, NY), 2003. **5**(2): p. 161.

108. Lankelma, J., et al., *Simulation model of doxorubicin activity in islets of human breast cancer cells.* Biochimica et Biophysica Acta (BBA)-General Subjects, 2003. **1622**(3): p. 169-178.

109. Eliaz, R.E., et al., *Determination and modeling of kinetics of cancer cell killing by doxorubicin and doxorubicin encapsulated in targeted liposomes.* Cancer research, 2004. **64**(2): p. 711-718.

110. Yuan, F., et al., *Vascular permeability in a human tumor xenograft: molecular size dependence and cutoff size.* Cancer Res, 1995. **55**(17): p. 3752-6.

111. Pennes, H.H., *Analysis of tissue and arterial blood temperatures in the resting human forearm.* J Appl Physiol, 1948. **1**(2): p. 93-122.

112. Curra, F.P., et al., *Numerical simulations of heating patterns and tissue temperature response due to high-intensity focused ultrasound.* Ultrasonics, Ferroelectrics and Frequency Control, IEEE Transactions on, 2000. **47**(4): p. 1077-1089.

113. Filonenko, E. and V. Khokhlova, *Effect of acoustic nonlinearity on heating of biological tissue by high-intensity focused ultrasound.* Acoustical Physics, 2001. **47**(4): p. 468-475.

114.	Solovchuk, M.A., et al., *Simulation study on acoustic streaming and convective cooling in blood vessels during a high-intensity focused ultrasound thermal ablation.* International Journal of Heat and Mass Transfer, 2012. **55**(4): p. 1261-1270.

115.	O'Neil, H., *Theory of focusing radiators.* The Journal of the Acoustical Society of America, 1949. **21**: p. 516.

116.	Hilmas, D.E. and E.L. Gillette, *Morphometric analyses of the microvasculature of tumors during growth and after x-irradiation.* Cancer, 1974. **33**(1): p. 103-10.

117.	Pappenheimer, J.R., E.M. Renkin, and L.M. Borrero, *Filtration, diffusion and molecular sieving through peripheral capillary membranes.* Am. J. Physiol, 1951. **167**(13): p. 2578.

118.	Nugent, L.J. and R.K. Jain, *Extravascular diffusion in normal and neoplastic tissues.* Cancer Res, 1984. **44**(1): p. 238-44.

119.	Wu, N.Z., et al., *Measurement of material extravasation in microvascular networks using fluorescence video-microscopy.* Microvasc Res, 1993. **46**(2): p. 231-53.

120.	Curry, F.E., V.H. Huxley, and R.H. Adamson, *Permeability of single capillaries to intermediate-sized colored solutes.* Am J Physiol, 1983. **245**(3): p. H495-505.

121.	Ribba, B., et al., *A mathematical model of Doxorubicin treatment efficacy for non-Hodgkin's lymphoma: investigation of the current protocol through theoretical modelling results.* Bull Math Biol, 2005. **67**(1): p. 79-99.

122.	Gerlowski, L.E. and R.K. Jain, *Microvascular permeability of normal and neoplastic tissues.* Microvasc Res, 1986. **31**(3): p. 288-305.

123.	Granath, K.A. and B.E. Kvist, *Molecular weight distribution analysis by gel chromatography on Sephadex.* J Chromatogr, 1967. **28**(1): p. 69-81.

124.	Saltzman, W.M. and M.L. Radomsky, *Drugs released from polymers: diffusion and elimination in brain tissue.* Chemical Engineering Science, 1991. **46**(10): p. 2429-2444.

125.	Swabb, E.A., J. Wei, and P.M. Gullino, *Diffusion and convection in normal and neoplastic tissues.* Cancer Res, 1974. **34**(10): p. 2814-22.

126.	Tong, R.T., et al., *Vascular normalization by vascular endothelial growth factor receptor 2 blockade induces a pressure gradient across the vasculature and improves drug penetration in tumors.* Cancer Res, 2004. **64**(11): p. 3731-6.

127.	Aukland, K. and R.K. Reed, *Interstitial-lymphatic mechanisms in the control of extracellular fluid volume.* Physiol Rev, 1993. **73**(1): p. 1-78.

128.	Wolf, M.B., P.D. Watson, and D.R. Scott, 2nd, *Integral-mass balance method for determination of solvent drag reflection coefficient.* Am J Physiol, 1987. **253**(1 Pt 2): p. H194-204.

129. Saltiel, E. and W. McGuire, *Doxorubicin (adriamycin) cardiomyopathy.* West J Med, 1983. **139**(3): p. 332-41.

130. Singal, P.K. and N. Iliskovic, *Doxorubicin-induced cardiomyopathy.* New England Journal of Medicine, 1998. **339**(13): p. 900-905.

131. Barth, T.J. and D.C. Jespersen, *The design and application of upwind schemes on unstructured meshes.* 1989.

132. Benet, L.Z. and P. Zia-Amirhosseini, *Basic principles of pharmacokinetics.* Toxicologic pathology, 1995. **23**(2): p. 115-123.

133. Rodvold, K.A., D.A. Rushing, and D.A. Tewksbury, *Doxorubicin clearance in the obese.* Journal of Clinical Oncology, 1988. **6**(8): p. 1321-1327.

134. Dubois, A.B., Julie; Mentre, France *Mathematical expressions of the pharmacokinetic and pharmacodynamic models implemented in the PFIM software.* University Paris Diderot, 2011.

135. Raghunathan, S., D. Evans, and J.L. Sparks, *Poroviscoelastic modeling of liver biomechanical response in unconfined compression.* Annals of biomedical engineering, 2010. **38**(5): p. 1789-1800.

136. Zhao, J., H. Salmon, and M. Sarntinoranont, *Effect of heterogeneous vasculature on interstitial transport within a solid tumor.* Microvascular research, 2007. **73**(3): p. 224-236.

137. Jain, H.V., J.E. Nör, and T.L. Jackson, *Modeling the VEGF–Bcl-2–CXCL8 Pathway in Intratumoral Agiogenesis.* Bulletin of mathematical biology, 2008. **70**(1): p. 89-117.

138. Schiffelers, R.M., et al., *Anti-tumor efficacy of tumor vasculature-targeted liposomal doxorubicin.* Journal of Controlled Release, 2003. **91**(1): p. 115-122.

139. Arap, W., R. Pasqualini, and E. Ruoslahti, *Cancer treatment by targeted drug delivery to tumor vasculature in a mouse model.* Science, 1998. **279**(5349): p. 377-380.

140. Eatock, M., A. Schätzlein, and S. Kaye, *Tumour vasculature as a target for anticancer therapy.* Cancer treatment reviews, 2000. **26**(3): p. 191-204.

141. Schutt, D.J. and D. Haemmerich, *Effects of variation in perfusion rates and of perfusion models in computational models of radio frequency tumor ablation.* Med Phys, 2008. **35**(8): p. 3462-70.

142. Grüll, H. and S. Langereis, *Hyperthermia-triggered drug delivery from temperature-sensitive liposomes using MRI-guided high intensity focused ultrasound.* Journal of Controlled Release, 2012. **161**(2): p. 317-327.

143. Tagami, T., et al., *A thermosensitive liposome prepared with a Cu^{2+} gradient demonstrates improved pharmacokinetics, drug delivery and antitumor efficacy.* Journal of Controlled Release, 2012. **161**(1): p. 142-149.

144.   Dalmark, M. and H.H. Storm, *A Fickian diffusion transport process with features of transport catalysis. Doxorubicin transport in human red blood cells.* J Gen Physiol, 1981. **78**(4): p. 349-64.

145.   Gaber, M.H., et al., *Thermosensitive liposomes: extravasation and release of contents in tumor microvascular networks.* Int J Radiat Oncol Biol Phys, 1996. **36**(5): p. 1177-87.

146.   Keenan, J.H. and F.G. Keyes, *Thermodynamic properties of steam : including data for the liquid and solid phases.* 1936, New York, London ;: Wiley ; Chapman & Hall.

147.   Nagaoka, S., et al., *Intracellular uptake, retention and cytotoxic effect of adriamycin combined with hyperthermia in vitro.* Jpn J Cancer Res, 1986. **77**(2): p. 205-11.

148.   Afadzi, M., et al. *Ultrasound stimulated release of liposomal calcein.* in *Ultrasonics Symposium (IUS), 2010 IEEE.* 2010. IEEE.

149.   Ranjan, A., et al., *Image-guided drug delivery with magnetic resonance guided high intensity focused ultrasound and temperature sensitive liposomes in a rabbit Vx2 tumor model.* Journal of controlled release, 2012. **158**(3): p. 487-494.

150.   Monsky, W.L., et al., *Augmentation of transvascular transport of macromolecules and nanoparticles in tumors using vascular endothelial growth factor.* Cancer Research, 1999. **59**(16): p. 4129-4135.

151.   Bailey, M., et al., *Physical mechanisms of the therapeutic effect of ultrasound (a review).* Acoustical Physics, 2003. **49**(4): p. 369-388.

152.   Hariharan, P., M. Myers, and R. Banerjee, *HIFU procedures at moderate intensities—effect of large blood vessels.* Physics in medicine and biology, 2007. **52**(12): p. 3493.

153.   Marbeuf-Gueye, C., et al., *Inhibition of the P-glycoprotein and multidrug resistance protein-mediated efflux of anthracyclines and calceinacetoxymethyl ester by PAK-104P.* European journal of pharmacology, 2000. **391**(3): p. 207-216.

154.   Maitra, R., et al., *Differential effects of mitomycin C and doxorubicin on P-glycoprotein expression.* Biochem. J, 2001. **355**: p. 617-624.

155.   Demeule, M., M. Brossard, and R. Béliveau, *Cisplatin induces renal expression of P-glycoprotein and canalicular multispecific organic anion transporter.* American Journal of Physiology-Renal Physiology, 1999. **277**(6): p. F832-F840.

156.   Köhler, M.O., et al., *Volumetric HIFU ablation under 3D guidance of rapid MRI thermometry.* Medical physics, 2009. **36**(8): p. 3521-3535.

157.   Enholm, J.K., et al., *Improved volumetric MR-HIFU ablation by robust binary feedback control.* Biomedical Engineering, IEEE Transactions on, 2010. **57**(1): p. 103-113.

158. Primeau, A.J., et al., *The distribution of the anticancer drug Doxorubicin in relation to blood vessels in solid tumors.* Clinical Cancer Research, 2005. **11**(24): p. 8782-8788.

159. Murad, A.M., et al., *Modified therapy with 5‑fluorouracil, doxorubicin, and methotrexate in advanced gastric cancer.* Cancer, 1993. **72**(1): p. 37-41.

160. von der Maase, H., et al., *Long-term survival results of a randomized trial comparing gemcitabine plus cisplatin, with methotrexate, vinblastine, doxorubicin, plus cisplatin in patients with bladder cancer.* Journal of Clinical Oncology, 2005. **23**(21): p. 4602-4608.